The Geological Society of America
Special Paper 450
2009

Late Quaternary sedimentary features of Bear Lake, Utah and Idaho

Joseph P. Smoot
U.S. Geological Survey, M.S. 926A National Center, Reston, Virginia 20192, USA

ABSTRACT

Bear Lake sediments were predominantly aragonite for most of the Holocene, reflecting a hydrologically closed lake fed by groundwater and small streams. During the late Pleistocene, the Bear River flowed into Bear Lake and the lake waters spilled back into the Bear River drainage. At that time, sediment deposition was dominated by siliciclastic sediment and calcite. Lake-level fluctuation during the Holocene and late Pleistocene produced three types of aragonite deposits in the central lake area that are differentiated primarily by grain size, sorting, and diatom assemblage. Lake-margin deposits during this period consisted of sandy deposits including well-developed shoreface deposits on margins adjacent to relatively steep gradient lake floors and thin, graded shell gravel on margins adjacent to very low gradient lake-floor areas. Throughout the period of aragonite deposition, episodic drops in lake level resulted in erosion of shallow-water deposits, which were redeposited into the deeper lake. These sediment-focusing episodes are recognized by mixing of different mineralogies and crystal habits and mixing of a range of diatom fauna into poorly sorted mud layers. Lake-level drops are also indicated by erosional gaps in the shallow-water records and the occurrence of shoreline deposits in areas now covered by as much as 30 m of water. Calcite precipitation occurred for a short interval of time during the Holocene in response to an influx of Bear River water ca. 8 ka. The Pleistocene sedimentary record of Bear Lake until ca. 18 ka is dominated by siliciclastic glacial flour derived from glaciers in the Uinta Mountains. The Bear Lake deep-water siliciclastic deposits are thoroughly bioturbated, whereas shallow-water deposits transitional to deltas in the northern part of the basin are upward-coarsening sequences of laminated mud, silt, and sand. A major drop in lake level occurred ca. 18 ka, resulting in subaerial exposure of the lake floor in areas now covered by over 40 m of water. The subaerial surfaces are indicated by root casts and gypsum-rich soil features. Bear Lake remained at this low state with a minor transgression until ca. 15 ka. A new influx of Bear River water produced a major lake transgression and deposited a thin calcite deposit. Bear Lake quickly dropped to a shallow-water state, accumulating a mixture of calcite and siliciclastic sediment that contains at least two intervals of root-disrupted horizons indicating lake-level drops to more than 40 m below the modern highstand. About 11,500 yr B.P., the lake level rose again through an influx of Bear River water producing another thin calcite layer. The Bear River ceased to flow into the basin and the lake salinity increased, resulting in the aragonite deposition that

Smoot, J.P., 2009, Late Quaternary sedimentary features of Bear Lake, Utah and Idaho, *in* Rosenbaum, J.G., and Kaufman, D.S., eds., Paleoenvironments of Bear Lake, Utah and Idaho, and its catchment: Geological Society of America Special Paper 450, p. 49–104, doi: 10.1130/2009.2450(03).

persisted until modern human activity. The climatic record of Bear Lake sediment is difficult to ascertain by using standard chemical and biological techniques because of variations in the inflow hydrology and the significant amount of erosion and redeposition of chemical and biological sediment components.

INTRODUCTION

The history of Bear Lake hydrology and climate resides within its sedimentary record. All mineralogical, chemical, biological, and magnetic measurements are derived from these deposits as recovered from cores and grab samples. The sedimentological framework is essential for interpreting the significance of the various measurements and for providing additional information on past physical conditions of Bear Lake.

This chapter provides sedimentary descriptions of all cores collected from Bear Lake except the GLAD 800 cores (Dean, this volume; Kaufman et al., this volume) and short gravity cores that were sampled in the field. Grab samples and trenches in and around Bear Lake are also included in this study. Data derived from these sources provide an overview of shallow-water to deep-water sedimentation for about the last 26,000 yr.

Physiographic Setting

Bear Lake is nestled in a valley between Paleozoic carbonate rocks of the steep mountains bordering the west side and the Mesozoic and Tertiary sandstones, conglomerates, and shales of the Bear Lake Plateau to the east (see Reheis et al., this volume). Faults that bound the valley offset drainages and other geomorphic features (McCalpin, 1993; Reheis et al., this volume), including the lake floor (Colman, 2005, 2006), indicating active Holocene tectonism. In its natural state, Bear Lake is primarily fed by spring-fed streams draining the adjacent highlands, and there has been little if any surface outflow (Fig. 1). A series of canals, completed in 1912, divert water from the Bear River into the lake and allow lake waters to drain northward back into the Bear River. The lake waters are alkaline, but not very saline, supporting a population of fish and invertebrates with many endemic species (Dean et al., this volume).

Sedimentation

Most of the information on modern sedimentation in Bear Lake is from studies presented in this volume. The bulk of the sediment currently being deposited in Bear Lake is either chemically precipitated or biologically formed (Fig. 2). Prior to completion of the canals, aragonite was the principal carbonate mineral precipitated for most of the Holocene, but low-magnesium calcite is now the primary mineral (Dean et al., 2006; Dean, this volume). The most important biological components of the sediments include diatom tests (Moser and Kimball, this volume) and ostracode shells (Bright, this volume). Very little clastic sediment is being introduced into the lake from the surface drainages (Rosenbaum et al., this volume). Geomorphic features that resemble deltas at the mouths of some creeks (particularly North and South Eden Creek) appear to have formed during the Pleistocene (see Colman, 2006). Wave transport disperses clastic sediment around the lake, mostly reworking older deposits. Shorelines are composed of siliciclastic sand, and boulders and cobbles reflecting the lithology of adjacent mountains. In shoreline areas more distant from the mountains, the coarse material includes abundant shells of snails, clams, and ostracodes.

The primary mechanical sedimentation processes occurring in Bear Lake today are wave transport and sediment gravity flows, mostly induced by wave activity (Fig. 2). Direct evidence of wave sorting in the modern lake is mostly limited to depths of less than 10 m. Grain-size distributions in surface sediments (see Smoot and Rosenbaum, this volume) suggest that wave winnowing occurs to depths of 30 m or more. Coarser grain sizes persist at greater depths where the lake floor is steeper, suggesting that underwater gravity flows are more important in those areas. A model for maximum wave depth indicates that silt-sized material is deposited well beyond the depth for wave movement even in the areas with low bottom slopes (Smoot and Rosenbaum, this volume). Therefore, it is believed that underwater gravity currents are an important mechanism for redistributing sediment throughout the lake. The resedimentation of shallow-water deposits lakeward is called sediment focusing (Davis and Ford, 1982; Hilton, 1985). Dean et al. (2006) and Dean (this volume) observed that near-surface sediment traps collected calcite precipitated at the surface, but sediment traps closer to the lake floor collected mostly aragonite, presumably older sediment that was mechanically resuspended.

Analytical Techniques

Three cores (BL96-1, -2, -3) were obtained with a Kullenburg piston apparatus, and the other ten cores (BL2K-2, -3; BLR2K-1, -2, -3; BL02-1, -2, -3, -4, -5) were collected with a UWITEC piston corer that is hammered into the sediment (Rosenbaum and Kaufman, this volume). Shoreline sample localities were trenched to just below the water table by hand, and 1 gal rectangular cans (25 cm deep, 18 cm wide) were pushed into two overlapping samples from the surface (total depth ~45 cm). All cores were split lengthwise with a steel wire and the surfaces were cleaned of smear marks and irregularities with a straight razor. Initial descriptions were made with a 10× hand lens and additional information was obtained by using a Nikon zoom stereoscopic microscope (up to 6×) with a 10-power ocular lens. The cores were photographed with 35 mm film in 14–20 cm overlapping segments, and the film was scanned at 3000 dpi to

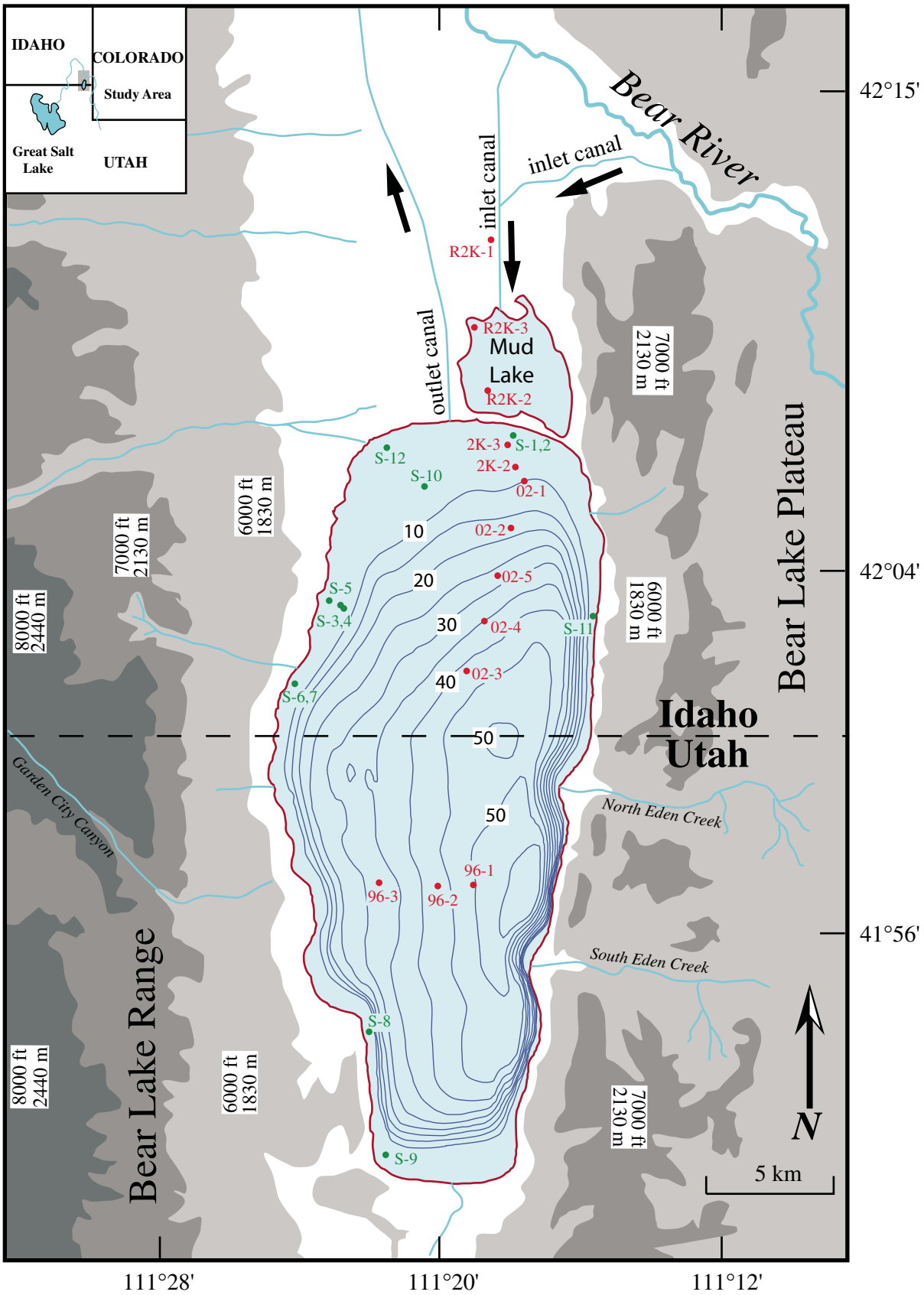

Figure 1. Map of Bear Lake and surrounding areas. Elevation zones are divided into 1000 foot intervals. Isobaths are at 5 m intervals except for depths less than 10 m. Red dots show locations of cores described in this paper and green dots show locations of trenches used in this paper.

4000 dpi. X-radiographs were made of 1-cm-thick slabs of the three Kullenburg cores in a Picker Minishot 1 using 17-inch Agfa Structurix D4DW film. The images were digitized at 4000 dpi with a UMAX 2100 scanner using the UTA-2100XL transparency adaptor. The images were examined with a hand lens and stereoscopic microscope. Smear slides were collected at 10 cm intervals and at visible changes in sediment character in all cores. A subsequent set of smear slides was collected in the Kullenburg cores at intervals where changes in fabric are visible in the X-radiographs. The smear slides were examined with a Zeiss binocular petrographic scope with 10× ocular and 40× objective lens. Selected smear slides (~100 samples) were counted along a 10 µm grid to establish variability in diatoms and grain types. Three hundred diatoms were counted on each slide, whereas abundance of grain types was estimated by using a shadow diagram (Terry and Chilingar, 1955). Polished thin sections were made at select intervals from chips imbedded with Spurr resin as described by Kemp et al. (2001). These were examined both by petrographic microscope and SEM. About 250 samples were dried and sieved into silt and sand fractions that were examined under the stereoscopic microscope. Diatoms species observed in smear slides were identified from photographs by Katrina Moser. Other biological identification, mineralogical analyses, biological identification, and radiocarbon dates cited in this paper were provided by the authors of other chapters in this volume.

Core Descriptions

The locations for the cores described in this paper are shown in Figure 1. The sedimentary characteristics of the cores are

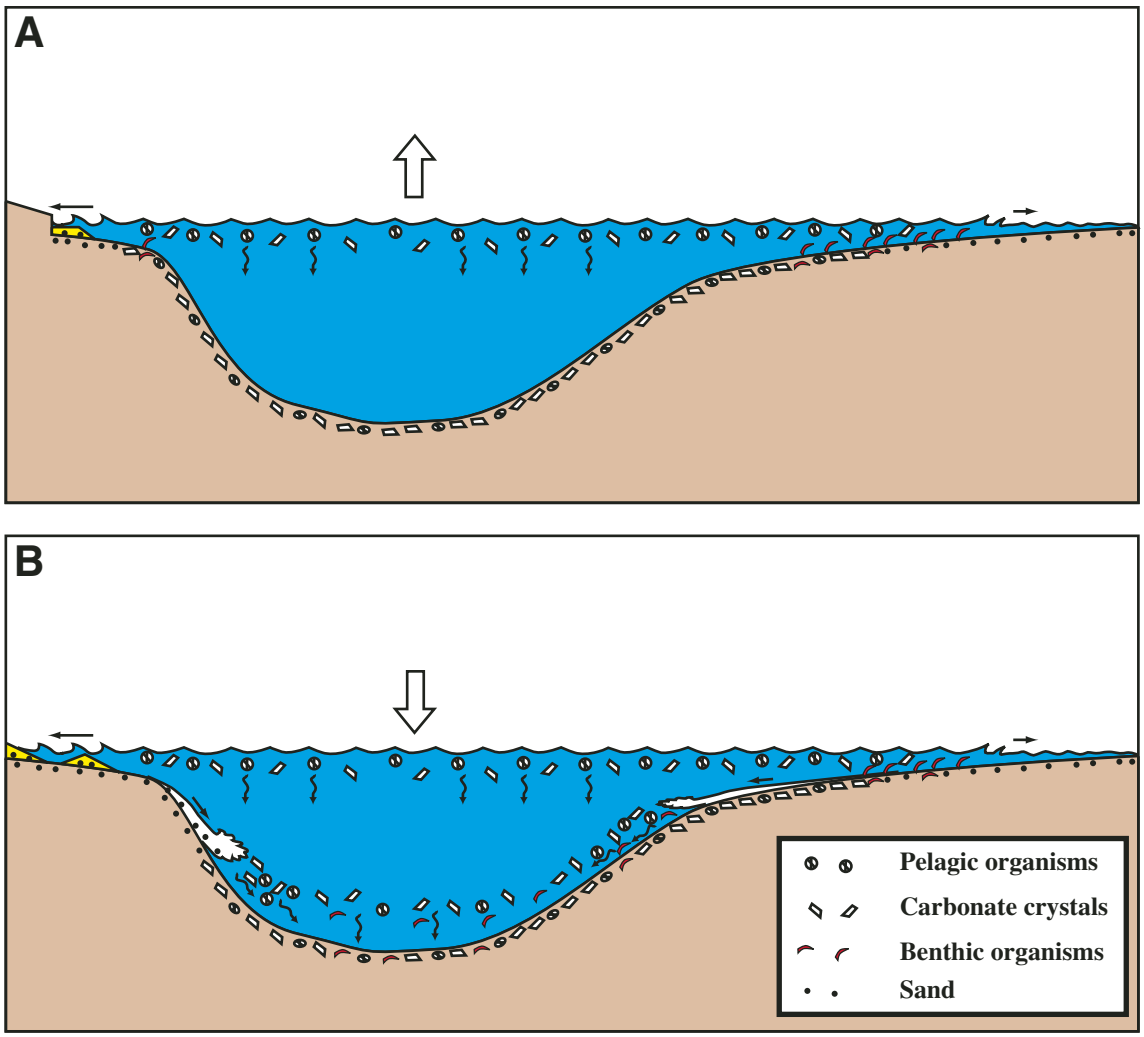

Figure 2. Schematic illustration of modern sedimentation in Bear Lake. (A) Rising lake level. Aragonite precipitation and pelagic organisms dominate deeper water and benthic organisms are mostly restricted to shallow water. Shoreline cuts into older deposits, particularly on margins with steep bottom slopes. (B) Falling lake level. Sediment focusing through wave transport and gravity flows is mixed with aragonite precipitation and biogenic sedimentation in deep water. Shoreline deposits build out into lake.

presented schematically in Figures 3–6. The details about sedimentary designations and sedimentary features are provided in the following sections. The text is organized to describe first the Holocene record from the cores and the trenches, and then the more poorly constrained late Pleistocene core record from 32 ka. The conditions that produced the assemblage of sedimentary features in the different settings and time periods are discussed following their descriptions.

MODERN AND HOLOCENE SEDIMENTS

The Holocene sediments deposited prior to diversion of Bear River into Bear Lake are dominated by aragonite. Calcite is the dominant mineral in sediment formed after diversion of the river, and in sediments deposited during a short interval in the early Holocene (Dean et al., 2006). Holocene and modern marsh deposits north of the lake largely consist of a mixture of calcite and siliciclastic clay and silt.

Deep-Water Aragonite Deposits

The variability of Holocene deep-water aragonite sediments is best illustrated in core BL96-1 (Fig. 3). Although the modern calcite-rich sediments are missing, the core contains a sedimentary record from ca. 7500 yr B.P. to less than 1000 yr B.P. (Colman et al., this volume). The sediments are uniformly fine grained and obvious layering is absent. Subtle changes in the sediment texture are discernable, as are variations in the bioturbation patterns, particularly in X-radiographs. The aragonitic sediments in core BL96-1 are divided into three varieties that are gradational in character.

Aragonite Type I

This type of sediment is characterized by centimeter-scale alternation of smooth tan mud and more poorly sorted tan mud with silt-sized black grains (Fig. 7). Random burrows with diameters ranging from 0.3 cm to 0.5 cm disrupt the poorly sorted intervals. These intervals are also less dense than the smooth intervals in X-radiographs. The smooth tan intervals typically have smaller (less than 0.2 cm) burrows that are mostly oriented parallel to the bedding surface (Fig. 8). Smear slides show a subtle contrast between the smooth and poorly sorted intervals (Fig. 9). Aragonite needles with a small range of crystal sizes (2–5 μm) dominate the smooth intervals, whereas the poorly sorted intervals include a variety of aragonite crystal sizes and shapes, as well as a significant component of calcite crystals and grain aggregates. Smear slides of smooth intervals also show that diatoms are dominated by one or two species, particularly *Navicula oblonga* and *Cymbella messiana*, whereas the poorly sorted layers also contain notable increases of a wider variety of diatom genera. A variation in the bioturbation is limited to the upper 40 cm of BL96-1 and coeval intervals in other cores. Random burrows have diameters as much as 1 cm and show dense outer rims in X-radiographs. Another variation within mud assigned to Aragonite I includes scattered coarse-silt- to sand-sized ostracodes in the poorly sorted intervals.

Aragonite Type II

This type of sediment is generally finer grained than Type I and characteristically has alternations of tan mud with no readily visible structure and tan mud with dark tubes (Fig. 10). The dark tubes are burrows 1–3 mm in diameter. The dark color is due to the presence of sulfide minerals that either line the burrows (Fig. 11) or are distributed in the sedimentary fill of the burrows. The burrows are typically oriented parallel to the bedding surface in the lower part of a dark tube interval and become larger and more randomly oriented toward the top of an interval (Fig. 11). The tan mud intervals that lack dark tubes have small (~1 mm in diameter) bedding-parallel burrows and the intervals are slightly denser in X-radiographs than the aragonite mud with dark tubes. Smear slides show mixtures of variously sized aragonite needles and some calcite aggregates in both sediment types, and a mixed assemblage of diatoms (Fig. 12). The intervals without dark tubes have a larger percentage of small pelagic diatoms, such as *Stephanodiscus* and *Cyclotella*, than the intervals with dark tubes. In contrast, the dark-tube intervals have a greater variety of diatom types, particularly the larger diatoms such as *Navicula oblonga* and *Cymbella mesiana*. The intervals with dark tubes also have a greater variety of aragonite crystal sizes and more calcite than the intervals without dark tubes. The dark-tube intervals are transitional in character to the poorly sorted intervals in Aragonite I.

Aragonite Type III

This type of sediment is characterized by yellowish silty to sandy mud alternating with tan mud (Fig. 13). The tan mud intervals are, in places, similar to the smooth tan mud of Aragonite I, and in other places resemble the poorly sorted mud of Type I aragonite or dark-tube intervals of Type II aragonites. In all occurrences, silt- to sand-sized ostracodes are a common component. In places, the contact of the yellowish silty interval with an underlying tan mud is very sharp with a concentration of sand grains. Random burrows (0.3–0.5 cm in diameter) occur throughout the yellowish intervals and sand-filled burrows extend from the sharp contacts into the underlying tan mud layers (Fig. 14). Small horizontal burrows are common in the denser tan mud layers. The yellowish silty intervals contain coarse silt- to sand-sized siliciclastic grains, rock fragments, and ostracodes in addition to a mixture of different aragonite crystals and calcite (Fig. 15). Diatoms in the silty intervals are characteristically fragmented and generally poorly preserved. The poorly sorted intervals of Type I aragonite that contain ostracodes could be reassigned to Type III aragonite, but the matrix is less silty and the diatoms are less fragmentary than is typical for Type III aragonite.

Interpretations

The relative grain sizes of each aragonite type and their distribution in the cores (Figs. 3, 4, and 5) suggest that Type II aragonite

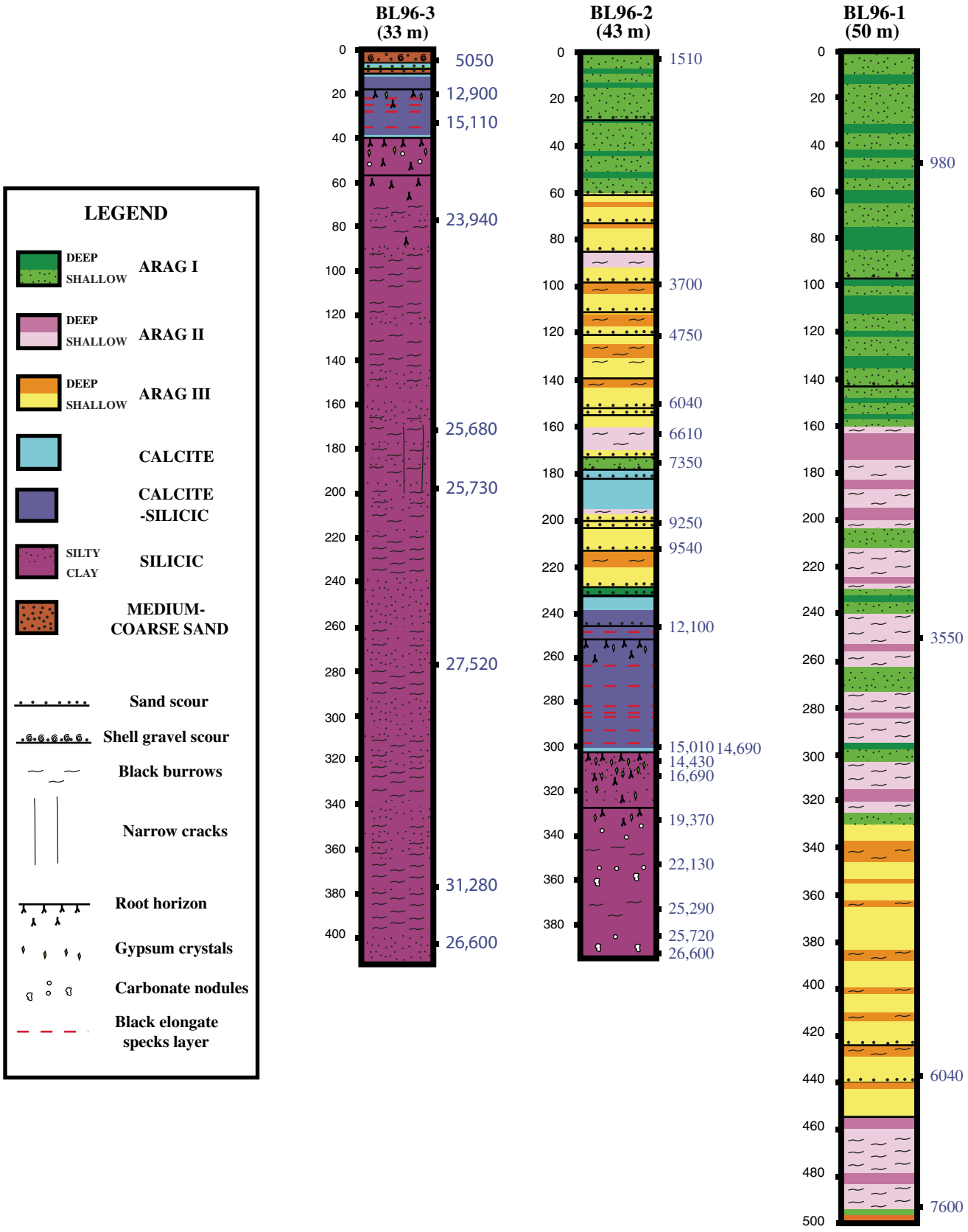

Figure 3. Schematic illustration of sediment types and sedimentary structures in the three Kullenburg cores whose locations are shown in Figure 1. Blue numbers are ages in calendar years derived from radiocarbon ages of pollen separates (Colman et al., this volume). Scales are in centimeters below the surface. Water depths of the coring sites (in parentheses below the core locations) are corrected to the modern highstand level (1805.5 m elevation).

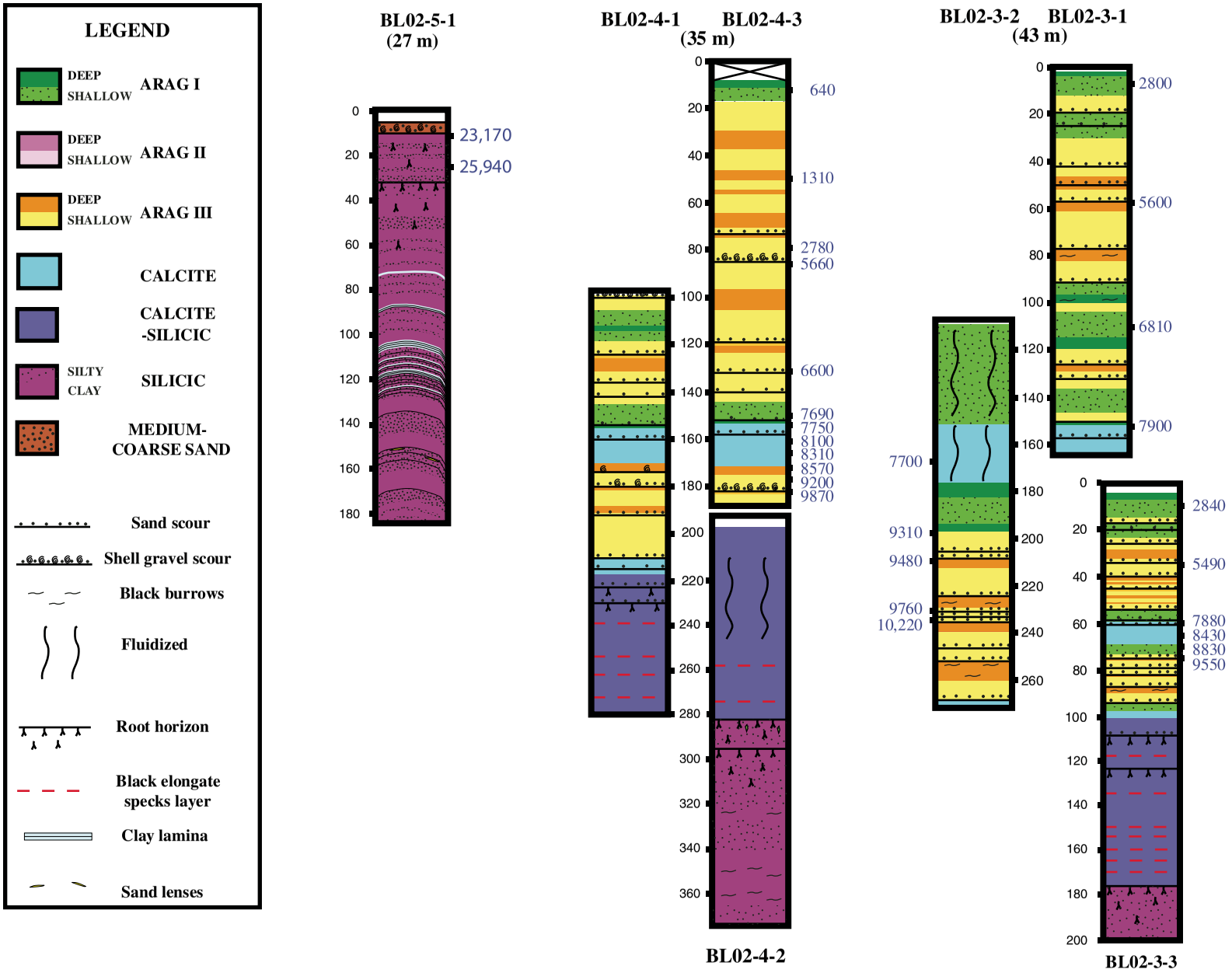

Figure 4. Schematic illustration of sediment types and sedimentary structures in UWITEC cores at deep-water sites (see Fig. 1). Scales are in centimeters and include composite depths of multiple cores. Blue numbers are ages as described in Figure 3. Water depths of the coring sites (in parentheses below the core locations) are corrected as described in Figure 3.

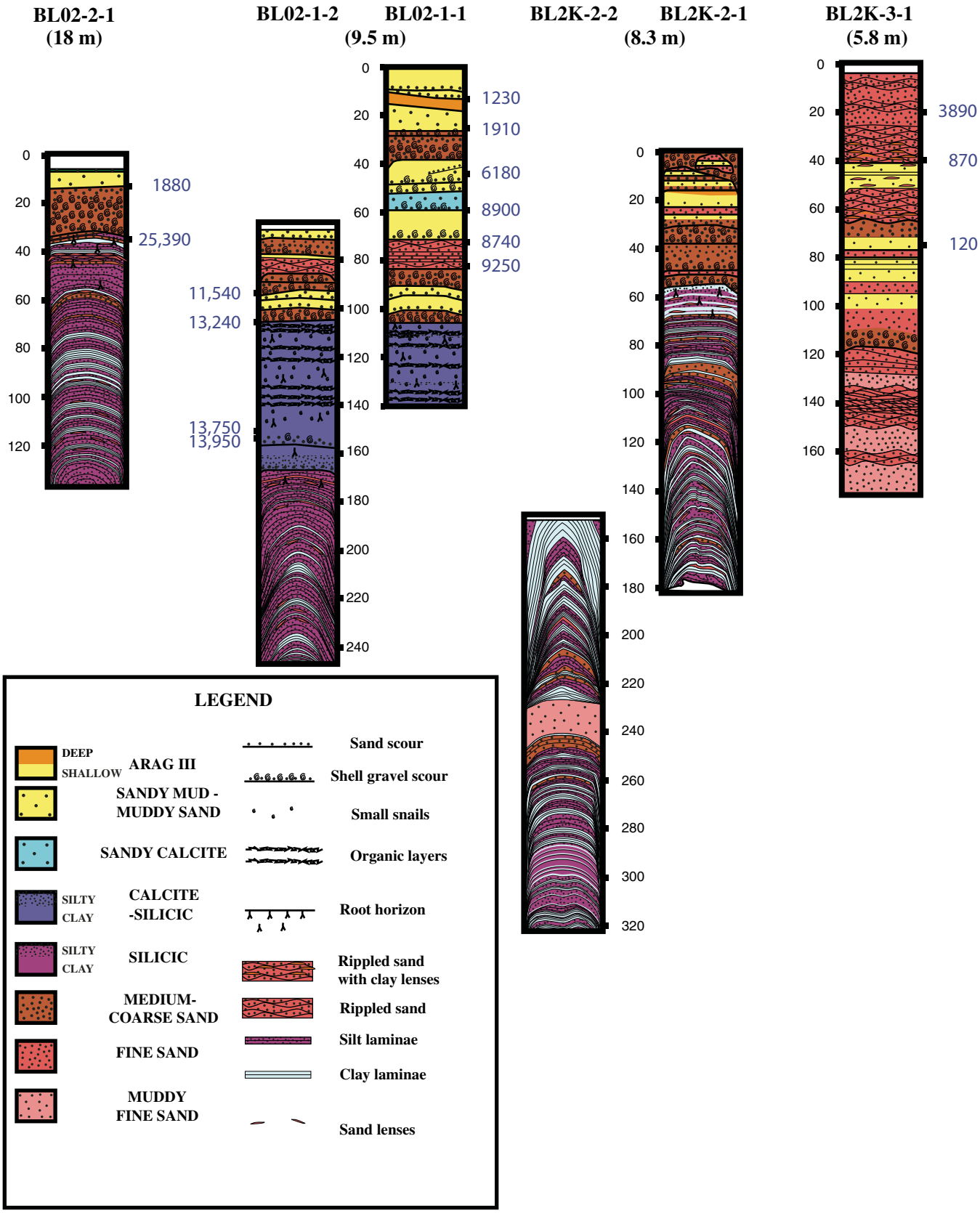

Figure 5. Schematic illustration of sediment types and sedimentary structures in UWITEC cores at shallow-water sites (see Fig. 1). Scales are in centimeters and include composite depths of multiple cores. Blue numbers are ages as described in Figure 3. Water depths of the coring sites (in parentheses below the core locations) are corrected as described in Figure 3.

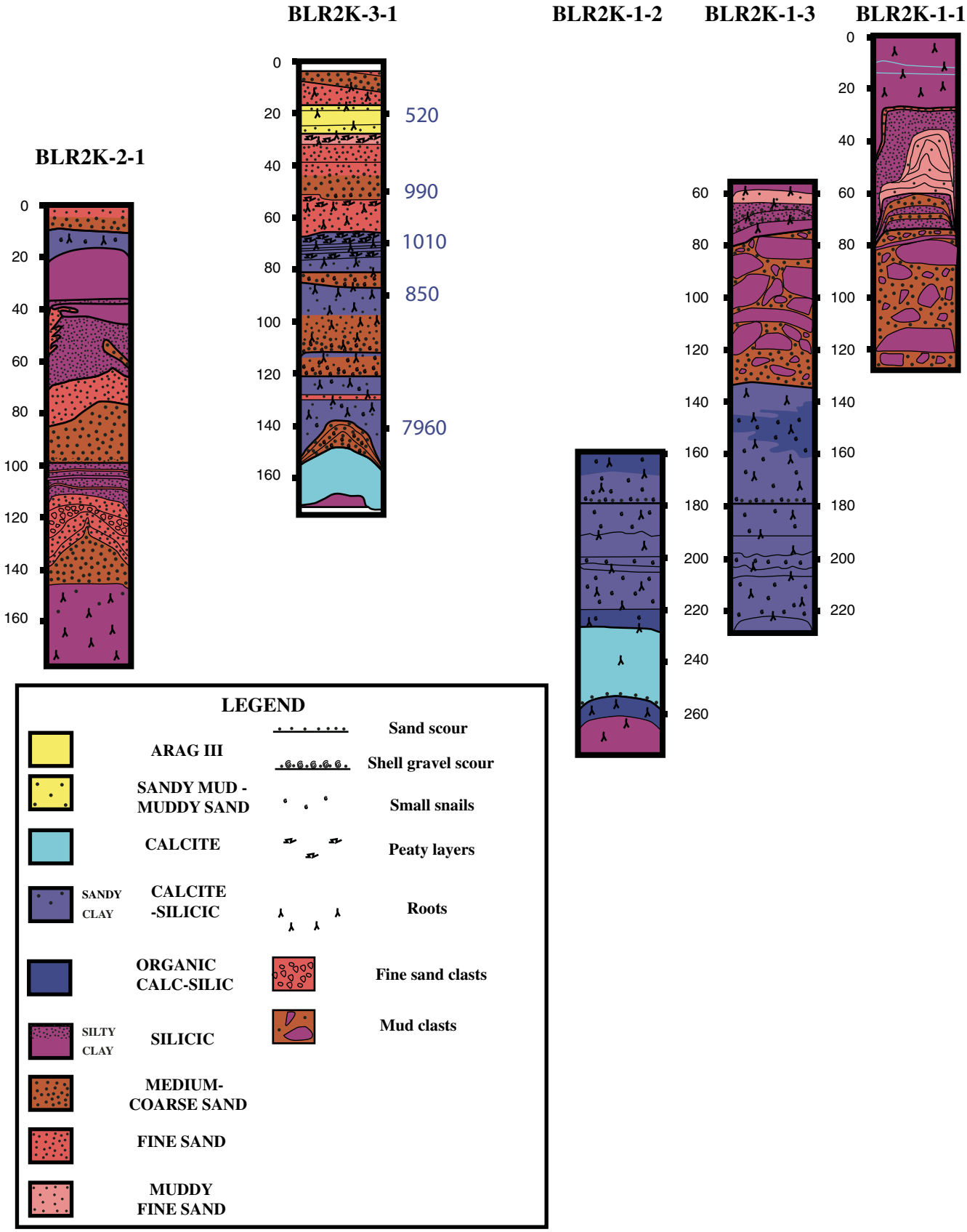

Figure 6. Schematic illustration of sediment types and sedimentary structures in UWITEC cores north of Bear Lake (see Fig. 1). Scales are in centimeters and include composite depths of multiple cores. Blue numbers are ages as described in Figure 3. Water depths of the coring sites (in parentheses below the core locations) are corrected as described in Figure 3.

represents the deepest water conditions and Type III aragonite represents the shallowest. Type I aragonite is found in the upper part of BL02-4 (35 m water depth), indicating that it formed at that depth in the pre-canal historical lake. Type III aragonite at the top of BL02-1 (9.5 m water depth) is less than 1000 yr old, and was probably deposited in the historical, pre-canal lake at similar depths. The abundance of broken diatoms in Type III aragonite is probably due to reworking by waves. Type II aragonite was not observed in any cores with historical-age deposits. The small pelagic diatoms in the Type II aragonite without dark tubes include *Stephanodiscus medius*, which is an indicator of cool fresh water (Moser and Kimball, this volume). Part of the overall

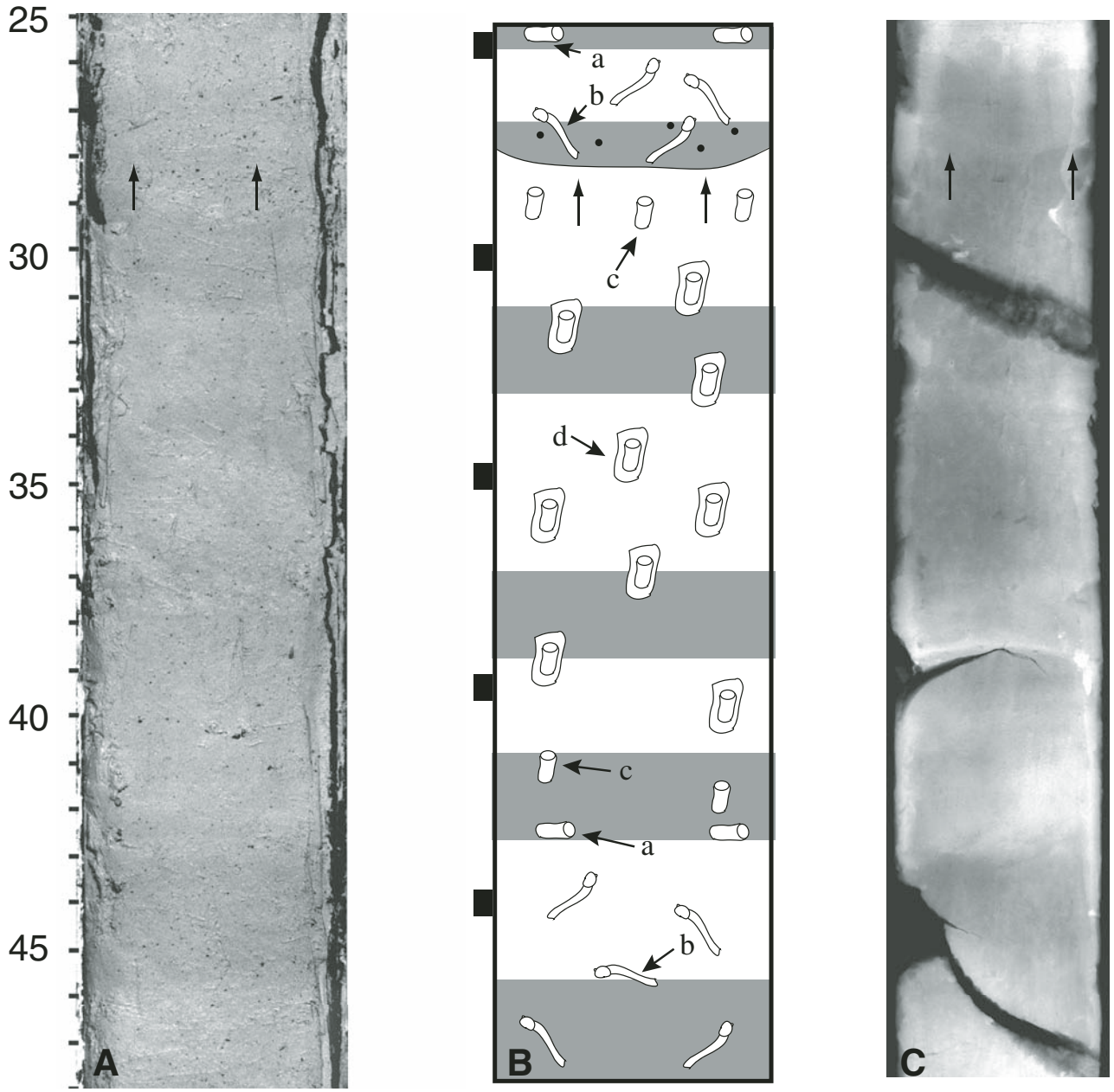

Figure 7. Aragonite I showing core segment on cut surface (A), schematic drawing of X-radiograph image (B), and X-radiograph (C) of BL96-2. The smooth tan intervals appear as denser (lighter) intervals in the X-radiograph (C) and poorly sorted intervals are less dense (darker). High-density intervals are shaded in B. Arrows point to scour surface filled with sand composed mostly of ostracodes. The features shown in B (not to scale) are small horizontal burrows (a), large random burrows (b), small random burrows (c), and random burrows with dense rims (d). Some of the density differences in C are due to irregularities in the sample thickness. The cut-surface photo was digitally enhanced to contrast the layers. Scales are in centimeters. The X-radiograph scale (B and C) differs slightly from the core (A) due to differential shrinkage from drying.

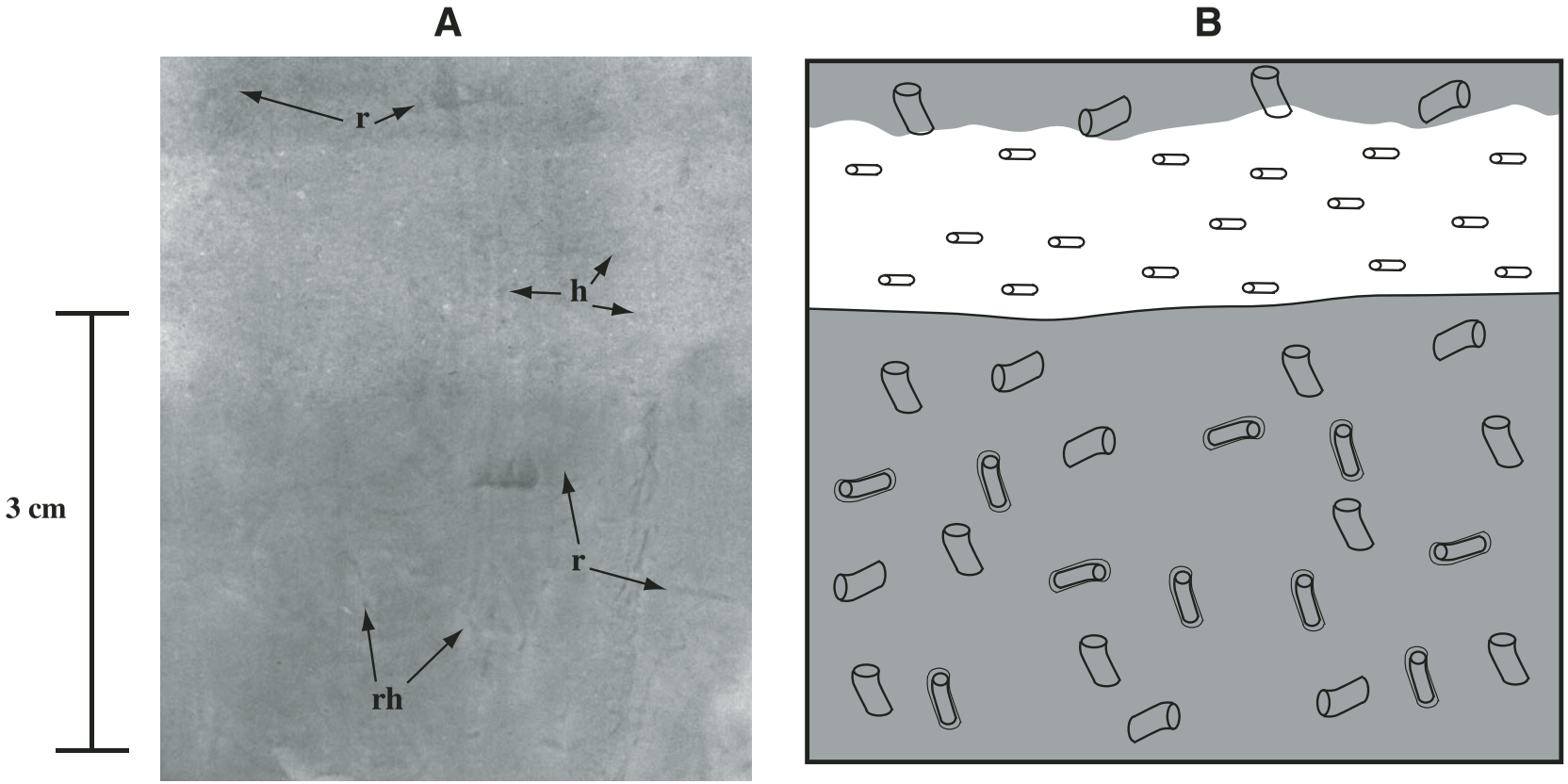

Figure 8. Aragonite I in BL96-1 showing detail of bioturbation patterns in X-radiograph (A) and schematic drawing (B). The denser (lighter) fine-grained interval contains small horizontal burrows (h). The less dense (darker), poorly sorted interval contains random burrows (r). Some random burrows have a denser outer rim (rh). The schematic depiction of sedimentary features does not show them to scale.

finer grain size in comparison to Type I aragonite is the relative dearth of the larger diatoms rather than a finer aragonite crystal size. It is possible that Aragonite II may represent a shift in lake temperature and/or salinity rather than a greater depth than Aragonite I. The argument against this interpretation is that Type II aragonite is apparently age correlative to Type I aragonite in cores from shallower water (Smoot and Rosenbaum, this volume).

The alternations of layers with relatively more and less mixing of diatoms and different mineral types and sizes is interpreted as indicating different degrees of sediment focusing. At Pyramid Lake (Smoot, 2003; Smoot and Benson, 2004), sediment focusing increases during falling lake levels. By analogy, rising lake levels would show less evidence of sediment focusing, particularly in deeper water, accounting for the

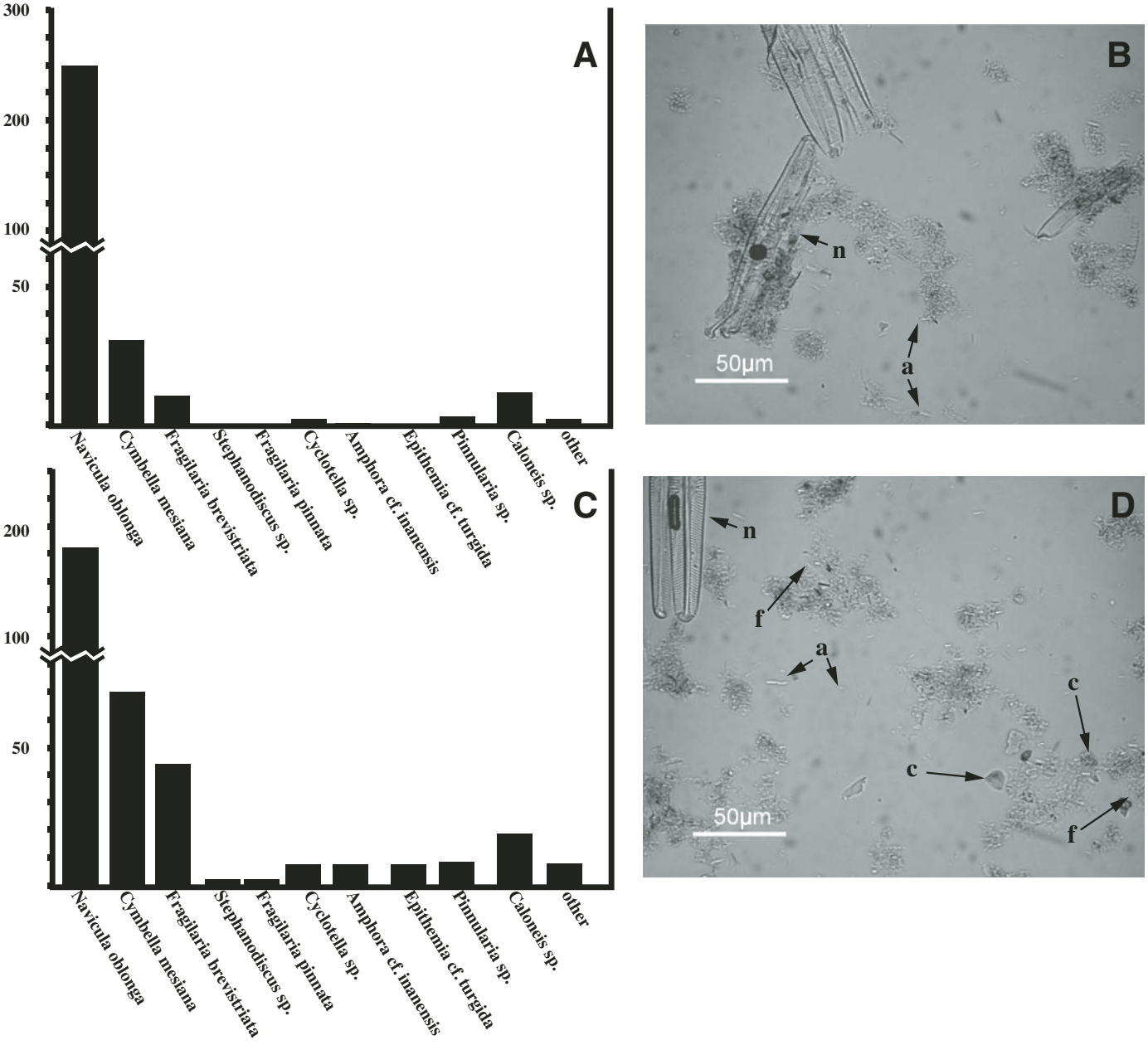

Figure 9. Aragonite I showing comparison of diatom count for a smear slide in a smooth tan interval (A and B) to that for a poorly sorted interval (C and D) in BL96-1. The smooth interval smear slides are dominated by one or two diatom species (A). The smear slide (B) shows *Navicula oblonga* (n) and 2–5 µm aragonite needles (a). The grainy intervals have more diverse diatom assemblages (C). The smear slide (D) shows *Navicula oblonga* (n) plus *Fragilaria brevistriata* (f) and calcite crystals (c) mixed with 2–20 µm aragonite needles (a). Note the compression of graphs and change of scale for counts over 100.

simpler mineralogies and diatom assemblages. The pronounced grading of some layers in Type III aragonite is consistent with deposition by turbidity currents. The variation in burrow styles in Type I and Type II aragonites is coincident with this shift in sediment focusing. The limitation of burrows to bedding planes may reflect an oxygen deficit (as in Smoot and Benson, 1998), whereas random burrowing represents a more oxygen-rich lake floor. Another possibility is that the substrate controlled the burrow style, with more random burrowing occurring in coarser sediment. The dark burrows in Type II aragonite may indicate more oxygen depletion than in Type I or Type III aragonite, or they may reflect a different organism that provided an organic

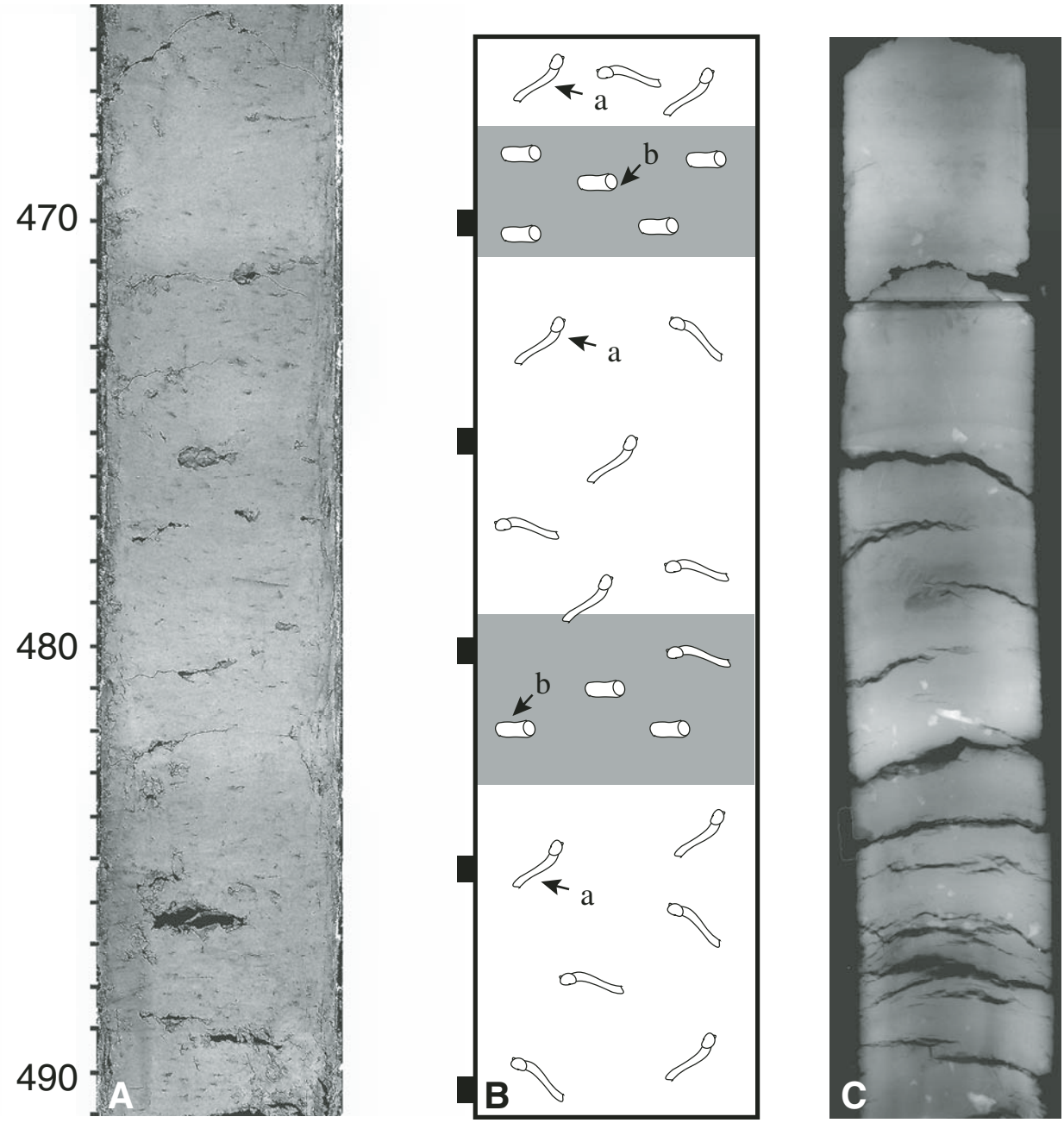

Figure 10. Aragonite II showing core segment cut surface (A), schematic drawing of X-radiograph image (B), and X-radiograph (C) of BL96-1. Random burrows (a) dominate intervals with dark tubes. These intervals are slightly less dense (darker) in C. Intervals without dark tubes are dominated by small, horizontal burrows (b). These intervals are denser (lighter) in C and shaded in B. Sedimentary features schematically shown in B are not to scale. Some of the density differences in C are due to variations in sample thickness. The cut-surface photo was digitally enhanced to contrast the layers. Scales are in centimeters. The X-radiograph scale (B and C) differs slightly from the core (A) due to differential shrinkage from drying.

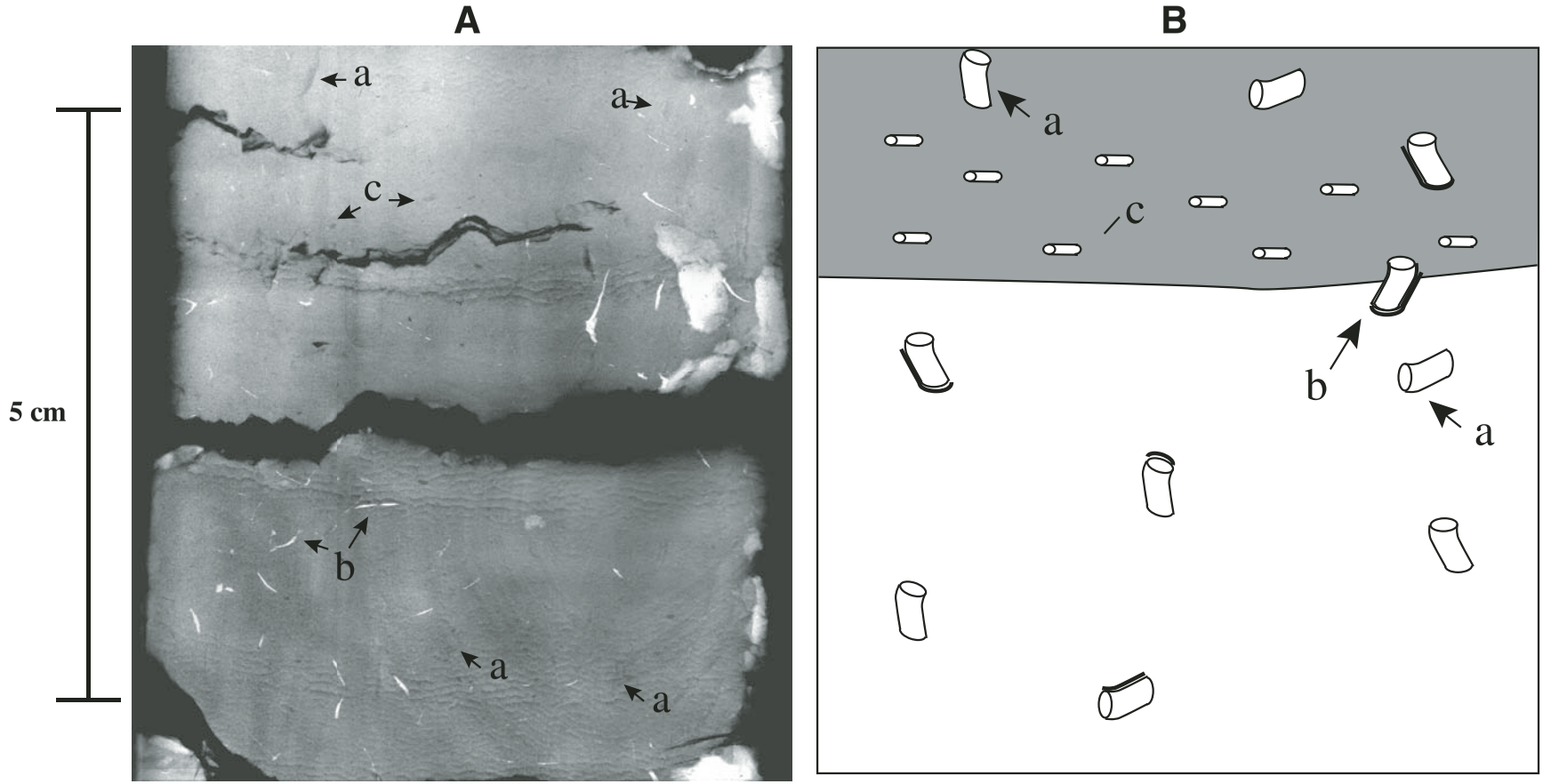

Figure 11. Aragonite II in BL96-1 showing detail of the bioturbation pattern in an X-radiograph (A) and schematic drawing (B). Sedimentary features in B are not drawn to scale. The dark-tube intervals are slightly less dense (darker in A) than the interval without dark tubes (light in A and shaded in B). The less dense intervals contain random burrows (a), some which have partial linings of sulfide minerals (b) that are very dense (white). The denser interval is dominated by small horizontal burrows (c), but some larger random burrows also occur.

substrate for sulfide precipitation (like a slime coating). The actual organisms that produced the burrows are not known. The limited literature on burrowing organisms in lakes does not provide sufficient criteria to recognize different types or even to differentiate between different burrowing strategies of the same type of organism.

Deep-Water Calcite Deposits

Gray mud dominated by euhedral to subhedral calcite crystals (2-10 µm) is found in the Holocene portion of cores BL96-2, BL96-3, BL02-3, BL02-4, and BL02-1. This layer is underlain and overlain by aragonite mud (Fig. 16). Radiocarbon ages are

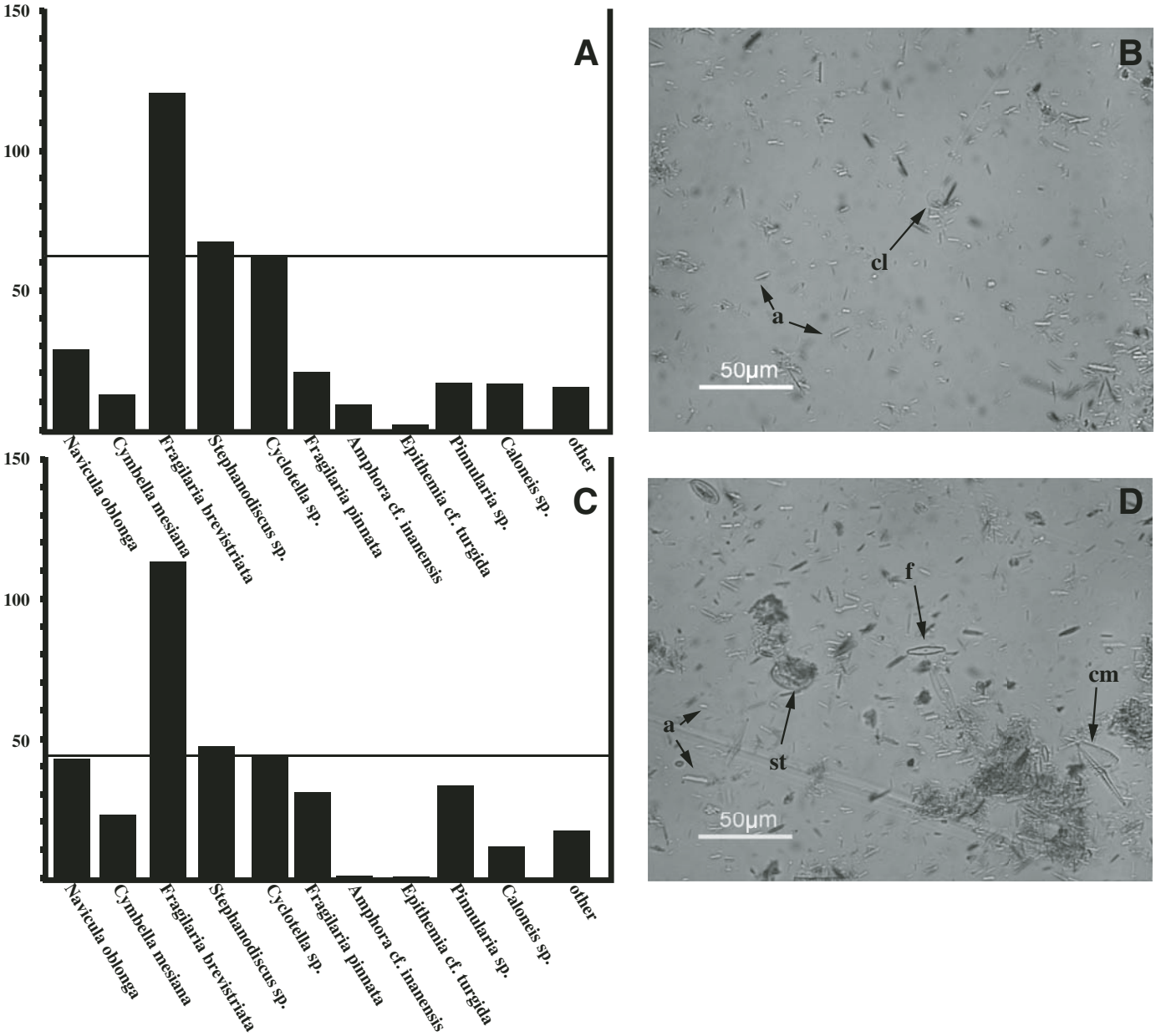

Figure 12. Aragonite II in BL96-1 showing comparison of diatom count for a dense interval without dark tubes (A and B) with that for an interval with dark tubes (C and D) of BL96-1. Both intervals show a variety of diatoms, although A has a higher percentage of small pelagic diatoms such as *Cyclotella* and *Stephanodiscus*, whereas in C, the small pelagic diatoms are mixed with nearly equal amounts of other diatoms such as *Navicula oblonga* and *Fragilaria pinnata*. Smear slide of the dense interval (B) shows variable aragonite crystal sizes (a) and the pelagic diatom *Cyclotella* (cl); compare this with the smear slide for a random burrow interval (D), which shows a wider range of aragonite crystal sizes (a) and a mixture of diatoms including *Stephanodiscus* (st), *Fragilaria brevistriata* (f), and *Cymbella mesiana* (cm).

consistent with the calcitic mud's representing the same lakewide sedimentation event. Cores BLR2K-1 and BLR2K-3 have similar beds that may also be correlative. In the cores from the deepest water (BL96-2, BL02-3, and BL02-4), the calcite-rich interval has a similar stratigraphy (Fig. 17). At the base, there is a 1- to 2-cm-thick bed that appears very dense in X-radiographs and contains small burrows (1–3 mm in diameter) that are oriented parallel to the bedding surface. Smear slides show this layer to be composed entirely of uniform euhedral calcite crystals and small planktonic diatoms (Fig. 18). This thin bed is overlain by 5–10 cm of more poorly sorted calcitic mud that has more randomly distributed burrows. Smear slides of this poorly sorted

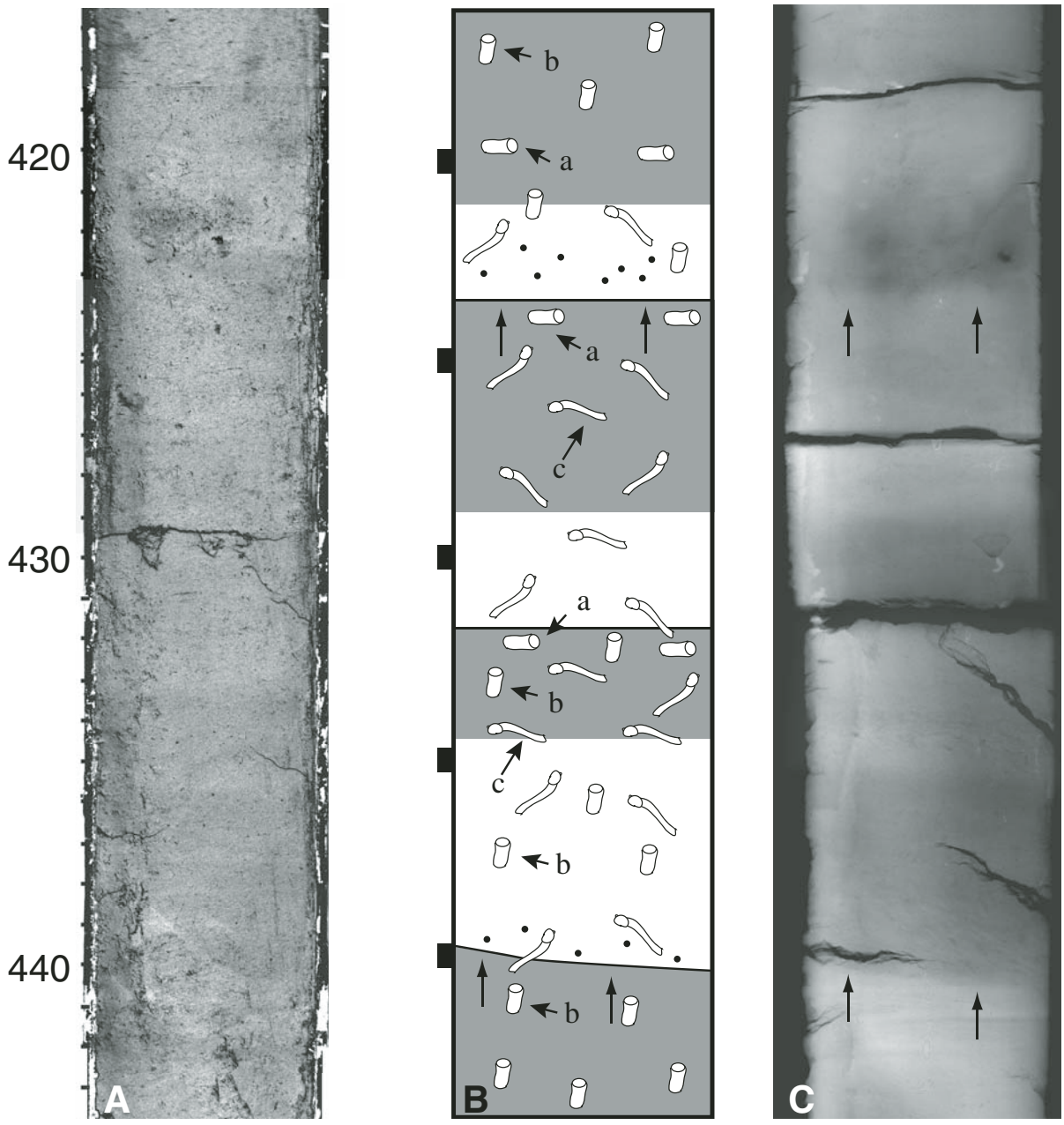

Figure 13. Aragonite III showing core segment in cut surface (A), schematic drawing of X-radiograph (B), and X-radiograph (C) of BL96-1. Sedimentary features in B are not drawn to scale. Coarse-grained intervals are less dense (dark) and have sharp, often irregular bases (vertical arrows). Burrows are less variable than in the other aragonite types but there are more small horizontal burrows (a) in the denser, finer-grained intervals (shaded in B). The coarser-grained interval contains random burrows including small, simple burrows (b) and larger more sinuous black burrows with high-density sulfide rims (c). Some of the density differences in C are due to irregularities in the sample thickness. The cut-surface photo was digitally enhanced to contrast the layers. Scales are in centimeters. The X-radiograph scale (B and C) differs slightly from the core (A) due to differential shrinkage from drying.

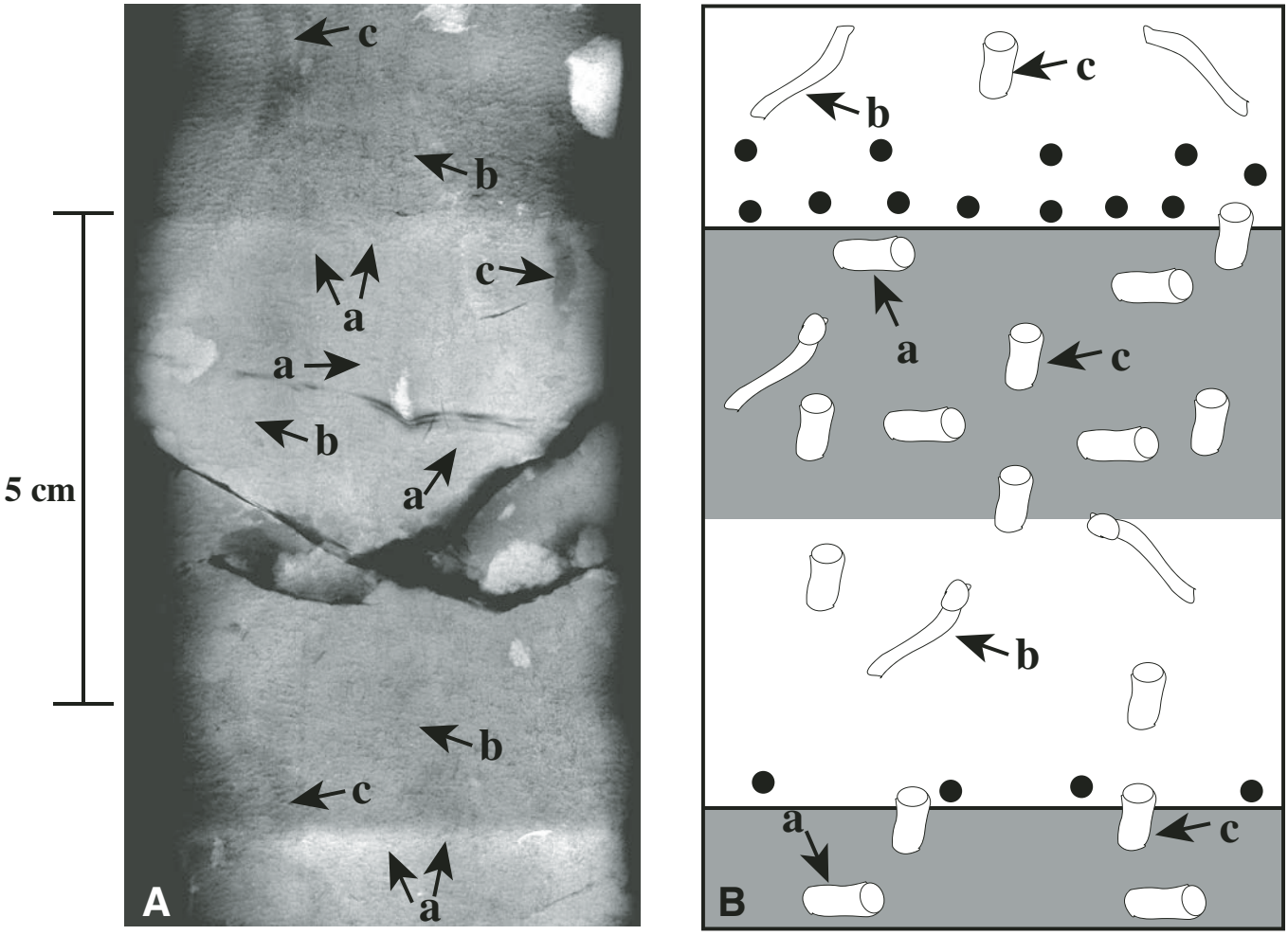

Figure 14. Aragonite III in BL96-2 showing detail of the bioturbation pattern in an X-radiograph (A) and a schematic drawing (B). Coarse-grained intervals (darker in A) have a sandy base overlying a sharp contact. Fine-grained intervals are denser (light in A and shaded in B) and have more abundant small, horizontal burrows (a). Random burrows cross all units and range from small, sinuous burrows (b) to large burrows (c).

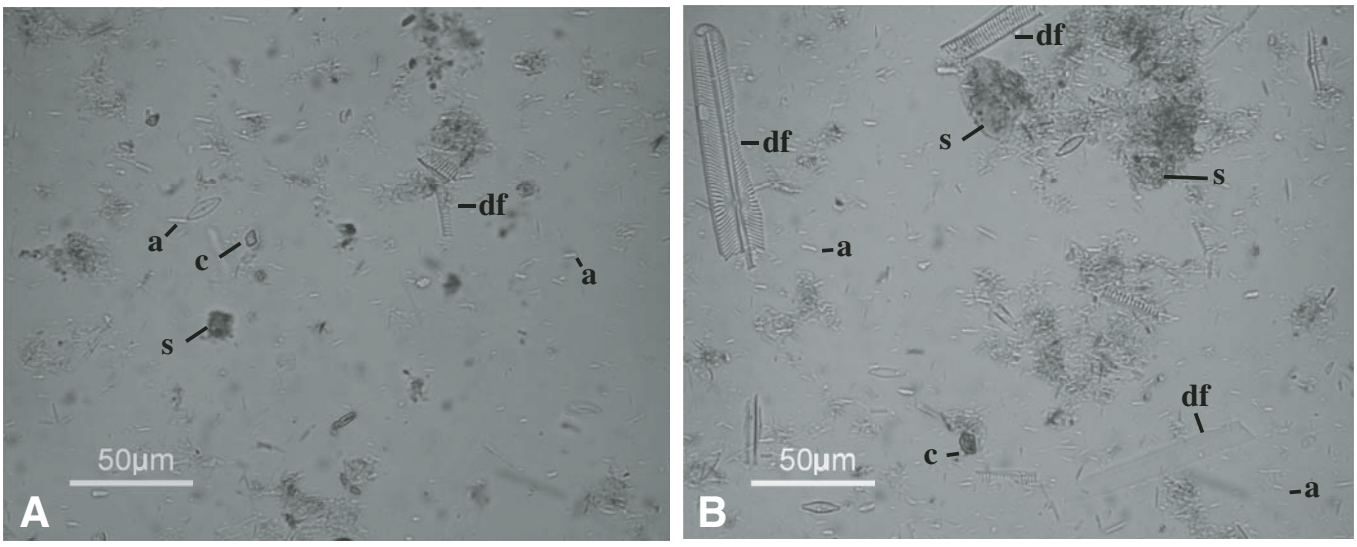

Figure 15. Aragonite III in BL96-1 showing comparison of smear slides from a fine-grained interval (A) and a coarse-grained interval (B). Both slides have a mixture of diatoms and a mixture of aragonite (a) and calcite (c). Diatom fragments (df) and silt-sized rock fragments (s) are present in both slides, but the abundance and size range in the coarse-grained interval (B) is much greater.

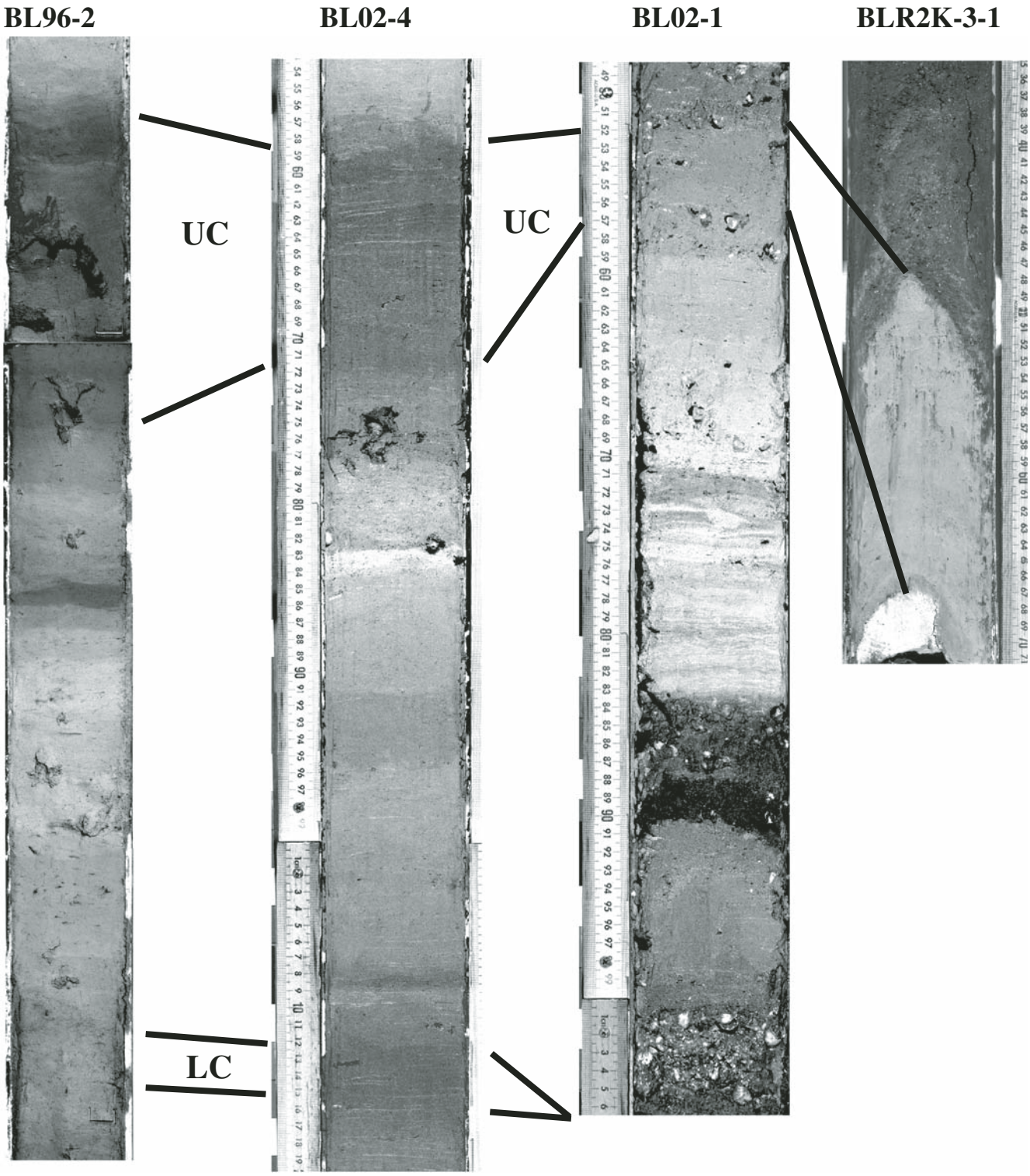

Figure 16. Correlation of four core segments containing Holocene deep-water calcite intervals (UC) from 43 m water depth (left), 34.9 m, 9.5 m, and Mud Lake (right). The calcite portions show only slight changes, whereas the underlying aragonite changes radically between the cores. A Pleistocene calcite layer (LC) underlies an aragonite interval in the deep-water cores. The calcite layer in the Mud Lake core overlies Pleistocene siliciclastic silt and is overlain by Holocene calcitic marsh deposits. The photos were enhanced digitally to contrast the layers. The scales are in centimeters.

unit show that the calcite also includes a mixture of rock fragments, scattered aragonite needles, and siliciclastic silt and that the diatoms include a number of shallow-water forms (Fig. 18). The mixed calcitic layer is sharply overlain by an ostracode-rich sand that is 1–2 cm thick. This sand is gradationally overlain by a mixed calcite and aragonite layer similar to the underlying one, but with more aragonite. Aragonite in this layer gradually increases upward to a poorly sorted Type I aragonite. In BL96-3 and BL02-1, the calcitic interval is thinner (1–5 cm thick) and is composed of calcite mixed with aragonite. These occurrences are rich in silt- to sand-sized ostracodes. The calcite-rich mud layers in BLR2K-1 and BLR2K-3 are 10–15 cm thick and dominated by euhedral calcite crystals and small planktonic diatoms. Silt- to sand-sized ostracodes are common at these locations and siliciclastic silt is an important component.

Applying the logic of the aragonite mud to calcite, the basal layer of calcite crystals represents a lake transgression. The rapid transition from aragonite to calcite is consistent with a major freshening of the lake. The remaining thickness of mixed calcite and aragonite represents sediment focusing in a falling lake before it changed to a strictly aragonite-precipitating lake. Geochemical data (Dean et al., 2006; Dean, this volume) indicate that the calcite layer precipitated in response to an influx of Bear River water. The occurrence of the calcitic layer north of Bear Lake in Mud Lake cores (Fig. 1) is consistent with a lake that extended well beyond the modern boundaries. The mixed calcite and aragonite probably does not represent the co-precipitation of these minerals, but rather the mixing of old aragonite with precipitated and reworked calcite as the lake level dropped. The ostracode-rich sand layer near the top of the calcitic layer is interpreted as indicating a drop in lake level. It could represent a lag deposit of storm wave activity, but was probably deposited as a wave-formed turbidite (as in Smoot and Benson, 1998, p. 140). The calcitic interval in the shallow-water localities is probably mostly reworked material representing the falling lake. The thicker calcitic interval in the cores within the marsh area

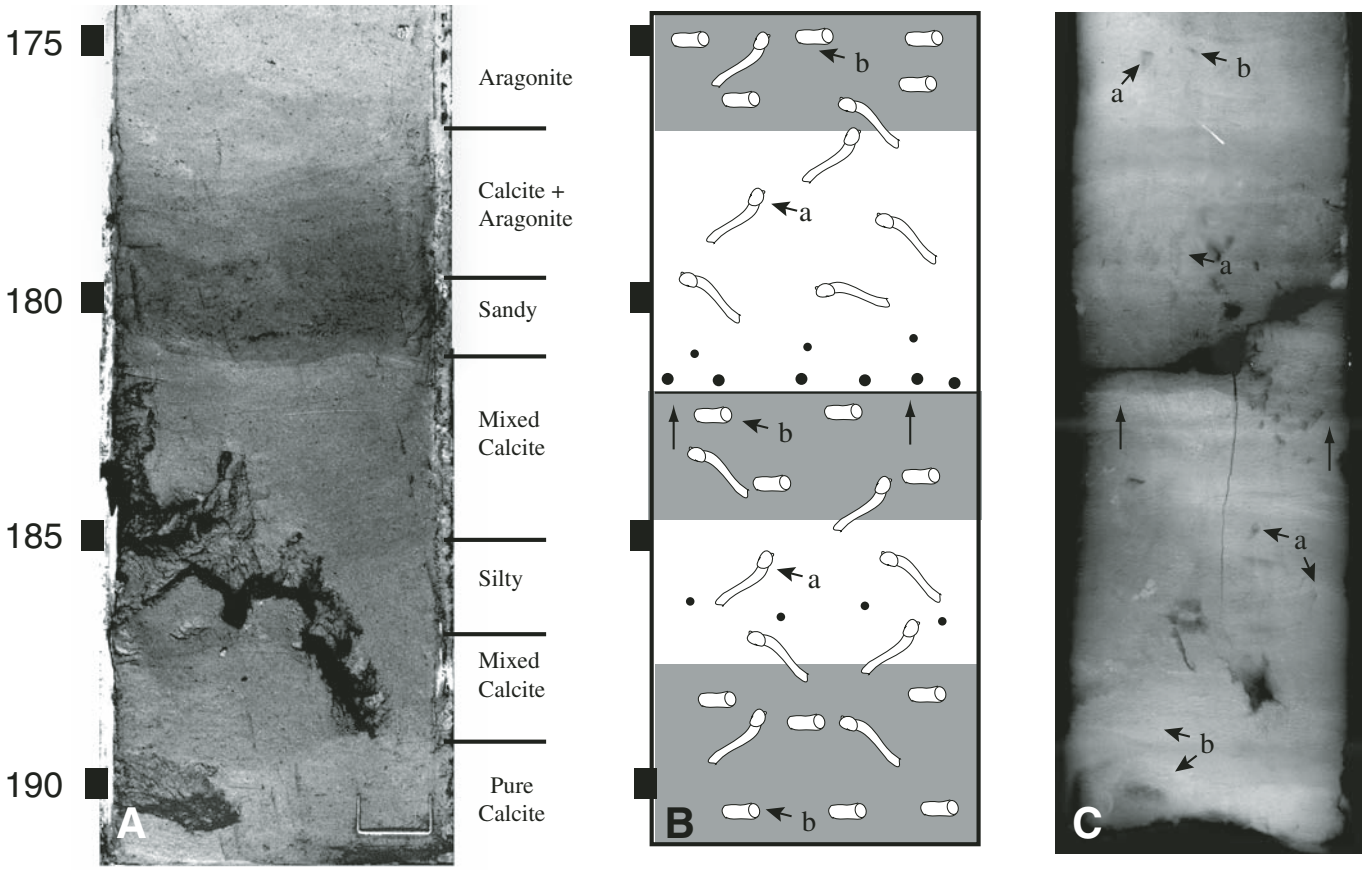

Figure 17. Deep-water calcite in core segment cut surface (A), schematic drawing of X-radiograph image (B), and X-radiograph (C) of BL96-2. Pure calcite is at base overlain by calcite mixed with minor aragonite. Silt-sized ostracode shells and rock fragments define a diffuse graded layer within the mixed interval. A sandy layer overlying a sharp surface (vertical arrows) separates sediment that is mostly calcite from sediment containing ~50% aragonite. The X-radiograph shows variations in sediment density (more dense is lighter) and pervasive bioturbation by random burrows (a). Small horizontal burrows (b) are abundant in the densest layers. Some of the density differences in C are due to variations in the sample thickness. The cut-surface photo was digitally enhanced to contrast the layers. Scales are in centimeters. The X-radiograph scale (B and C) differs slightly from the core (A) due to differential shrinkage from drying.

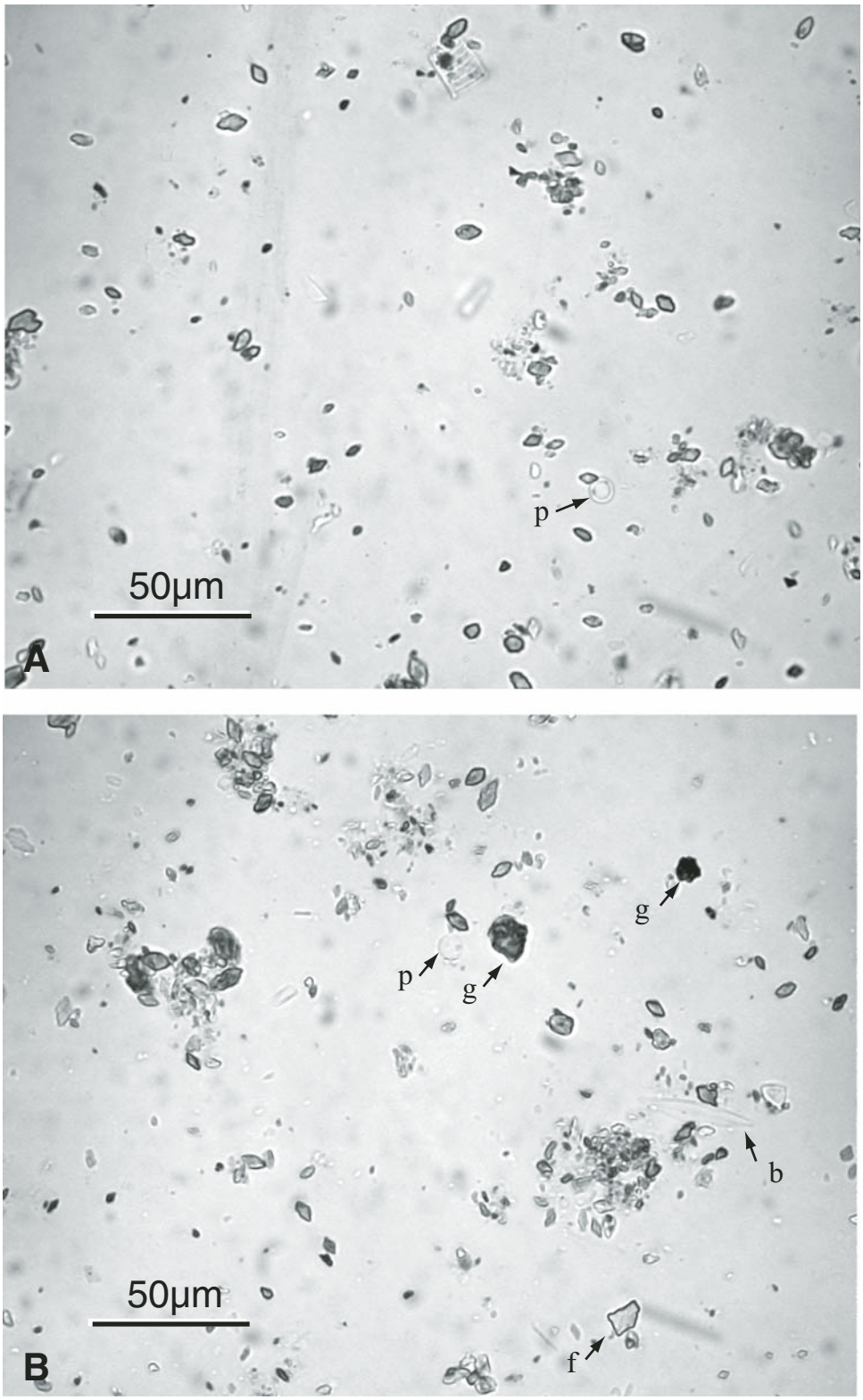

Figure 18. Deep-water calcite from BL96-2 showing comparison of pure calcite smear slide (A) with that of the silty mixed calcite (B). The pure calcite is composed of euhedral to subhedral calcite crystals and pelagic diatoms (p). The mixed calcite also contains benthic diatoms (b) and more irregular calcite composite grains (g) and calcite crystal fragments (f).

may indicate less erosion because the lake rapidly fell below that level, or the layer may have started thicker in that area due to mixing of detrital material closer to the mouth of the Bear River.

Shallow-Water and Shoreline Deposits

Cores taken in lake depths less than 35 m have sandy Holocene deposits that are generally less than 1 m thick (Figs. 3 and 5). These sediment thicknesses are consistent with the reflection profiles of Colman (2005, 2006), which illustrate a profound thinning of Holocene deposits at depths of less than 30 m. Modern shoreline deposits were examined from shallow trenches and short cores at different sites along the lake edge (Fig. 1), mostly during a prolonged drought in the summer of 2004. Three cores were also taken in the area north of Bear Lake (Fig. 1). Reheis et al. (2005, this volume) described 2–4 m thick sequences exposed along the Rainbow Canal north of the lake. They noted that Pleistocene deposits were mostly sand and gravel, but that Holocene deposits included peat, peaty mud, and the calcitic marl unit described earlier.

Bioturbated Sandy Mud and Muddy Sand

These are the most common deposits observed in cores and are transitional in character to Type III aragonite deposits. These deposits typically have vague layers or patches of different grain sizes with no distinct boundaries (Fig. 19). The sand component is commonly dominated by ostracode shells, particularly in cores taken in deeper water. In cores taken near the modern shoreline, the sand component may be dominated by siliciclastic sand. The patchy character includes well-defined burrow tubes as much as 1 cm in diameter. Bioturbated muddy sand with patches of plant debris and roots were observed in shallow cores along the northern shore of Bear Lake (see Fig. 23B in section on shoreline deposits) in less than 1 m of water. Such muddy sand is a common component of deposits in BL2K-1, -2, and -3, and BL02-1. Bioturbated sandy mud occurs in those cores, as well as in BL02-2 and BL96-3.

Bioturbated muddy sand and sandy mud represent variations on the same theme. Sediment transport was relatively infrequent, allowing organisms to homogenize the sediment, which therefore shows only vague bedding contacts. Differences in the sand-to-mud

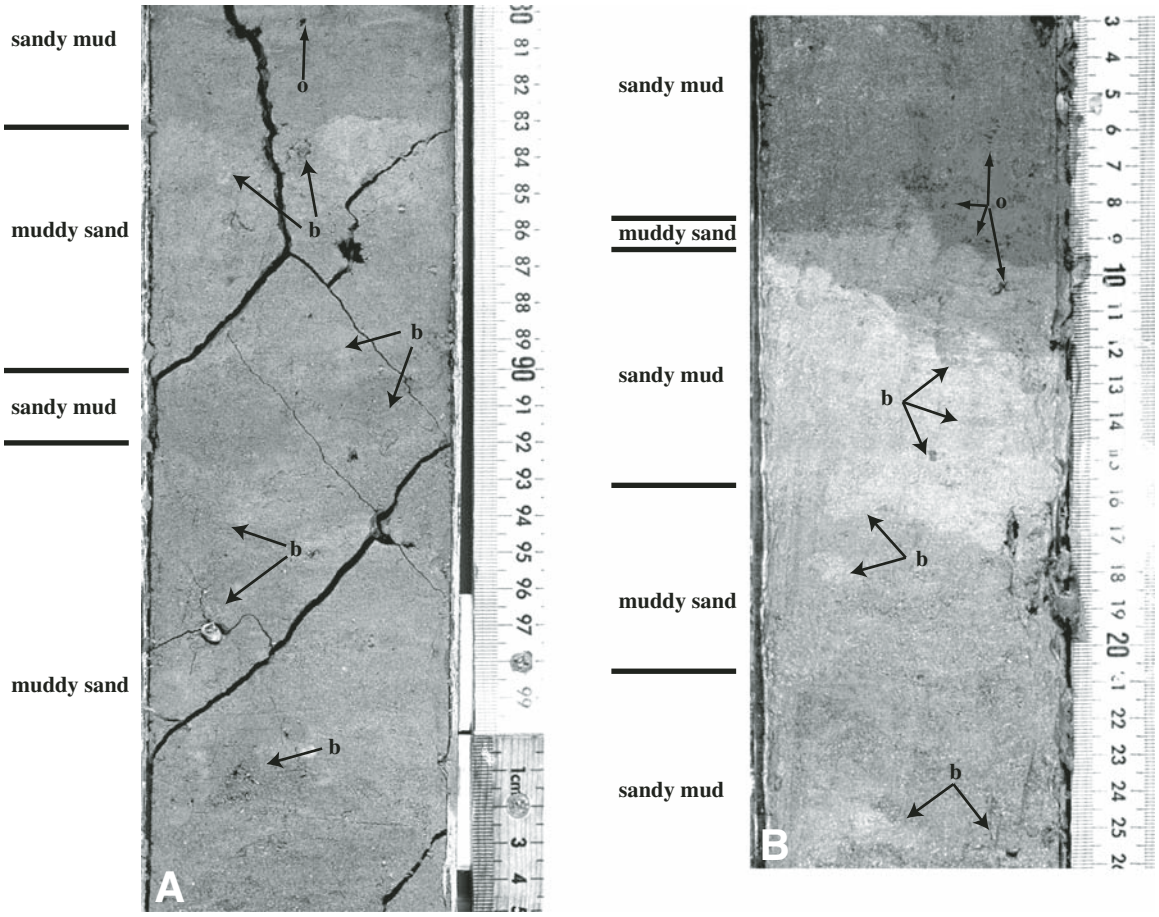

Figure 19. Shallow-water sandy mud and muddy sand in cores at BL2K-3-1 (A) and BL02-1 (B). Numerous burrows (b) homogenize the bedding including sand-mud contacts. Organic flecks (o) probably represent root hairs and fragments of aquatic plants. Scales are in centimeters.

ratio are interpreted as indicating the relative impact of winnowing of fine-grained material by wave action. Trenches and can cores from the north shore of the lake show abrupt transitions with muddy sediment beneath a surface veneer of sand or shell gravel. An abundance of sediment-filled burrows and open burrows within the upper 10 cm attests to the activity of worms and insects. Aquatic plants densely colonize the surface with small, hairlike holdfasts (e.g., Hutchinson, 1975), and their leaves provide dark organic material to the sediment. Terrestrial plants also occur less abundantly into water depths of several tens of centimeters, but are more common in areas that are subaerially exposed during lake fluctuations.

Rippled Sand Deposits

Where the lake-floor slope is relatively steep, oscillatory ripples are common in a few meters of water. These appear as well-defined sand lenses or sand layers with interspersed mud lenses. Sand lenses are characteristically well sorted and may be composed almost entirely of shells or shell fragments. Thin elongate lenses have flat bases and broad, rounded tops (Figs. 20 A and 20B), whereas thicker shorter lenses have more trough-shaped bases and steeper sides (Fig. 20C). Sand layers with mud lenses are actually superimposed sand lenses, each of which may comprise very different grain sizes, with a mud parting filling the troughs (Fig. 20B). These were observed in shallow can cores taken in less than 1 m of water on the west-central shore of the lake. The surface was composed of long-crested oscillatory ripples whose crests shifted with passing waves, but whose troughs were still and muddy. Ripple troughs may also be filled by coarser material such as shells that also form lenticular bodies (Fig. 21).

Sand lenses are formed by migration of wave-formed ripples on the lake floor. Thin, flat-bottomed, elongated lenses represent rolling-grain ripples which are the lowest-velocity bedforms produced by waves (see Harms et al., 1982, Chapter 2, p. 25–41). Thicker lenses with trough-shaped bases are produced by fully turbulent ripples under higher wave-bottom shear stress. The wave energy that produces the ripple deposits is intermittent and variable in strength. In areas where wave energy is felt only during the largest storms, isolated sand lenses in mud will form. These lenses will be preserved if the bottom bioturbation is insufficient to mix the radically different grain sizes. In areas where wind velocities are sufficient to cause wave sand movement frequently, beds composed of superimposed ripple lenses will form. Obviously, shallower water conditions favor this development as do steeper lake floors and long fetch distances. In transition to shorelines, wave-formed ripples may be erased by planar lamination during large storms or they may be intercalated with wave-formed bars (see below).

Shoreline Deposits

The modern shorelines around Bear Lake are mostly sandy deposits that are composed of a relatively narrow beach face and low-relief nearshore bars. Locally, these deposits are inset within wave-cut terraces eroded into older deposits mostly during lake-level rises. Where the lake floor has a very low slope in the northwest corner of the lake, the shoreline is a broad, flat expanse of shell gravel. Older shoreline deposits above the historical lake level include strandlines of boulders and cobbles.

On the northwestern corner of Bear Lake, the lake floor has a very low slope (Fig. 1), so shallow depths occur for kilometers away from the shoreline. Storm waves entering this part of the lake rapidly lose energy as they drag on the lake floor. Under these conditions, the shoreline deposits form very thin, shell-rich sheets (Fig. 22), reflecting the effect of bottom drag on all waves entering the area. The deposits observed in trenches were 10–20 cm thick and consisted mostly of snail shells at the base with coarse siliciclastic sand matrix grading upward to fine sand with scattered snail and clam shells (Fig. 23). These graded layers were traceable shoreward as a continuous sheet for kilometers. The sheet had a sharp base overlying bioturbated sandy mud and muddy sand. In the occurrences closer to the historical high-stand shoreline, the underlying mud had polygonal desiccation cracks filled with shelly sand. Graded shell beds that resemble these shoreline deposits were observed in several cores (Fig. 24) including BL2K-2, BL2K-3, BL02-1, BL02-2, and BL02-5. Two thin (3 cm) graded shell layers in BL02-4 may also be shoreline deposits, but they appear to be thinner and muddier. These deposits could represent storm wave deposits or wave-formed turbidite deposits farther offshore.

Sheet-like graded beds are formed on a shoreline by the rise and fall of lake level exposing large areas to wave action (Fig. 23A). On the very low slopes of the northwestern part of the lake, storm waves break kilometers from the edge of the lake. where they erode muddy sediment and concentrate coarse-grained material (mostly shells). Smaller waves can move closer to the shore, moving smaller grain sizes. Only mud and silt are moved at the actual water edge. The progressive landward loss of energy produces the characteristic graded bed. There is a hint of very low relief changes in gravel thickness over distances of tens of meters that could reflect a very low relief bar form. During falling lake levels, the wave sheets build lakeward, overlying bioturbated sandy mud (Fig. 23B). During rising lake levels, the gravel sheet may overlap previously mud-cracked mud (Fig. 23C).

The eastern side of Bear Lake has a steep transition from 40 to 50 m depth to the lake margin (Fig. 1), and the western side has a steep transition from 20 to 30 m deep to the lake margin. Under these conditions, storm waves impinge on the shoreline with much more energy than for the northwestern low-slope lake floor. The northeastern and southern ends of the lakes are transitional into low-slope shorelines as described above. The shoreline deposits adjacent to steep lake floors are thicker and more pronounced than the deposits formed adjacent to low slopes. These deposits consist of thinner sediment veneers over wave-cut terraces or thicker accumulations of bars and shoreface sand (Fig. 25).

Small wave-cut terraces are commonly overlain either by imbricated gravel or by lakeward-dipping tabular foresets. The imbricate gravel consists of coarser ridges (cobbles or boulders), with both lakeward and shoreward imbrication overlying finer

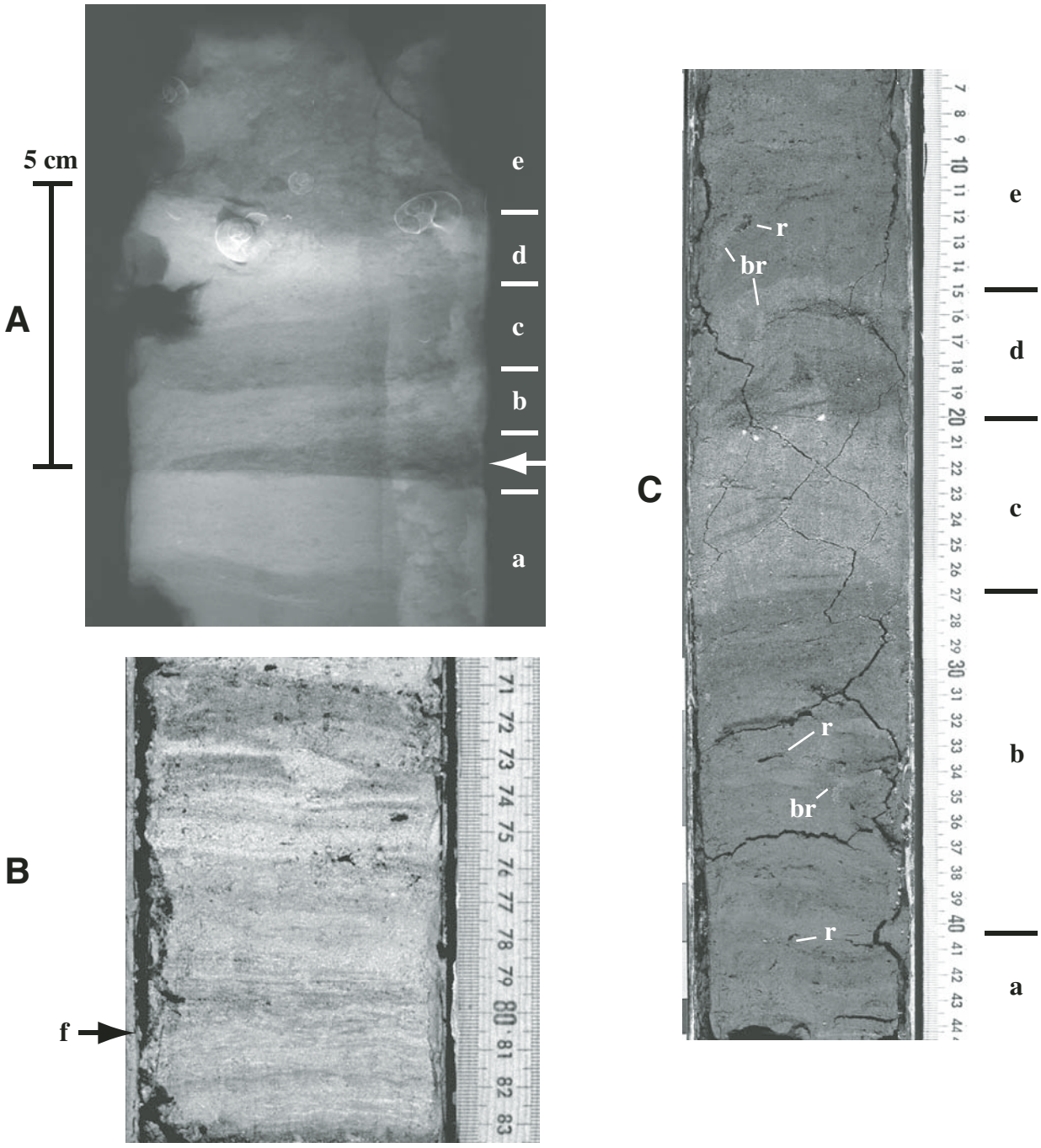

Figure 20. Wave-rippled deposits. (A) X-radiograph of top of BL96-3 showing convex-upward ripple lens of ostracode shells (arrow). The lens overlies bioturbated aragonite mud (a) and is draped with calcite mud (b). Graded aragonite sand (c) is overlain by sandy aragonite mud (d). Graded aragonite sand with snail shells at the base (e) is at the surface. (B) Quartz-rich fine sand (light) interbedded with aragonitic sandy mud (dark) in BL02-1. Wavy character is due to sand lenticularity reflecting rolling-grain ripples. Note mud lenses at ~80 cm (f) that were probably deposited in ripple troughs (flasers). (C) Ripple sequence in BL2K-3-1 consists of isolated very fine sand lenses in sandy mud (a), very fine sand with fine sand and muddy sand lenses (b), fine to medium sand with cross-lamination (c), fine sand with medium to coarse sand lenses (d), and muddy sand with fine sand lenses (e). Note burrows (br) and carbonaceous roots (r). Scales are in centimeters.

gravel with a shoreward imbrication. These produce steplike lenses perpendicular to the shore. The lakeward-dipping tabular sets may be sand, shelly sand, or gravel built over wave-rippled sand (Fig. 26). The foresets thicken lakeward from the erosional surface to as much as 30–40 cm.

Lakeward-dipping steep foresets are produced by waves piling up on shore and then sweeping sediment lakeward (Smoot and Lowenstein, 1997, p. 241–242). These are only produced on a small scale at Bear Lake, reflecting the generally shallow shoreline slopes and low sediment availability.

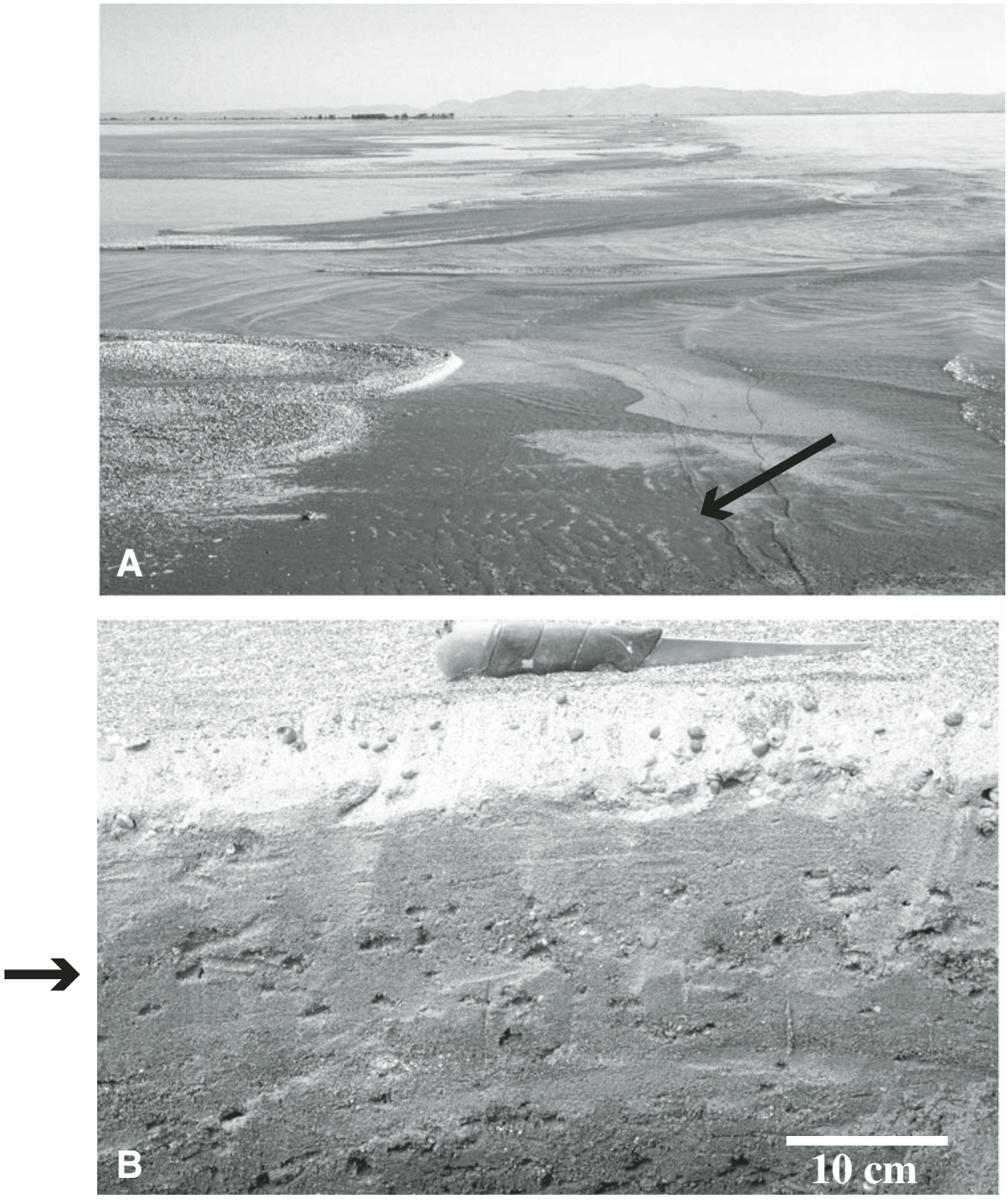

Figure 21. (A) View of shoreline at locality S7 showing wave-formed bars of coarse, shelly sand with ripples forming in shallow water in the foreground (arrow). Note the coarse material (light bands) trapped in the ripple troughs. The foreground of picture is ~2 m wide. (B) Cross section of rippled sand with coarse sand in the troughs (arrow) from a trench just shoreward of A.

Sandy beachfront deposits consist of sandy bars that have steep shoreward-dipping fronts and lower-angle lakeward dips that overlap at the lake edge into a ridge-and-furrow strandline. This type of deposit is generally thicker on the eastern side of the lake than on the western side. In cross section, the bars produce landward-dipping tabular foresets ranging in thickness from ~15 cm to over 50 cm. Each foreset bed is graded, with coarsest grain sizes at the base and progressively finer grain sizes toward the top. Adjacent beds vary in average grain size and composition. The foresets overlie wave-rippled sand deposits. The lakeward surface acts as a shoreface, accreting low-angle planar lamination that thickens gently lakeward where it grades into rippled sand (Fig. 27). The shoreface sands are generally finer grained than the bar foresets, but may include coarser layers or erosional insets of shoreward-dipping tabular sets 5–20 cm thick. The bar and shoreface deposits in broad beach areas are commonly modified by wind, which erodes sand from the crests and redeposits it into the troughs.

As surface waves impinge on shallower water, they become progressively more asymmetric with a stronger shoreward component. The offshore bars are composite bedforms produced by these asymmetric waves. The size and thickness depends upon the wave strength, water depth, and availability of sediment. Most of the coarse sediment in the modern Bear Lake is derived from reworking of older deposits. There is not much evidence for well-developed long-shore drift or influx of river-deposited sediment. The barforms are pushed shoreward during storms and then modified by lower-energy waves. Once a bar is pushed into shallow enough water, its back side becomes the surface for wave run-up and that side builds lakeward as a shoreface deposit.

Marsh Deposits

The cores taken in Mud Lake (Figs. 1 and 6) include sediments from the present-day shallow lake, and deposits formed when the area was a heavily vegetated swamp before completion

Figure 22. Gravel sheet at shoreline of locality S10. The bottom slope is very flat, with water depth remaining shallow for several hundred meters from shore. Snail shells and sand form a continuous layer for more than a kilometer inland. The picture foreground is ~2 m wide.

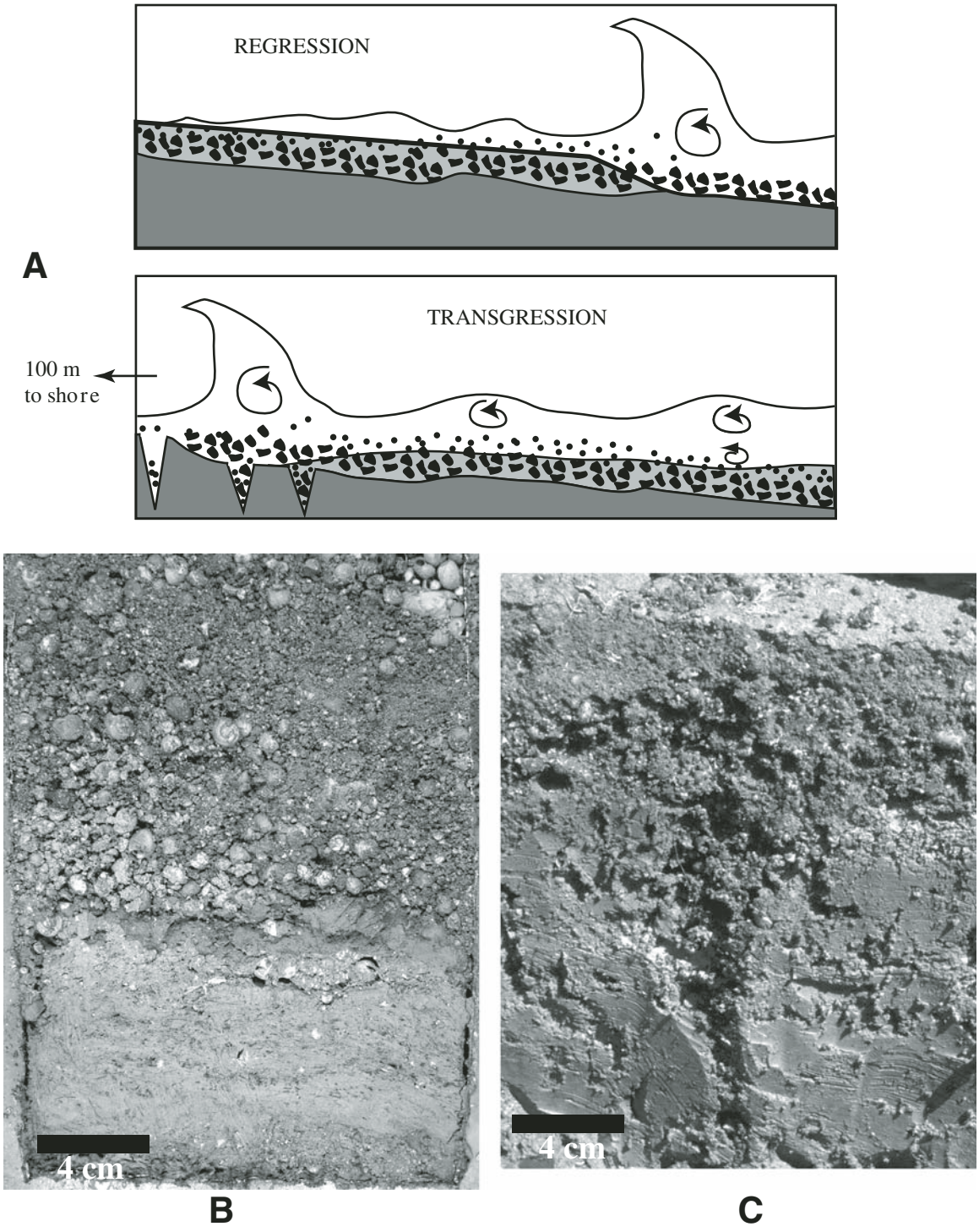

Figure 23. Cross sections through shoreline gravel sheet at locality S10. (A) Schematic drawing of how gravel sheets are formed during a dropping and rising lake level. Storm waves break hundreds of meters from shore, eroding the surface and depositing coarse sand and shells. Waves lose energy shoreward, depositing sand and mud. Transgression over previous subaerial deposits is initially fine grained then coarser. (B) Can core taken at modern shoreline showing graded shell gravel overlying burrowed sandy mud with small aquatic plant rootlets. (C) Trench in gravel sheet ~600 m shoreward showing graded shell gravel overlying sandy mud with desiccation cracks.

of the canals. A breccia composed of irregular mud clasts occurs 74 cm below the surface in a core taken near the canal (Fig. 28). The clasts reflect sedimentary units below the breccia in the same core. The sediment above the breccia is mostly a reddish sandy mud with abundant burrows and carbonaceous root casts. Thin sand layers are mostly siliciclastic sand. The mud includes a mixture of subhedral calcite crystals, with very few diatoms visible in the smear slides. Below the breccia, the mud is more organic rich and less siliciclastic. Diatoms are abundant, dominated by a mixture of attached diatoms (Moser and Kimball, this volume). Carbonized roots and plant fragments are locally abundant, in places making a muddy peat deposit. Shells and shell fragments, mostly small snails, are randomly scattered in the mud and concentrated into thin layers. Thin gray to tan layers are mostly calcite with a mixture of diatoms, charophyte fragments and oogonia, and silicate grains (Fig. 29). Sand beds with sharp bases contain mostly siliciclastic grains (Fig. 28), but also contain abundant shell fragments and snails. These beds are commonly graded, but are fairly well sorted into layers. There appears to be a loss of Holocene section in the areas closer to the barrier bar separating Mud Lake from Bear Lake. The sand beds also appear to be thicker and more common in that direction.

The pre-canal marsh environment was dominated by biological production and carbonate precipitation. Siliclastic material was probably introduced by floods from the mountain streams, windblown dust, and storm wash over the barrier ridge of northern Bear Lake. Storm wash would account for the apparent increase of sand layers in the southern cores and for the high sorting of those sands. The mud breccia in BLR2K-1 is interpreted as material dredged from the canal and dumped into the adjacent swamp. After construction of the canal, there was a source for muddy sediment from the Bear River. The muddy sequence in BLR2K-1 was above water level at the time of coring, but may be a local area of high sedimentation. The dearth of diatoms within the sediments supports the idea of high sedimentation rates. The aragonite layer in BLR2K-3 suggests that

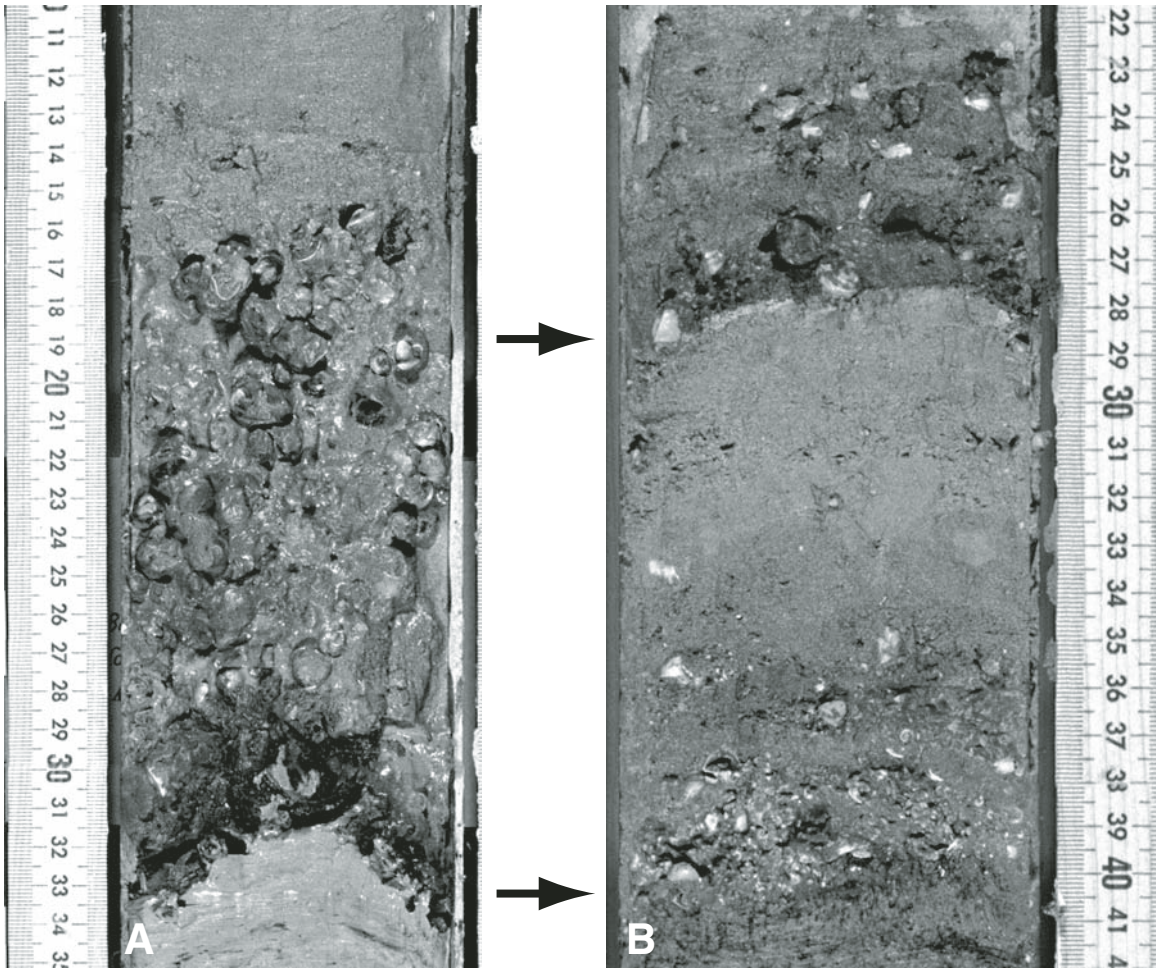

Figure 24. Graded shell gravel beds in BL02-2-1 (A) and BL02-1 (B). The graded gravel in B (arrows) is very similar to the shoreline gravel illustrated in Figure 23. The gravel in A is muddier due to infiltration of material during deposition of deeper-water sediment following a transgression. Scales are in centimeters.

Figure 25. Shoreline deposits at locality S8 (A) and locality S11 (B). (A) Recently notched shoreline from a minor transgression has small wave-built platforms building lakeward (arrows) over rippled sand. (B) Beach face developed on a stranded bar deposit. Note the depression behind the beach front (with tire tracks) and the erosional terrace in the background (with cars parked on top).

the lake rose above the barrier bar and flooded the swamp. The 5.2 ka age of that layer (Fig. 6) indicates that it is a fairly recent deposit. The calcite-precipitating lake stage of the early Holocene also flooded the swamp (Fig. 28). Sandy deposits overlying the gray calcitic mud probably represent lake lowering and re-establishment of the vegetation.

Modern Dam Breach

In BL2K-3, a 35-cm-thick sequence of fining-upward sand with ripple cross-lamination is overlain by an upward-coarsening sand sequence with climbing-ripple cross-lamination (Fig. 30). This sand overlies burrowed muddy sand and is overlain by bioturbated mud and graded shell gravel. Radiocarbon ages through

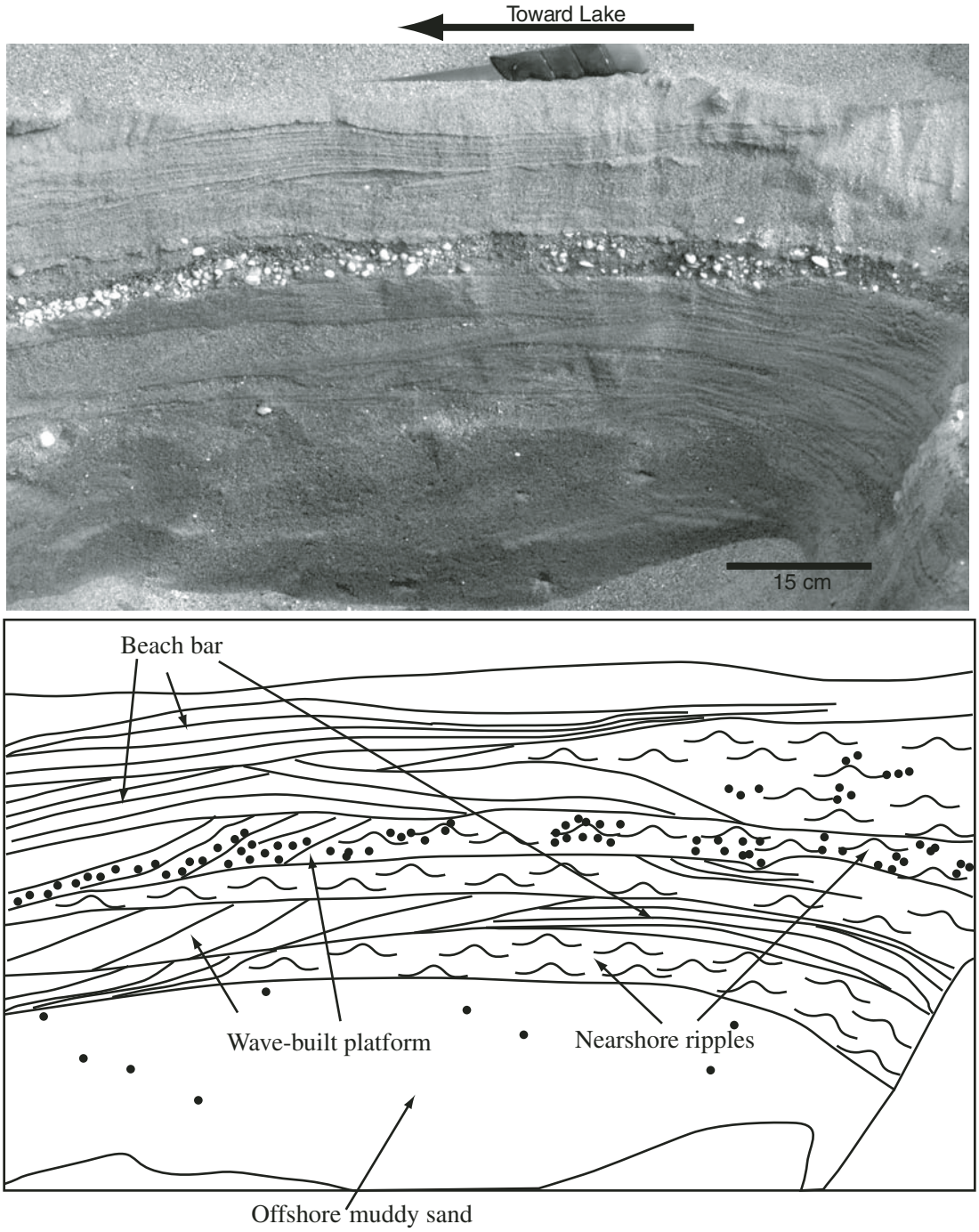

Figure 26. Trench cross section of shoreline deposits at locality S8. Base of trench is burrowed muddy sand. Series of lakeward-dipping tabular foresets are small wave-built platforms of quartz sand and shells. Beach-bar deposits include shoreward dipping sets with wave-rippled sand.

this sequence (Fig. 5) are inverted. The upward-fining sand layer is interpreted as the initial pulse of sediment when a dam used to regulate Mud Lake water levels was breached during a spring flood, causing a rush of Mud Lake water and sediment to enter Bear Lake in 1993. The upward-coarsening sequence is due to the continued erosion of older deposits from the dam breach and their deposition as a clastic wedge on the lake floor. The stratigraphically reversed ages reflect the erosion of older deposits and their redeposition into the lake. Prior to the breached-dam flood, burrowed muddy sand formed at this locality. The shallower water conditions produced by the addition of sediment caused this locality subsequently to be more nearshore in character.

Holocene Depositional Model

The reconstruction of Holocene sedimentary facies at Bear Lake relies heavily on the calibrated ages derived from radiocarbon ages (Colman et al., this volume). The ages based on pollen separates (pollen+ of Colman et al., this volume) are considered more reliable than those for shells (370 yr reservoir effect correction from Colman et al., this volume). Comparison of coeval core records along north-south or east-west transects clearly show radical changes in the thickness of sedimentary packages, with much thicker records in deeper water (Figs. 31 and 32). This observation, coupled with the abundance of reworked sediment and the presence of sharp bedding contacts overlain by sand, suggests that erosion of the shallower deposits and redeposition in deeper water have been important components of the sedimentary record. The cores available for sedimentary analysis typically lack the modern surface sediments and often have sediment thousands of years old at the top. This, combined with the modern canal-fed lake chemistry, complicates direct comparisons to modern depositional conditions. Geochemical data for BL02-4 (Dean, this volume) suggest that the uppermost sediments were deposited after the opening of the canals, that BL2K-3 contains a thick sand sequence that is correlative to a recent event, and that the upper part of BLR2K-1 has a breccia attributed to the canal-digging process. A collection of surface samples along several transects from shallower to deeper water provided grain-size distributions of insoluble clastic sediment (Smoot and Rosenbaum, this volume). These data suggest that the modern surface sediments are consistently finer grained than most of the Holocene

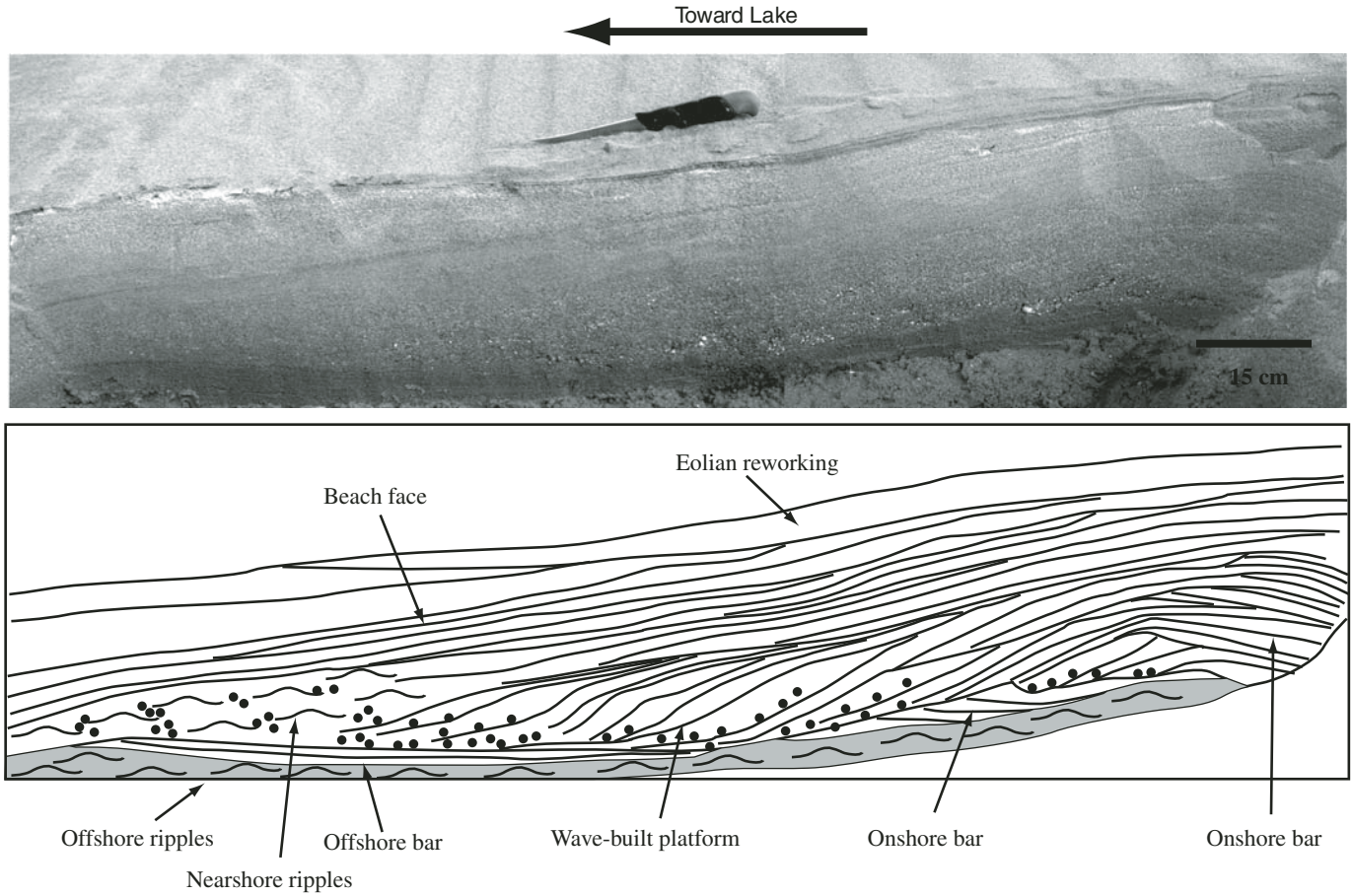

Figure 27. Trench cross section of shoreline deposits at locality S6. Beach-face deposit of predominantly quartz sand is superimposed on a shoreline bar that was modified by wave-built platforms. Offshore rippled fine sand forms lenses in muddy sand.

sediments and that the grain-size distribution is not uniform to depth. Therefore, the depositional model for the Bear Lake Holocene record is forced to use relative depth relationships with only broad constraints on absolute depth.

According to the distribution of the sediments in cores (Figs. 31 and 32) and trenches, the ideal Bear Lake depositional model has Aragonite II forming in the deepest water (greater than 50 m) and Aragonite I (35–50 m) followed by Aragonite III (20–35 m) forming in progressively shallower water (Fig. 33). Sandy mud and muddy sand are deposited at depths less than 20 m, with rippled sand beds grading to shoreline sands on the steeper lake margins and muddy sand directly overlain by sheet gravels on the low-angle lake margins. Although this type of arrangement is suggested by the core records, the reality of the facies distribution is much more complicated. The correlation used in Figures 31 and 32 assumes that most of the deviation is due to the degree of erosion, with progressively more erosion at shallower depths. Erosion is more pronounced along the east-west transect than the north-south transect, perhaps reflecting the different slopes. Shoreline deposits are notably absent in east-west seismic profiles in the middle of the lake, suggesting they are systematically eroded during transgressions. Aragonite II is the least well behaved of the

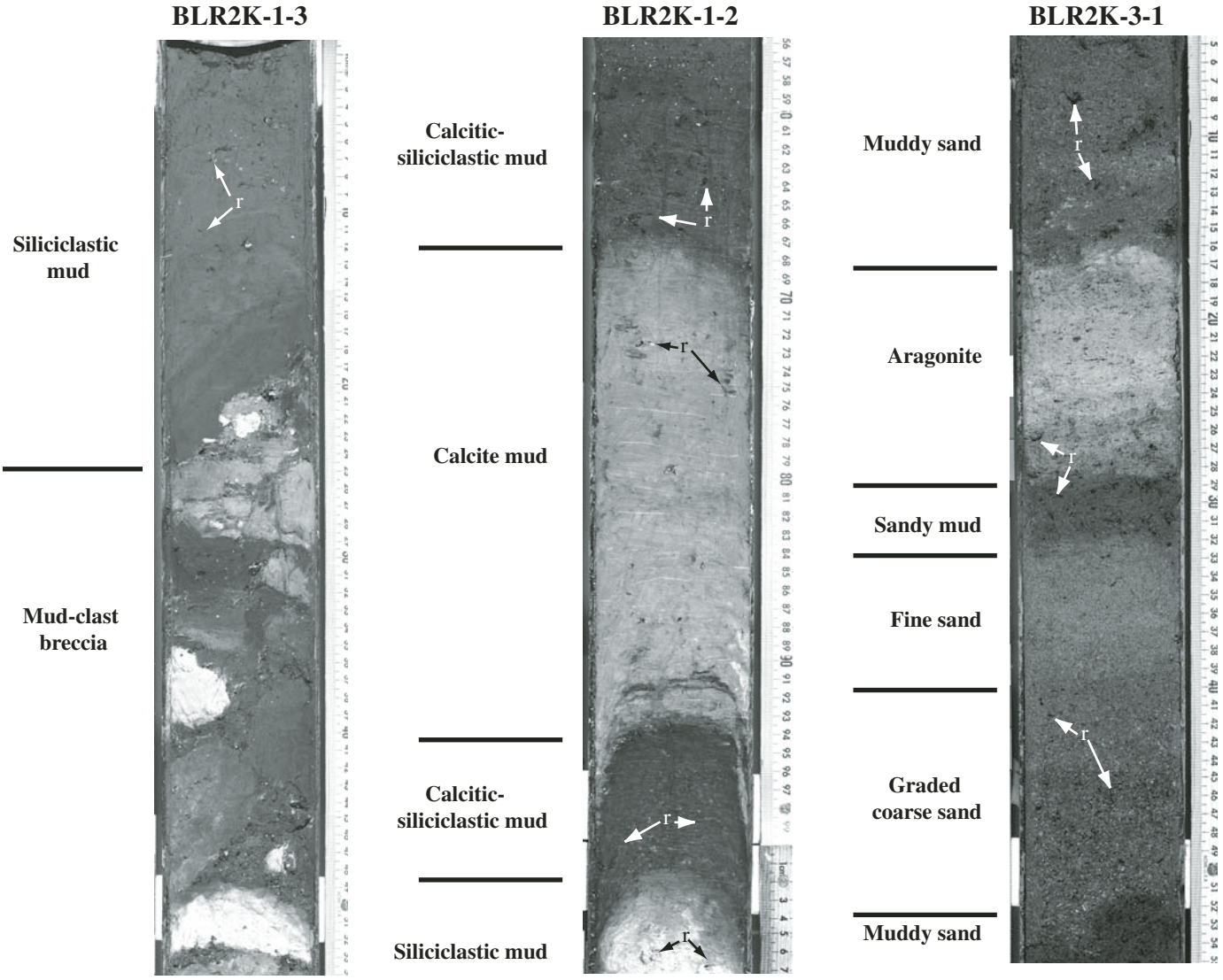

Figure 28. Core segments from the area north of Bear Lake at localities shown in Figure 1. In BLR2K-1-3, lower breccia includes fragments of mud and muddy sand from Holocene and Pleistocene deposits in the area. Upper brown silty mud with root casts (r) shows very little diatom or calcite content. In BLR2K-1-2, calcitic siliciclastic mud is organic rich and contains abundant small snails (white dots). Calcite mud contains pelagic diatoms similar to those in the Holocene calcite layer in Bear Lake. Siliciclastic mud at the base appears to be mostly glacial flour. BLR2K-3-1 reflects proximity to narrow bar separating the marsh from the lake. The graded sand and fine sand are composed mostly of quartz and shell fragments, similar to the bar deposit. Sandy mud and muddy sand contain calcite crystals, small snails, and organic matter, similar to typical marsh deposits. The aragonite layer is burrowed sandy mud, similar to shallow-water lake deposits. All scales are in centimeters.

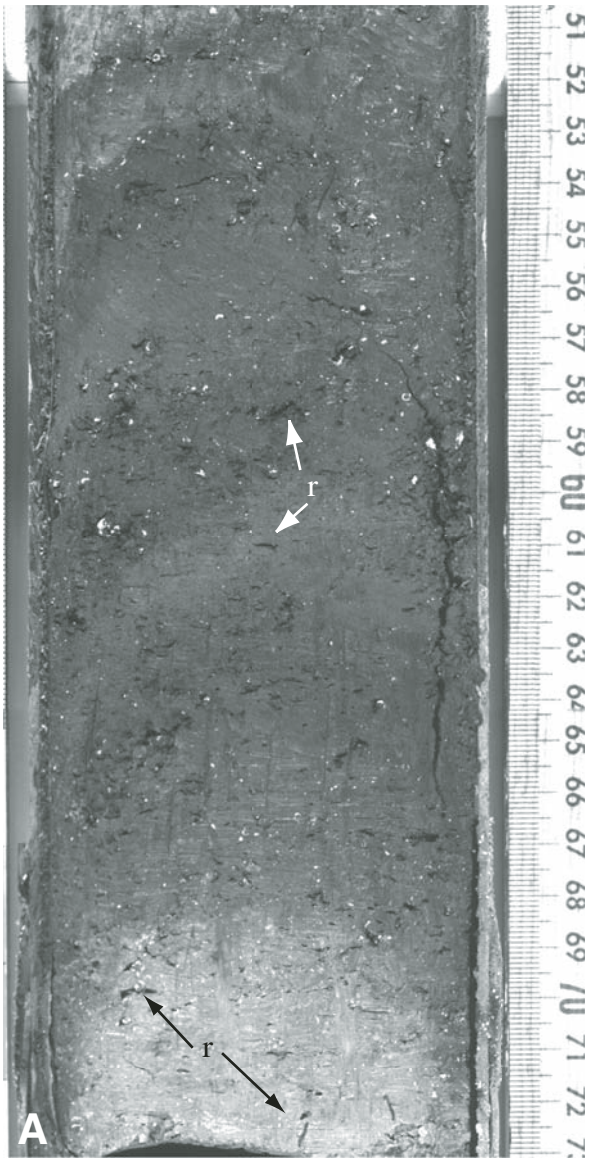

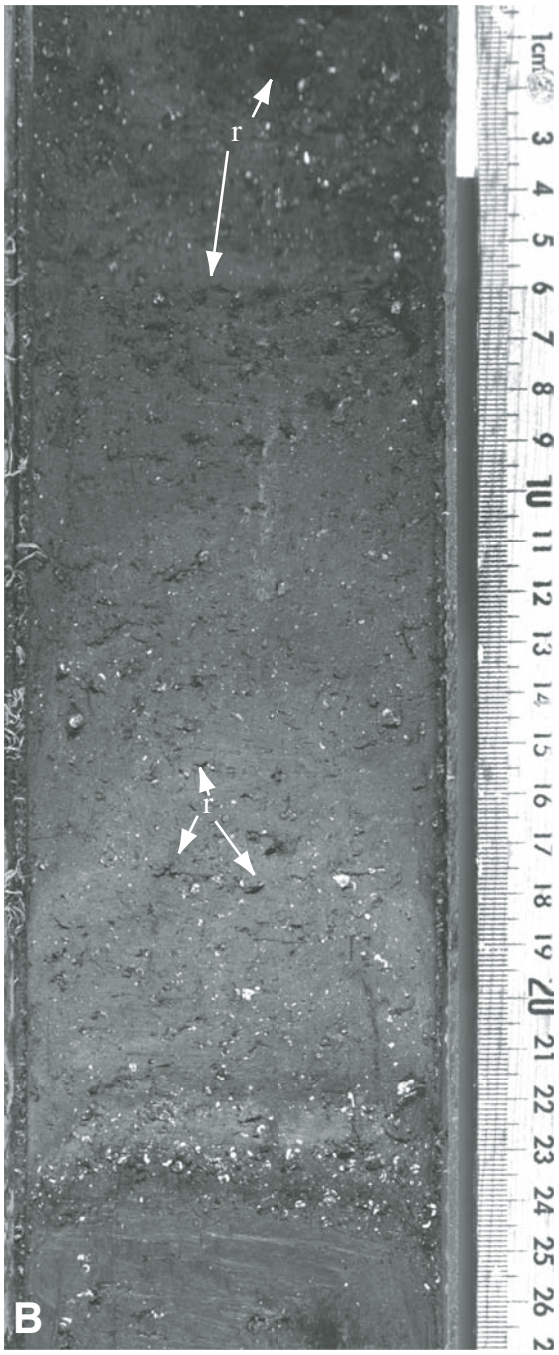

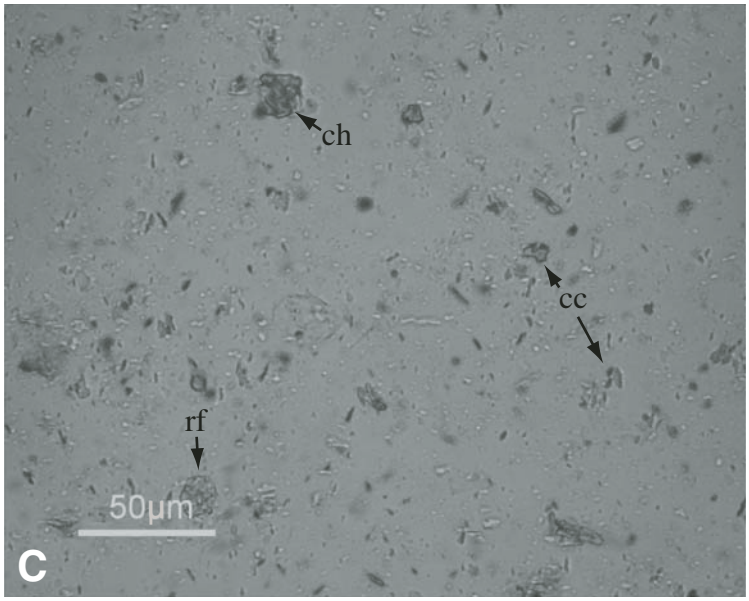

Figure 29. Core segments showing variations in typical marsh deposits. (A) Calcitic siliciclastic mud in BLR2K-1-3 with abundant carbonized roots (r) and small snails (white dots). Faint banding in upper part of sample is due to organic-poor, calcite rich layers (lighter). Light layer at base is mud containing abundant glacial flour. (B) Calcitic siliciclastic mud in BLR2K-3-1 with abundant carbonized roots (r) and small snails (white dots). Snails are concentrated into a layer near base. Banding represents organic-poor, calcite-rich layers (light) and peat-like, organic-rich patches, and irregular bands (very dark). (C) Smear slide of calcitic siliciclastic mud showing calcite crystals (cc), rock-fragment grains (rf), and a charophyte oogonium (ch). Tiny white dots are silicate grains (glacial flour?). Scales in A and B are in centimeters.

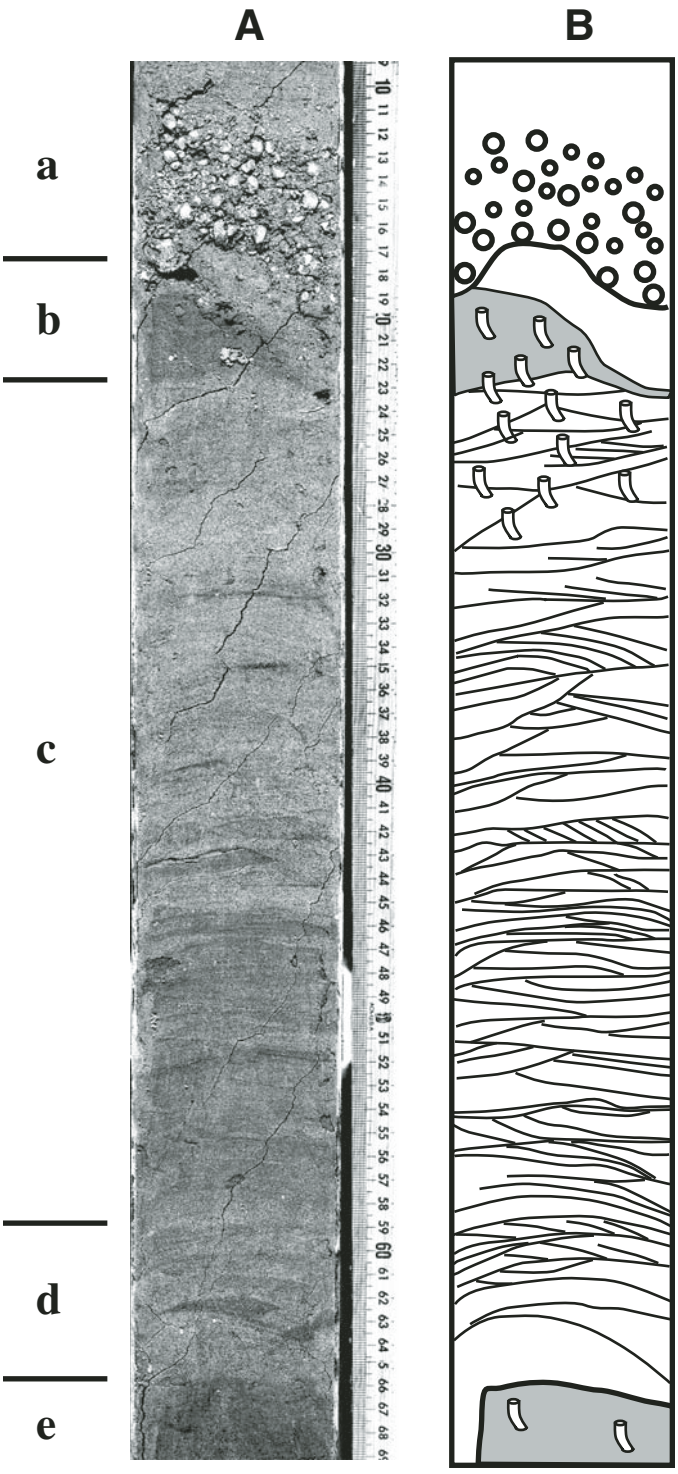

Figure 30. Core segment (A) and schematic sketch (B) from BL2K-3-1. (a) Graded shell gravel at the top is a shoreline deposit similar to gravel sheet in Figure 22. (b) Bioturbated sandy mud (shaded in B) with wave-sorted sand cap. (c) Upward-coarsening sequence of ripple cross-lamination. The upper part was modified by burrowing. (d) Upward-fining sequence of ripple cross-laminated sand. (e) Bioturbated sandy mud. Scale is in centimeters.

carbonate facies, requiring nearly systematic removal of equivalent strata in the shallower cores. This may indicate that Aragonite II represents a range of depths and may be more indicative of a change in water chemistry or temperature. It is interesting to note that the two Aragonite II horizons in BL96-2 and their correlative counterparts in BL96-1 are the only intervals that registered as distinctly different diatom populations in the study of Moser and Kimball (this volume). This suggests that the other Aragonite II intervals in BL96-1 may not be as distinct from Aragonite I. Another possible explanation is that Aragonite II represents very short lived lake-level rises during periods of rapid shifts in lake depth. This explanation would also explain the relatively poor mixing of Aragonite II in contrast to Aragonite I and the association of interbedded Aragonite I with the Aragonite II intervals that are equivalent to Aragonite III in BL96-2 and BL02-3.

The deepest-water core record (BL96-1) indicates there were four types of deep-lake conditions at Bear Lake during the Holocene. Aragonite I deposition appears to overlap with the modern lake conditions to ca. 2.5 ka. Aragonite II deposition occurred during two intervals, 2.5–4.5 ka and 6.5–7.5 ka, the younger one intermittently switching to Aragonite I. Aragonite III deposition dominated over a prolonged period around 5–6.5 ka and it also is found in 9–10 ka deposits in BL 96-2 and BL02-3, which were not penetrated in BL96-1. Calcite deposition (not penetrated in BL96-1) occurred ca. 8–8.5 ka. Aragonite III occurrences in BL96-1 indicate lake conditions much shallower than the modern lake. This interpretation is supported by the presence of sheet gravel shoreline deposits in cores at 35 m below the modern highstand in those core records equivalent to the Aragonite III in BL96-1. In contrast, the calcite depositional event is indicative of a major lake-level rise to depths greater than the modern highstand. The age range of the calcite is roughly coincident with that of the Willis Ranch shoreline, which is 9 m above the modern highstand (Laabs and Kaufman, 2003; Smoot and Rosenbaum, this volume). This rise in lake level coincides with an influx of Bear River water (Dean et al., 2006; Dean, this volume). Aragonite I deposits in BL96-1 appear to be coeval with conditions similar to the modern Bear Lake and conditions that were shallower. If Aragonite II represents aragonite deposition in a deeper lake, it suggests two time intervals with intermittent rises above the modern highstand without Bear River influence. The Aragonite II at 3.5 and 7.0 ka are the most likely associated with a deeper lake, whereas the other occurrences are more debatable.

The area now covered by Mud Lake was a shallow marsh for most of the Holocene. It was inundated with lake water during the calcite interval and possibly briefly during a lake-level rise ca. 500 yr B.P. The latter record is a thin aragonite bed in BLR2K-3 that may also represent a single depositional event during a storm rather than a lake-level rise. The area near the northern shoreline of Bear Lake experienced frequent episodes of storm washover depositing the graded sand beds found there. Following the opening of the canals, the marsh was replaced by Mud Lake and deposition of siliciclastic silt and mud was more rapid than before.

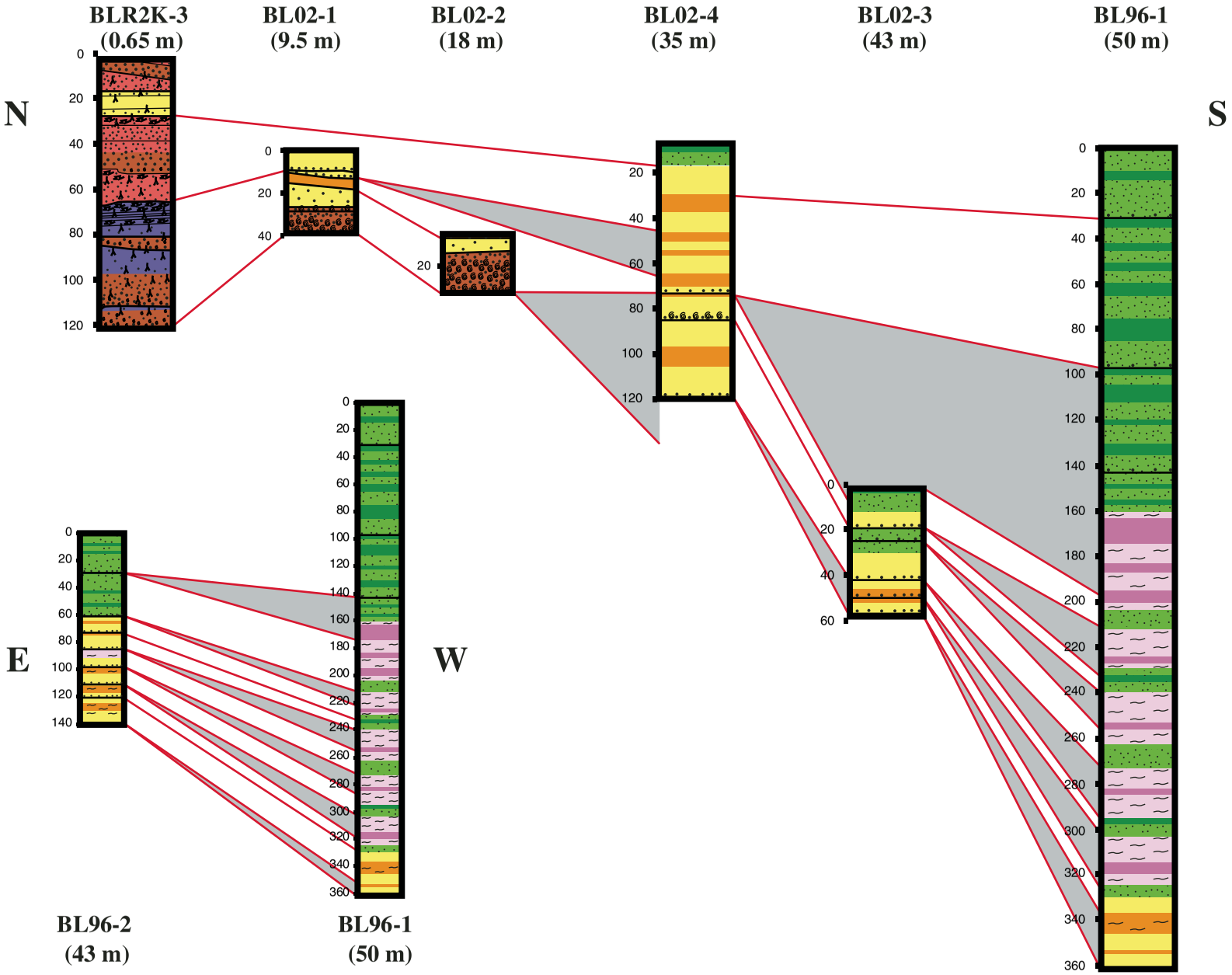

Figure 31. Correlation of core segments younger than 5 ka along a north-south and an east-west transect. Sediment types and sedimentary structures are provided in the legends for Figures 3–6 (p. 54–57). Note the change of scale for the east-west correlation. Red lines represent correlated horizons and gray shading indicates portions of sections missing, presumably due to erosion at the shallower core site. Section thicknesses may be composites of two or more cores. Correlations are from Smoot and Rosenbaum (this volume). Water depths of the coring sites (in parentheses below the core locations) are corrected to the modern highstand level (1805.5 m elevation). Vertical scales are depths below the surface in cm.

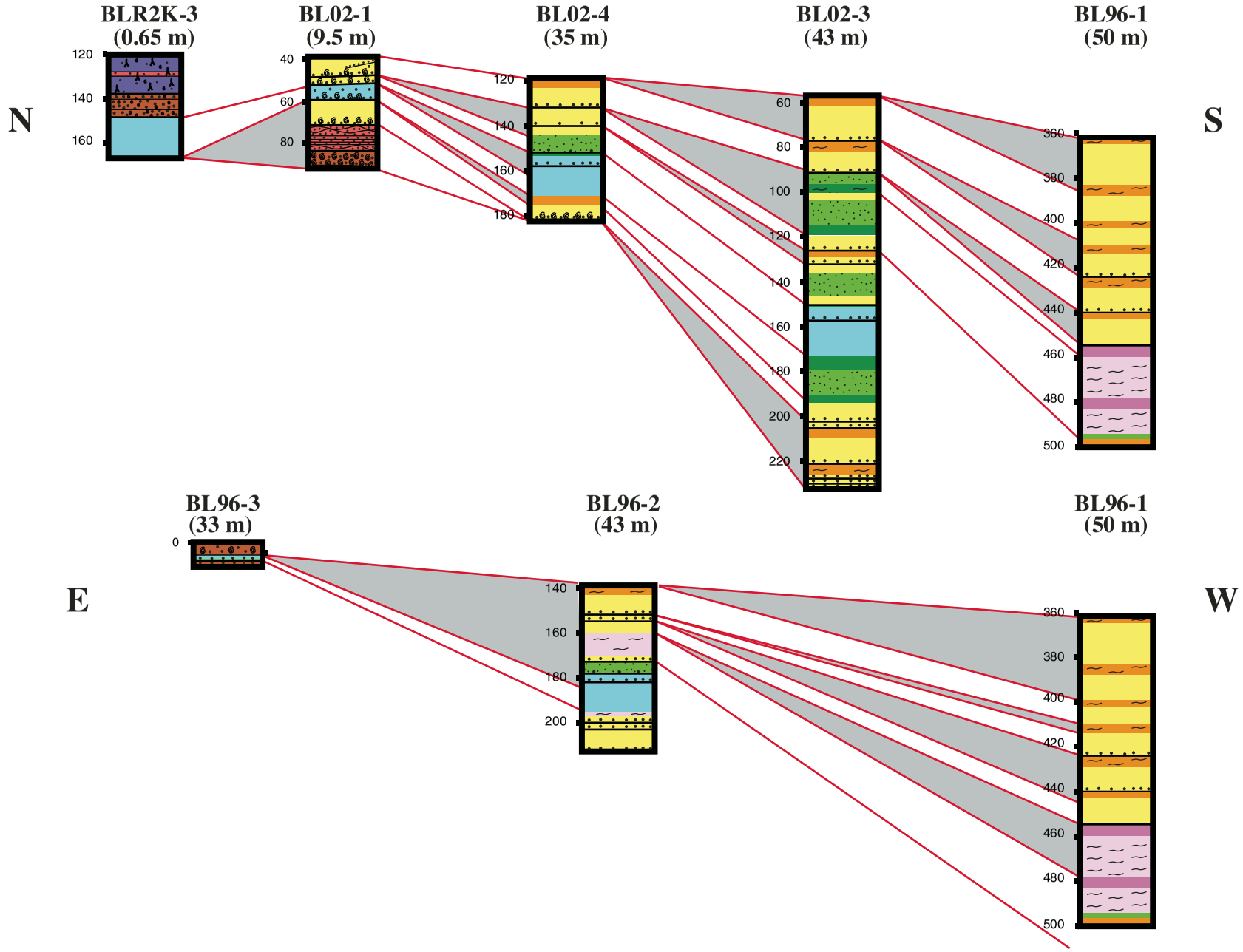

Figure 32. Correlation of core segments representing the time interval 10–5 ka along a north-south and an east-west transect. Formatting, scales, and data sources are the same as for Figure 31.

PLEISTOCENE SEDIMENTS

Pleistocene age sediments are found in a few exposures of shoreline deposits around the lake margin (Laabs and Kaufman, 2003; Reheis et al., this volume) and in cores (Figs. 3–6). The longest sequence of Pleistocene sediments collected was in the GLAD800 cores, which penetrated 120 m of sediment spanning ~220 k.y. (Dean, this volume; Kaufman et al., this volume). These cores, however, have not been thoroughly examined. The preliminary data suggest that the character of these deposits is similar to the range of Pleistocene sediment types observed in shallower cores, including some aragonite intervals (Dean, this volume; Kaufman et al., this volume). The longest core through Pleistocene sediments that has been thoroughly examined (BL96-3) is ~4 m long and dates to ca. 26 ka (Colman et al., this volume; Smoot and Rosenbaum, this volume). The shoreline exposures were not examined for this study but have been described by Robertson (1978) and Laabs and Kaufman (2003).

Deep-Water Sediments

The majority of the deep-water sediments in the cores examined consist of siliciclastic mud and mud consisting of a mixture of siliciclastic sediment and calcite. The youngest Pleistocene deep-water deposits are aragonite, mostly Aragonite III. The Pleistocene aragonite deposits are underlain by a thin calcitic mud. Another thin calcitic mud occurs lower in the Pleistocene section below the mixed calcitic-siliciclastic mud interval. The aragonite deposits are effectively identical to those of the Holocene and will not be redescribed. The calcitic mud intervals are also like the Holocene calcitic interval previously described. Both are characterized by a basal nearly pure calcite that becomes more

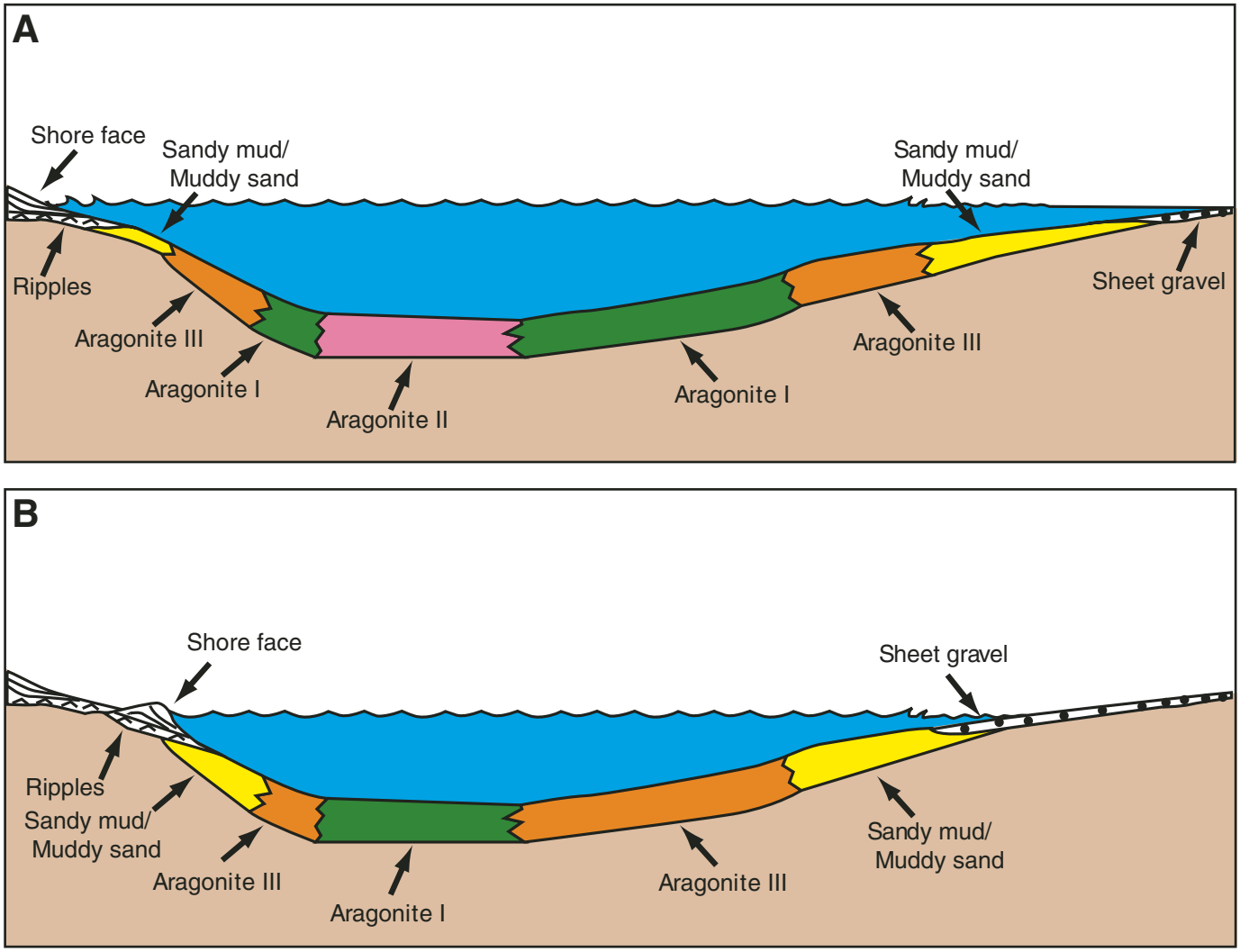

Figure 33. Schematic illustration of aragonite depositional facies in Bear Lake during the Holocene for conditions slightly deeper than the modern lake (A) and conditions slightly shallower than the modern lake (B). The left side represents a lake margin with a relatively steep slope (as in the eastern side of the lake), whereas the right side represents a shallow slope (as in the northern side).

siliciclastic rich with rock fragments upward. These will not have any further description.

Mixed Calcitic-Siliciclastic Mud

Mixed calcitic-siliciclastic mud is mostly gray colored with vague decimeter-scale lighter and darker bands and horizons of dark blebs (Fig. 34). This sediment type occurs in BL96-2 from ~235–330 cm depth, and is also found in BL96-3, BL2002-4, and BL2002-3. It contains 30%–40% calcite mixed with silty clay (Dean, this volume). The calcite is a mixture of subhedral to anhedral crystals (2-10 μm) and a variety of polycrystalline or irregular calcite grains (2-100 μm) (Fig. 35). The silt and clay are a mixture of silicate minerals and rock fragments with only minor clay minerals. Diatoms are varied and include both attached and pelagic forms. The relative amount of calcite is variable, with the darker, more calcite-poor layers containing more rock fragments and fewer visible diatoms. There is an ostracode-rich sandy layer with a sharp contact at 242 cm in BL96-2, but the typical sediment is mostly silt and clay. Burrows are typically small (1–3 mm diameter) and random, and some zones of burrows appear more horizontal. The most conspicuous layering in mixed calcitic-siliciclastic mud consists of bands containing abundant head capsules and sulfide-coated egg casings of the aquatic crustacean *Daphnia*. The latter resemble concentrations of dark blebs on the split core surfaces (Fig. 34). In the X-radiographs, the *Daphnia* concentration zones appear to display an upward size increase of very dense bleb-shaped features (Fig. 36). The largest blebs (as much as 1 mm) are horizontally elongated and may be tubes, whereas the smaller blebs (~0.5 mm) are clearly *Daphnia* egg casings.

The depositional conditions for the mixed calcitic-siliciclastic mud are difficult to determine. The mixture of carbonate crystals,

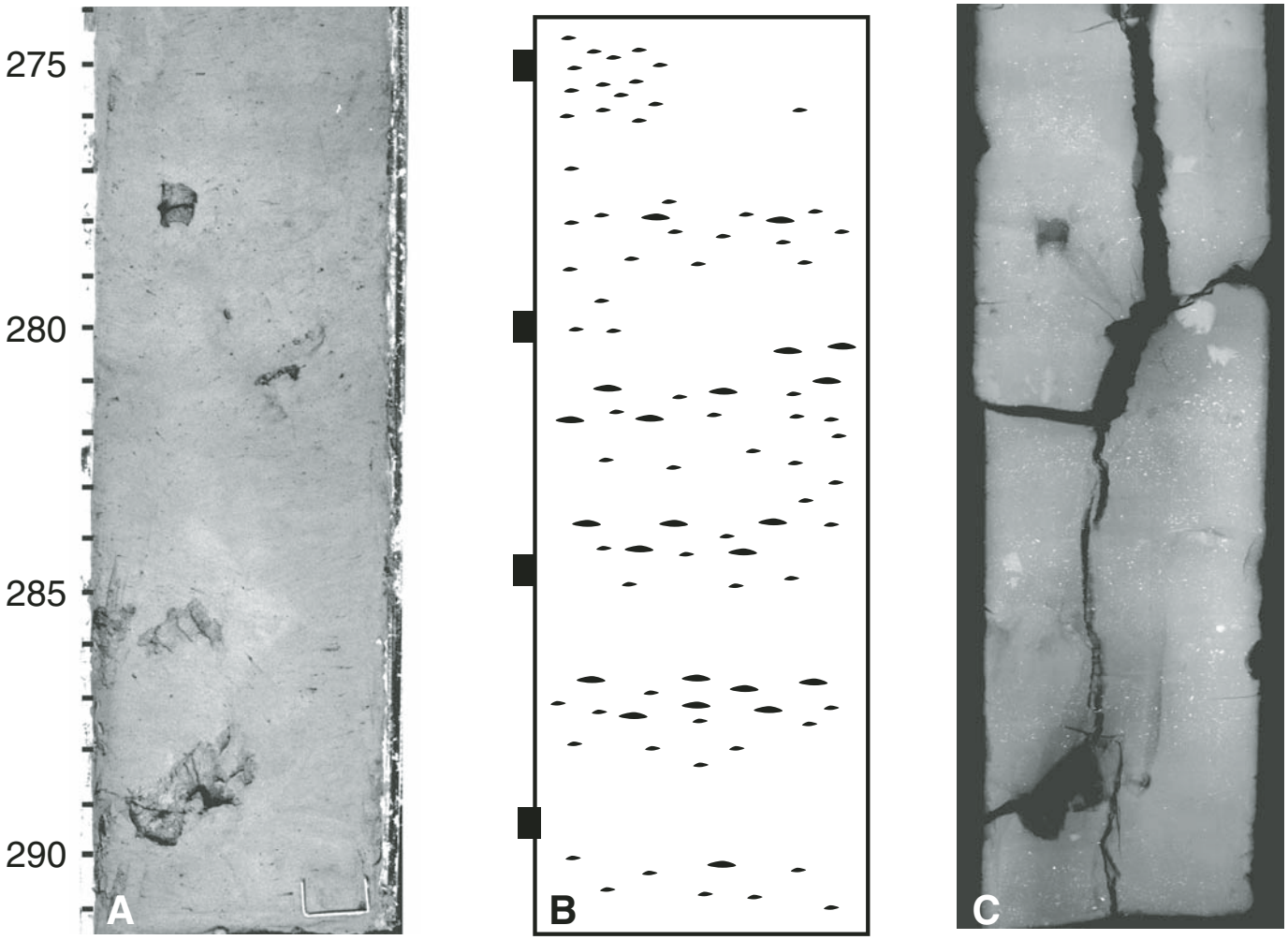

Figure 34. Mixed calcitic and siliciclastic mud in core segment cut surface (A), schematic drawing of X-radiograph image (B), and X-radiograph (C) from BL96-2. An irregular banding is defined by concentrations of sulfide-coated blebs (*Daphnia* egg casings and possible horizontal tubes) that appear black on the cut face and bright white in the X-radiograph. Scales are in centimeters. Some of the density differences in C are due to irregularities in the sample thickness. The large light patches in C are fragments under the sample. The cut-surface photo was digitally enhanced to contrast the layers. The irregular light patches in A are due to uneven oxidation around sample plugs (holes).

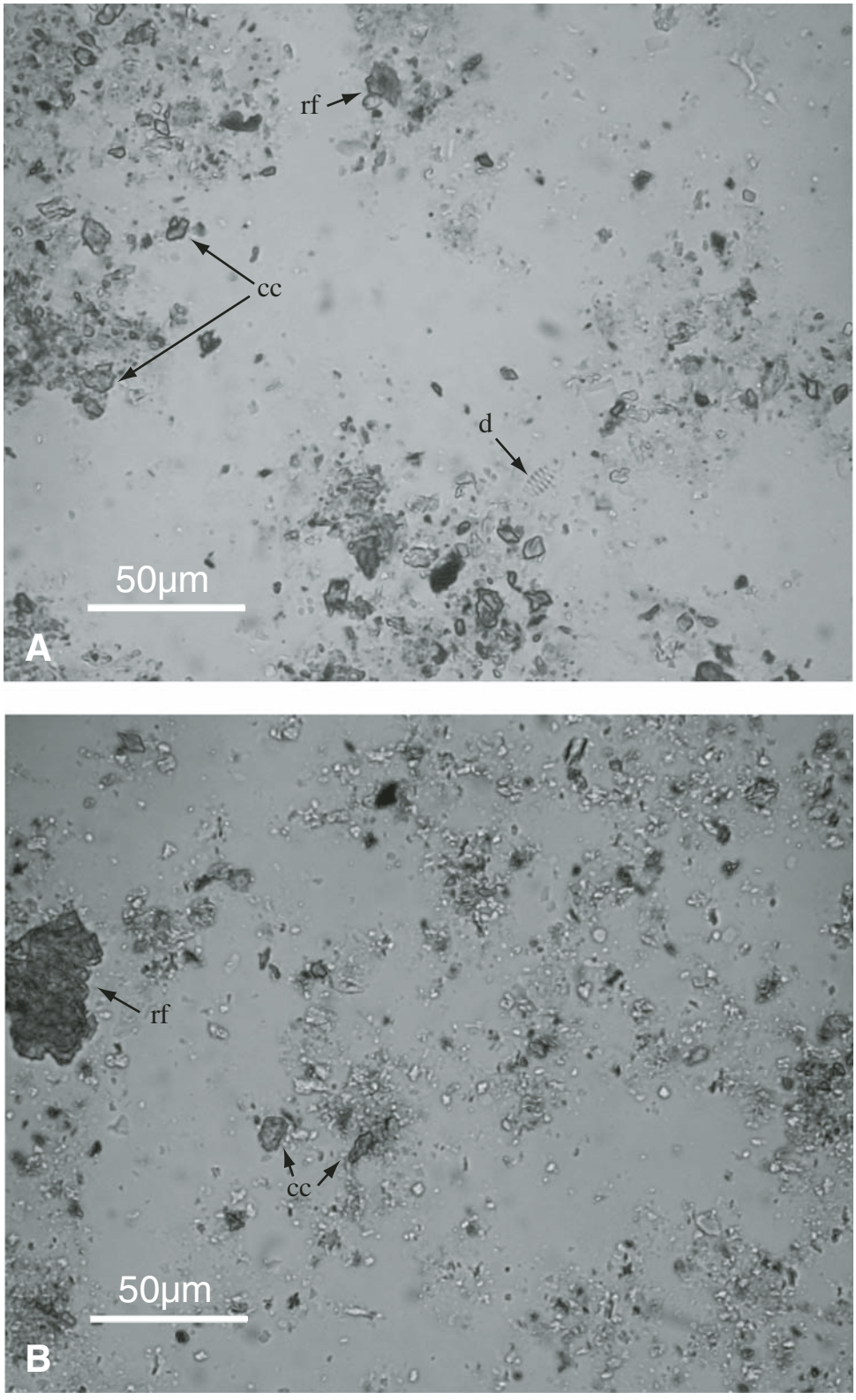

Figure 35. Smear slides of mixed calcitic and siliciclastic mud. (A) More calcite rich interval with calcite crystals (cc), small rock fragments (rf), and diatoms (d). (B) Calcite-poor interval with calcite crystals (cc) and larger, more plentiful rock fragments (rf). Diatoms are less abundant.

siliciclastic grains, and carbonate grains suggests that sediment reworking was important. This is supported by the mixed diatom assemblage. The relative abundance of ostracodes is similar to that of the shallower-water deposits in the Holocene section. Because *Daphnia* live and produce eggs at the water surface, the concentration of their remains in the sediment provides no relative indication of water depth. The concentration does suggest that, at least intermittently, sedimentation rates were very low. Subaqueous plants produce tiny root hairs that are concentrated at the sediment surface. It is possible that the tiny, tube-shaped features associated with the *Daphnia* concentrations are actually sulfide-coated root casts of subaqueous plants. If so, the mixed calcitic-siliciclastic mud intervals represent a clear and probably shallow lake and the dearth of sandy mud and sand layers indicates it had a small surface area.

Siliciclastic Mud

The thickest section of deep-water siliciclastic mud is found in BL96-3, where it constitutes the lower 320 cm of the core. These deposits consist of alternations of reddish fine mud and slightly greenish to brownish silty mud (Fig. 37). The silt includes some carbonate clasts, but is mostly quartz and rock fragments. The clay-sized particles are predominantly small grains (rock flour?). Diatoms are uncommon in smear slides, and probably constitute a very small fraction of the sediment. Mud and silty mud alternations occur in 2–20 cm intervals. The coarser layer usually has an abrupt contact with the underlying finer layer, whereas the transition to finer material may be more gradational. Bioturbation patterns in the sediment are intense. Randomly oriented burrows ranging from 1 to 5 mm in diameter are filled with sediment and may have partial lining of sulfide minerals. The latter features appear as dense streaks in X-radiographs. The finer-grained intervals appear to have more horizontal burrows that are generally smaller than the random burrows. Many of these horizontal burrows appear as dark flattened ovals in the cut face of cores and as denser features in the X-radiographs. These features suggest sulfide concentrations in the burrows. At a larger scale, the distribution of coarser and finer sediment appears to define rhythmic upward-coarsening successions (Fig. 38). The thickest fine-grained intervals alternate with the thinnest coarse-grained intervals. Over a 20–60 cm thickness, the fine-grained portions of alternations become progressively thinner as the coarse-grained portions become progressively thicker. A thick fine-grained interval abruptly overlies this succession, indicating the next upward-coarsening sequence. These upward-coarsening successions are also recognizable in the grain-size data (Rosenbaum and Heil, this volume).

Siliciclastic mud in Bear Lake was largely derived from the Bear River, including a large amount of glacial flour from the Uinta Mountains (Rosenbaum and Heil, this volume). The smear-slide observations confirm that most of the clay-sized material in siliciclastic mud units is not clay minerals from weathering, but small silicate grains and rock fragments. The lack of bedding in deep-water siliciclastic mud is due to the intense bioturbation and suggests low sedimentation rates. The variability in bioturbation style may indicate changes in the accumulation rate, oxidation state of the lake floor, or substrate preference. The coincidence of changes in bioturbation style with changes in grain size does little to distinguish between the different possibilities. The 2- to 20-cm-thick alternations of mud and silty mud characteristic of the deep-water siliciclastic mud and the larger-scale upward-coarsening sequences have several possible

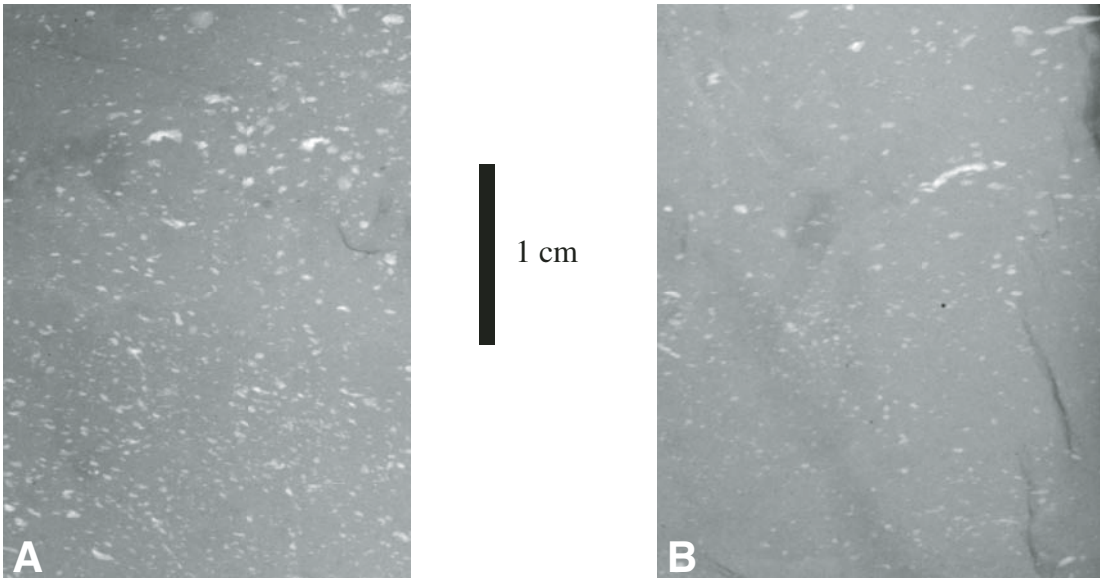

Figure 36. X-radiographs showing two examples of upward increase of size in sulfide-coated blebs in mixed calcitic and siliciclastic mud. In A, the larger blebs are only slightly more elongate, whereas in B, some larger blebs are very tubelike.

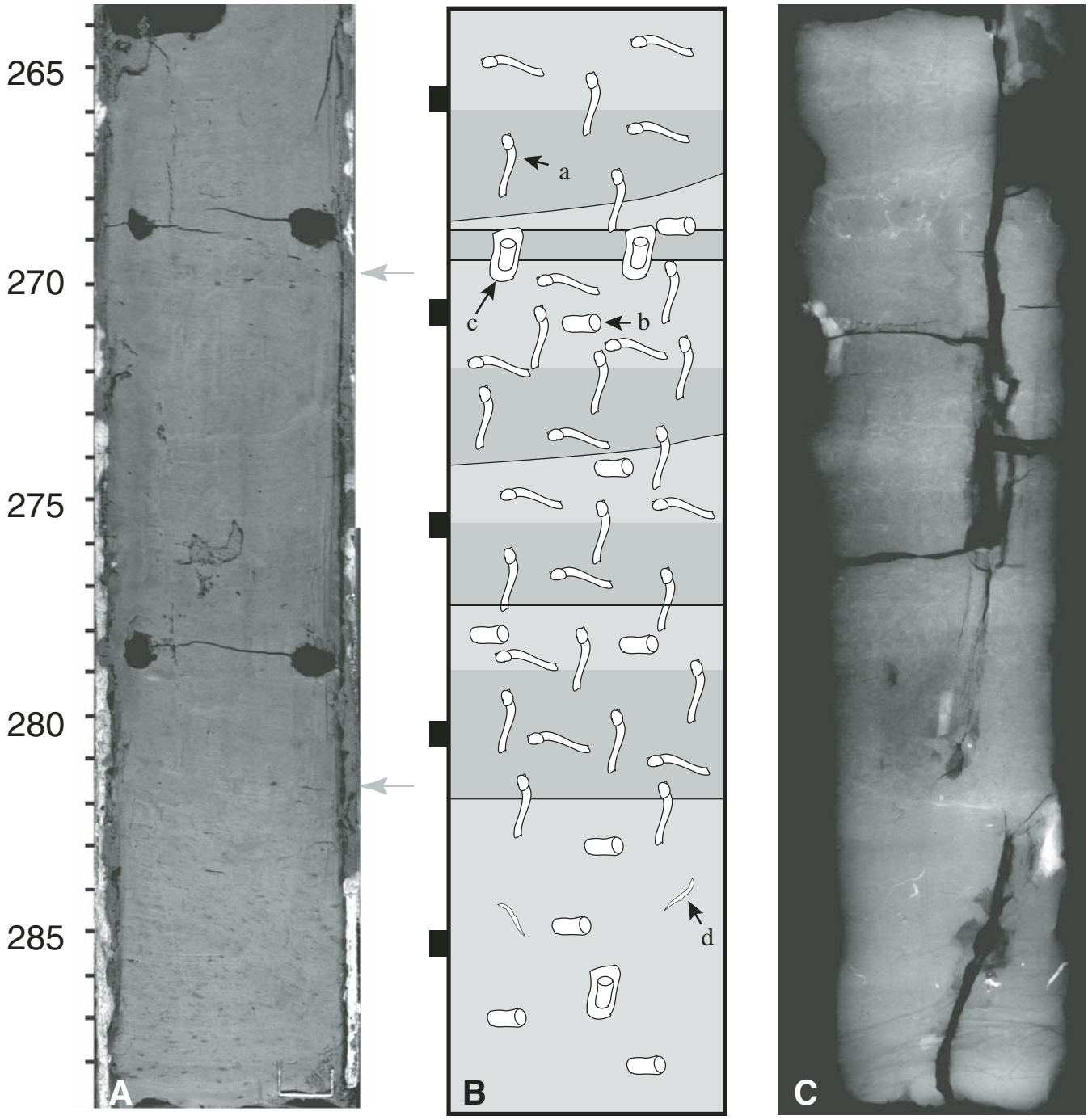

Figure 37. Siliciclastic mud in core segment cut surface (A), schematic drawing of X-radiograph image (B), and X-radiograph (C) of BL96-3. In the cut surface (A), the section appears to consist of a 10 cm greenish silty band (darker between gray arrows) overlain and underlain by reddish clay bands with black streaks. The X-radiograph (C) shows that the reddish intervals are denser (lighter), reflecting finer grain size, but each interval comprises smaller alternations of coarser and finer material. The schematic drawing (B) illustrates the sharp basal contacts of coarser layers (darker shading) and distribution of burrow types including large sinuous burrows (a), small horizontal burrows (b), and random burrows with denser rims (c). Bright gashes (d) are probably partial sulfide mineral coatings on large burrows. The sedimentary features shown in B are not to scale. Scales are in centimeters. The X-radiograph scale (B and C) differs slightly from the core (A) due to differential shrinkage from drying. Some of the density differences in C are due to irregularities in the sample thickness. The cut-surface photo was digitally enhanced to contrast the layers.

causes. Rosenbaum and Heil (this volume) note that the indicators of glacial flour are less pronounced in coarser layers, and suggest that the variations in grain size may reflect advance and retreat of glaciers in the Uinta Mountains. Although this is a very reasonable interpretation of the data, it neglects the observation that the clay-sized material in the presumed glacial-advance layers is identical to that of the presumed glacial-retreat layers. The shifts in indicators of glacial flour noted by Rosenbaum and Heil (this volume) may actually be indicating dilution by locally derived coarse sediment rather than changes in the influx of glacial flour. Changes in grain size in the deep-water siliciclastic mud might reflect changes in the discharge of the Bear River that may have caused turbiditic underflows to travel deeper into the lake (as in Sturm, 1979). The change in grain size may also represent slight changes in water depth, with coarser sediment deposited when lake level lowered, allowing coarser material to

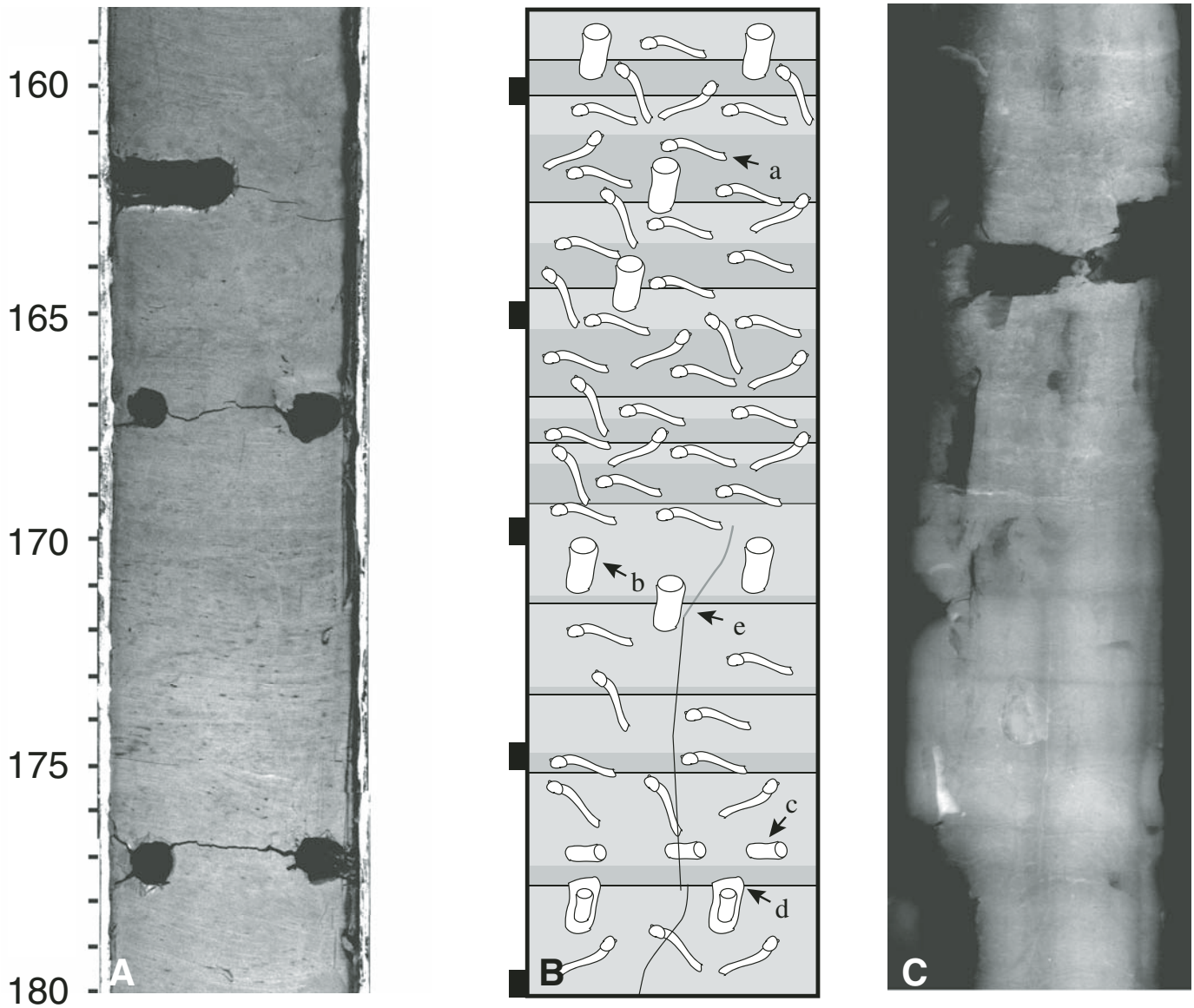

Figure 38. Siliciclastic mud in core segment cut surface (A), schematic drawing of X-radiograph image (B), and X-radiograph (C) of BL96-3. In the cut surface (A), there is an upward-coarsening sequence of reddish clay (lighter) to greenish silty mud (darker). The top is the base of another upward-coarsening sequence. The X-radiograph (C) shows that the sequence is composed of finer banding with a gradual increase in the thickness and number of less dense, coarser-grained beds (darker). The schematic drawing (B) illustrates the sharp basal contacts of coarser layers (darker shading) and distribution of burrow types, including large sinuous horizontal burrows (a) most abundant in coarser layers, random burrows (b), small horizontal burrows (c), and random burrows with denser rims (d). Hairline vertical cracks (e) cut bedding. The sedimentary features shown in B are not to scale. Scales are in centimeters. The X-radiograph scale (B and C) differs slightly from the core (A) due to differential shrinkage from drying. Some of the density differences in C are due to irregularities in the sample thickness. The cut-surface photo was digitally enhanced to contrast the layers.

move into the core localities. On the other hand, geochemical data suggest that the lake was spilling during deposition of the siliciclastic mud (Dean et al., 2006; Dean, this volume), which would limit the degree of lake-level fluctuation. A spilling lake at this time of sedimentation is also suggested by geomorphic data (Reheis et al., this volume) and shoreline data (Laabs and Kaufman, 2003; Smoot and Rosenbaum, this volume). A similar change of grain size could also have been caused by the rapid growth of delta fronts, combining components of increased discharge and increased proximity of inflow. The processes for making shifts in grain size could all have been precipitated by the advance and retreat of glaciers in the Uinta Mountains, which controlled the discharge and sediment supply of the Bear River. However, they were not necessarily a direct response to the glaciers themselves.

Shallow-Water Sediments

Carbonaceous Calcitic-Siliciclastic Mud

In core BL02-1, there is a 50-cm-thick interval of gray mixed calcitic-siliciclastic mud with bands of carbonaceous material (Fig. 39). This mud contains abundant small snail shells and irregular clumps of calcite and charophyte oogonia. Black carbonaceous tubes form both horizontal patterns and vertical disruptions. The horizontal tubes appear to be concentrated in horizons. Random burrows give the mud an irregular mottled appearance.

The organic-rich calcitic-siliciclastic mud deposit in BL02-1 is similar to the Holocene marsh deposits described earlier. The snails, charophytes, and carbonate crystals look to be the same and the concentrations of organic materials are similar. Carbonaceous tubes that are probably roots are common as was also observed in the Holocene marsh deposits. The concentrations of horizontal tubes are interpreted as roots of submerged plants.

Laminated Siliciclastic Deposits

Siliciclastic deposits that are laminated alternations of silt, sand, and clay were found in BL02-1, BL02-2, BL02-5, and BL2K-2 (Figs. 4 and 5). Most of the cores through this type of sediment were deformed by the coring process, in some cases causing extensive bowing and flowage of the originally horizontal laminae (Fig. 40). The lamina range from 0.5 to 5 mm in thickness. There is a range of lamina types. Graded laminae, which are continuous across the width of each core, are the ubiquitous sedimentary style. These laminae vary from mostly silt with a thin clay parting to mostly clay with a thin silty base (Fig. 41). Sand laminae are internally well sorted with sharp upper and lower contacts (Fig. 42). They commonly pinch out over the width of the core (10 cm) defining convex-upward lenses with flat bases. Although core deformation may account for some of the discontinuity of sand beds, most of them appear to be independent of their position along the deformation axis and independent of the thickness of the layer. Bioturbation is pervasive throughout the laminated beds, but burrows tend to mottle within the layering. Some thick sand beds appear structureless, which may be due to bioturbation. Within the laminated siliciclastic sequences the distribution of graded clay-rich laminae, graded silty laminae, and sand laminae appear to define upward-coarsening successions that are 2–15 cm thick (Fig. 40). Graded laminae become progressively thicker and coarser in upward-coarsening sequences, with sandy laminae at the top. These upward coarsening sequences are also stacked into successions 20–40 cm thick where each successive sequence has less clay at the base and more sand at the top. An example of laminated siliciclastic sediment that is transitional to the deep-water siliciclastic mud is in core BL02-5 from 27 m below the modern highstand. Intervals with graded clay-rich laminae and silty laminae are overlain and underlain by siliciclastic mud with vague, wispy bands of light (clay) and dark (silty) sediment (Fig. 43). The transition between these bedding styles is characterized by an increased density of bioturbation features disrupting the layering both above and below the layered intervals. There are no sand laminae in BL02-5.

The predominance of repeated graded silt layers with less common clay laminae is similar to prodeltaic deposits in glacial lakes (Smith and Ashley, 1985). In this setting, each graded layer represents an influx of sediment related to a melting event, such as summer warming. If each graded lamina were a varve, it would suggest a much higher sedimentation rate for the laminated deposits than is indicated by radiocarbon ages in the deeper-water siliciclastic sediments. The lenticular sand laminae are interpreted as wave deposits. The sharp bases and broad convex cross sections with no internal lamination are characteristic of cross sections of rolling-grain ripples (i.e., Harms et al., 1982, Chapter 2, p. 25–41). Rolling-grain ripples are low-relief, long-crested ripples that develop at the lowest velocities for wave movement. Upward-coarsening sequences in the laminated siliciclastic sediment may represent changes in the inflow or shifts in lake depth changing the loci of sediment input. Modern lakes fed by seasonal melting commonly show sequential variations in grain size of similar scale to those in Bear Lake. These changes may be due to increases in discharge to the lake during longer melting periods (i.e., Lamoureux and Bradley, 1996) or they could be due to more random processes such as delta lobe switching (i.e., Lamoureux, 1999). The occurrence of wave deposits in BL2K-2 and BL02-3 indicates that the lake depth was no more than 3 m above the historical highstand (Smoot and Rosenbaum, this volume). The interbedding of sand lenses and clay suggests that the occurrence of rippled sand is related more to decrease of silt input than to decrease of depth. The deposits in BL02-5 were deposited below wave base and in an environment transitional to the deep-water siliciclastic mud. The increase of bioturbation with depth is probably due to the decrease of sedimentation rates away from the delta.

Subaerial Features

Black carbonaceous tubes that are coated with pyrite cut vertically across lamination in siliciclastic sediment in BL2K-2 (Fig. 44).

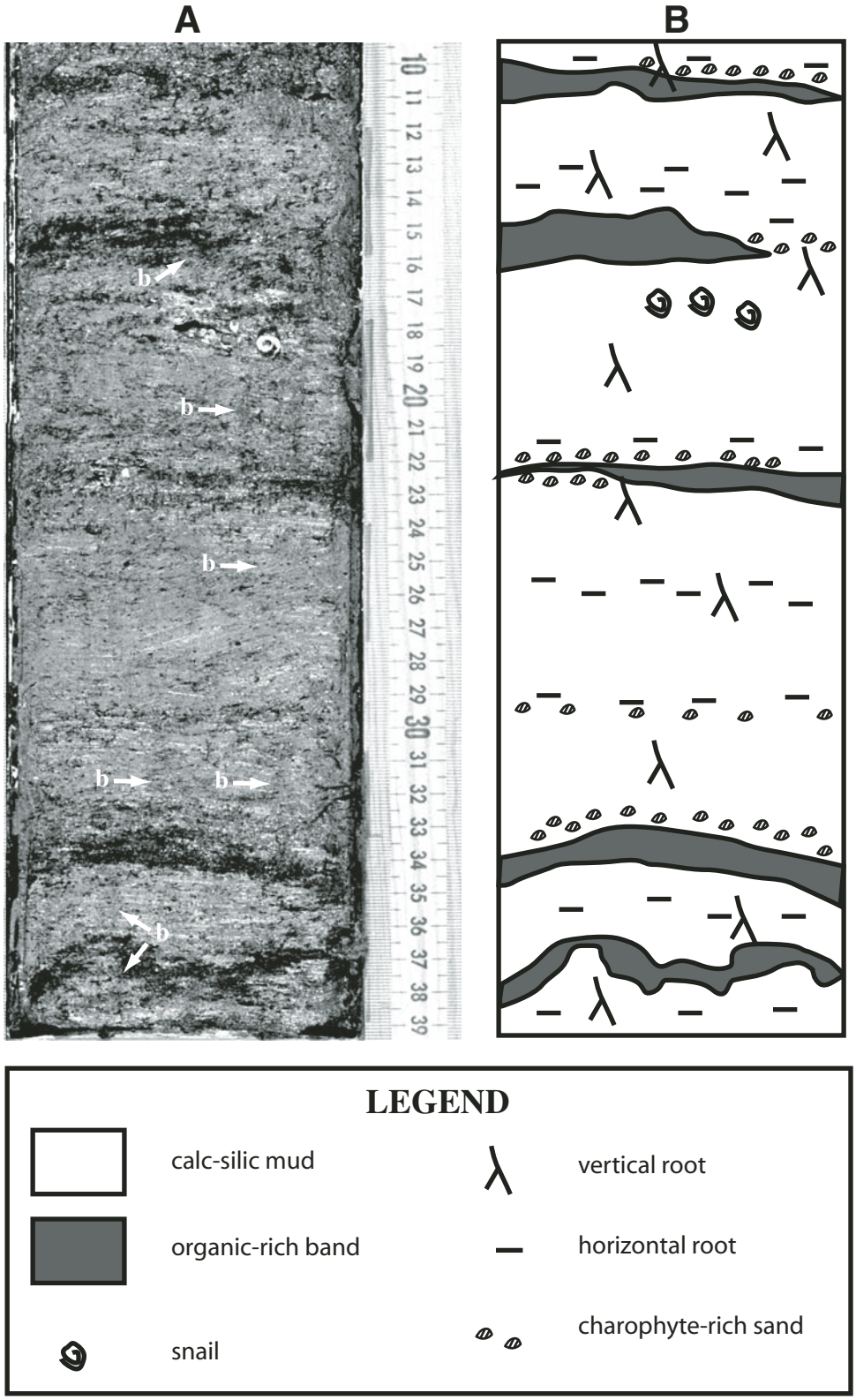

Figure 39. Mixed calcitic and siliciclastic mud with dark carbonaceous bands in core BL02-1. Mottled appearance of sediment is due to abundant random burrows. Some of these are indicated with "b." Carbonaceous tubes are oriented vertically or are concentrated in layers as horizontal features. Charophytes are mixed with unidentifiable calcite clumps, producing sandy clumps and layers. Scale is in centimeters.

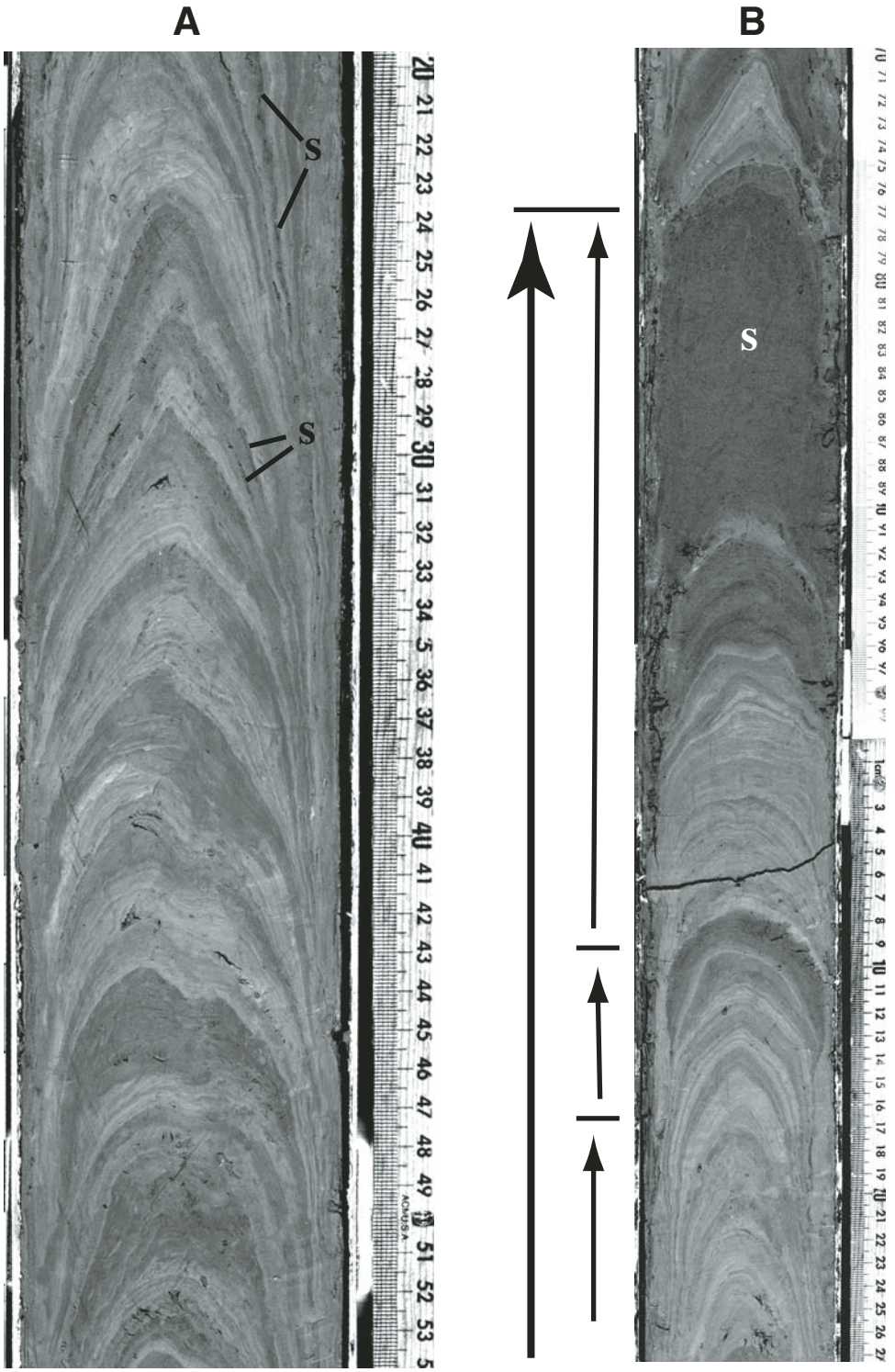

Figure 40. Core segments of laminated siliclastic interval in BL2K-2-1 (A) and BL2K-2-2 (B). The segment in A shows alternations of clay laminae (light), silt laminae (darker), and sand lenses (darkest, some are labeled "s"). The segment in B shows three small upward-coarsening sequences (arrows) that are part of a larger upward-coarsening sequence (heavy arrow). Sediments range from clay laminae (lightest) to unbedded medium sand (darkest). Layering was deformed by the coring process. Scale is in centimeters.

The tubes are thickest (~1 mm in diameter) and most abundant immediately below the contact of a graded shell gravel that marks the base of aragonitic sediment. The tubes become progressively smaller and less abundant downward over ~20 cm. Each tube commonly displays abrupt kinks, and some branch downward. Similar carbonaceous tube sequences ("root horizons" in Fig. 5) are in BL02-1 also below a graded shell gravel marking the transition to aragonitic sediment and in BL02-2 below the carbonaceous calcitic-siliciclastic mud deposit. In cores BL96-2 and BL96-3, the contact between siliciclastic mud and calcitic-siliciclastic mud contains numerous millimeter to sub-millimeter tubes coated with framboidal pyrite, which have a morphology similar to that of the carbonaceous tubes in BL2K-2, but they are hollow (Fig. 45). The tubes in BL96-2 and BL96-3 are abruptly concentrated at the contact then gradually become smaller and less abundant downward over 5–20 cm (Fig. 44). The sulfide-lined tubes in BL96-2 and BL96-3 are easily identified in X-radiograph images as bright dense objects. They are also recognizable in split cores, including BL02-3, BL02-4, and BL02-5, as dark tube-shaped lines. Each of these cores shows

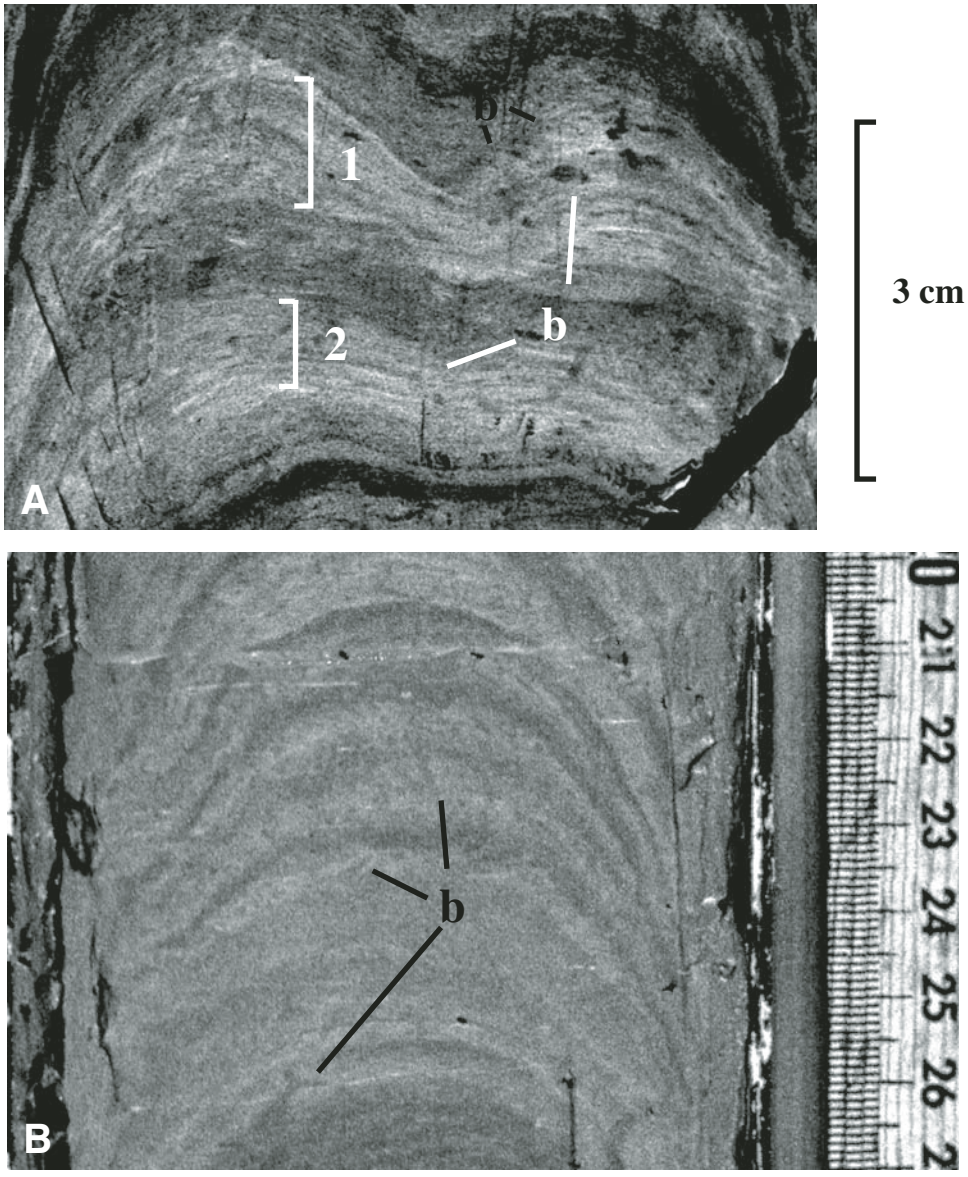

Figure 41. Clay- and silt-dominated graded layers in laminated siliciclastic sediments of BL02-2. (A) Laminated clay (light) with thin silt bases (dark lines). There are four graded laminae in the thickness marked "1" and seven graded laminae in the thickness marked "2." Note small burrows (b). (B) Silt (dark) grading to clay (light). There are eight graded laminae in the center of the picture. Note small burrows (b) and mottling of light clay layers. Scale is in centimeters. Layering was deformed by the coring process.

multiple horizons of these tubes including two within the upper part of the siliciclastic mud intervals and one or two within the calcitic-siliciclastic mud interval (Figs. 4 and 5). In BL96-2, a Scanning Electron Microscope (SEM) image of the mud containing the pyrite-lined tubes also contained numerous tiny hollow tubes (5–10 μm diameters) that are lined with thin sheets of clay (Fig. 45). In BL96-3, the lower tube horizon in the siliciclastic mud interval includes sediment-filled tubes as much as 1 cm in diameter that taper downward and branch (Fig. 46). The siliciclastic mud intervals associated with the pyrite-lined tubes in BL96-2, BL96-3, BL02-3, and BL02-4 show an abundance of clay minerals in smear slides in contrast to the rest of the siliciclastic mud deposits.

The morphology of the carbonaceous tubes in BL2K-2 indicates that they were plant roots. Plant stems as thin as these features would not cut across lamination, including sand layers, nor would they show the systematic decrease in size and abundance downward from the contact with the shell gravel. Given the morphology and distribution of the sulfide-coated tubes in BL96-2 and -3, the tubes in these samples are also interpreted as roots. The small diameters of most of the tubes suggest that the vegetation was mostly grasses or small bushes, although the larger features in BL96-3 could represent small trees. The clay-lined tubes are consistent with eluviated clay linings around root hairs (e.g., Kubiena, 1970, Plate 10). This suggests, along with the vertical orientation of the tubes, that the plants grew in a subaerial environment (Retallack, 2001, p. 13–19). The occurrence of clay minerals, rather than the glacial flour, in the horizons containing the structures interpreted as roots is also suggestive of soil formation. The downward decrease of root diameters and abundances is interpreted as representing protrusion of the roots down from the surface, but it could also reflect proximity to a larger taproot.

Gypsum crystals ranging from 0.05 to 0.3 mm long are associated with the black sulfide-coated tubes in two intervals in BL96-2 (Fig. 45). The thickest interval of gypsum (305–330 cm) has the largest crystals near the top and progressively smaller crystals downward. The crystals are organized into vertically elongate concentrations and horizontal bands (Fig. 47). The lowest occurrence consists of small, irregular concentrations of crystals. BL96-3 also has gypsum crystals associated with the black tubes, but the best developed occurrence (19–23 cm) consists of small, irregular patches of small crystals (around 0.5 mm), and the other interval (40–50 cm) is known only from silt-sized crystals in smear slides. Ovate carbonate concretions (1–5 mm diameter) are associated with the sulfide-coated tubes at the interval starting at 40 cm in BL96-3 (Fig. 48), and in the lower part of the interval starting at 330 cm in BL96-2.

The gypsum crystal concentrations, which coarsen upward, are similar to modern gypsum soil profiles (Dan and Yaalon, 1982). In gypsum soils, the gypsum is introduced as windblown dust and is then worked downward into the soil profile by rainfall (Drever and Smith, 1978). The crystals reprecipitate during

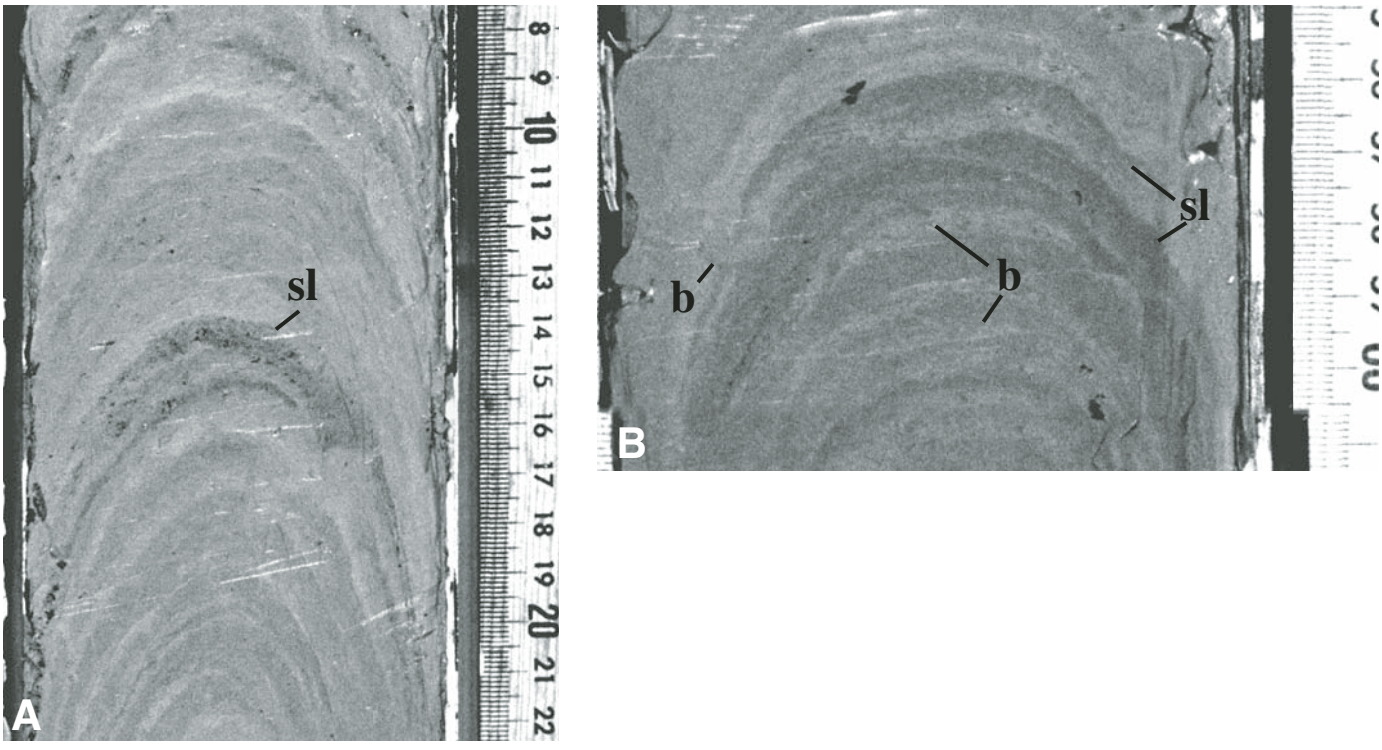

Figure 42. Core segments of BL02-2 with laminated siliciclastic sediment showing sand lenses. (A) Medium sand lenses (sl) at top of upward-coarsening sequence overlain by a thicker clay unit. (B) Fine sand lenses (sl) with thin clay partings. Note burrows (b) of various sizes. Scales are in centimeters. Layering was deformed by the coring process.

dry intervals, with larger crystals forming closer to the surface. Similarly, the carbonate nodules may represent caliche development in a soil horizon by reprecipitation of carbonate dust or silt-sized detrital limestone. The large calcitic concretions near the base of BL96-2, however, may not be related to the rooted zone, and could represent a later diagenetic feature.

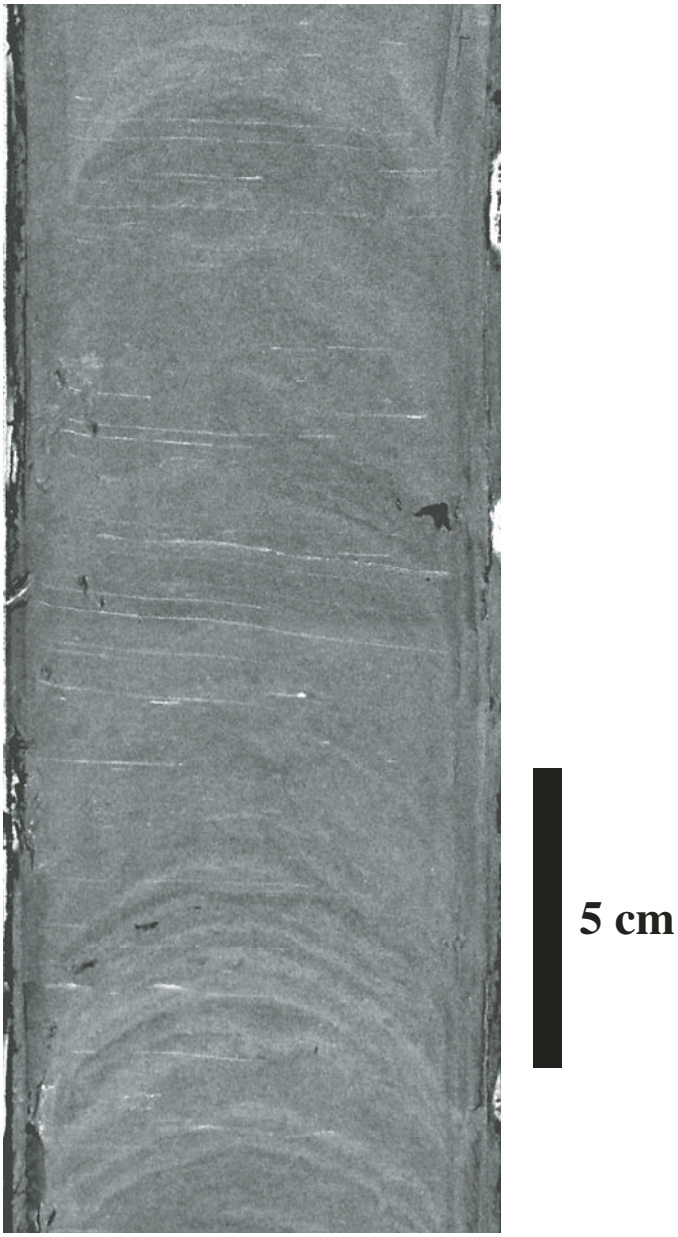

Figure 43. Core segment of BL02-5 showing transition between laminated siliciclastic sediment and unbedded siliciclastic sediment. Laminated interval is comprised of silt and clay (light). Dark upper interval is mottled silty mud with vague bands of coarser-grained (darker) and finer-grained (lighter) sediment.

Pleistocene Depositional Model

Age constraints on the Pleistocene sedimentation are poorer than those for the Holocene. Several dated intervals are in apparent conflict with other ages including two samples from the same depth in BL96-2 (Fig. 3). The change from siliciclastic to calcitic sedimentation and calcitic to aragonitic sedimentation are the most important correlative features that are consistent with the radiocarbon age. The reconstruction presented here assumes that the horizons marking the initiation of the structures interpreted as roots are correlative, and that they represent significant time breaks in the record. The correlation of core segments representing the age interval 15–10 ka (Fig. 49) and the age interval 26–15 ka (Fig. 50) rejects the two 14 ka ages in BL96-2 in favor of the older ages, and it also rejects both of the radiocarbon ages in BL02-5 (Fig. 4).

The youngest Pleistocene deposits in Bear Lake are aragonite deposits similar to those of the Holocene. Aragonite III is the most common sediment in deep-water cores (BL96-2, BL02-3) indicating conditions much shallower than the modern lake. There was at least one transgression that brought lake levels near the modern depth, very close to 10 ka as indicated by Aragonite III deposits in BL02-1 at depths similar to modern occurrences (~10 m). The graded shell gravel at the tops of BL2K-2, BL02-1, BL02-2, and BL02-5 may actually represent much younger shorelines that have eroded to the Pleistocene deposits. The oldest aragonite deposits, which include Aragonite II in the deepest core sites, are ca. 11.5 ka. These gradationally overlie calcite deposits and are interpreted as indicators of increasing lake salinity after the Bear River ceased to flow into the basin (Dean et al., 2006; Dean, this volume).

Calcitic sediment deposition occurred in Bear Lake over the period of 15–11.5 ka. Deep-water calcite similar to the Holocene deposit was precipitated at the very beginning and very end of this depositional interval, and it chemically indicates that the lake was receiving Bear River water. It is not known if the lake became as deep as inferred for the Holocene calcite during either of these intervals. Both calcites are found only in cores whose locations are deeper than 30 m below the modern highstand. Shoreline shell gravel overlying the correlative strata in the cores from shallower-water localities suggests that the younger calcite could have been eroded. Deposits of the Raspberry Square phase (Laabs and Kaufman, 2003) at ~9 m above the modern highstand are 15.9 k.y. old (Smoot and Rosenbaum, this volume). This could be equivalent to the older of Pleistocene calcite deposits, or the younger one if the shells that were dated had been reworked. The bulk of the calcitic interval consists of a mixture of calcite and siliciclastic mud. The sedimentation rate was probably low despite the increase of siliciclastic sediment, as indicated by concentrations of *Daphnia* egg casings and body parts. If the elongated blebs represent aquatic vegetation, the water must have been relatively clear to allow growth. The siliciclastic component includes glacial flour, but this may have been derived from older deposits exposed on the lake margin and reworked by local

drainages. This model explains the conflicting evidence of clastic deposition with low sedimentation rates and low turbidity. The rooted horizons indicate that at two times during the depositional interval, the lake fell to at least 43 m below the modern highstand. Because the mixed calcitic-siliciclastic mud deposits immediately above and below the root-disrupted horizons are nearly the same, the lake-level changes to produce the exposure surfaces must have been relatively small. The coeval occurrence of marsh-like deposits in BL02-1 indicates that the maximum lake level was lower than 9 m below the modern highstand (Fig. 51). If the marsh deposits in BL02-1 formed in a depression above the lake margin, it could have always been much shallower.

Siliciclastic mud contains abundant glacial flour brought in from the Bear River. The oldest deposits examined in this report date to 26 ka and the youngest siliciclastic sediments to 16 ka (Smoot and Rosenbaum, this volume). The lake during this period

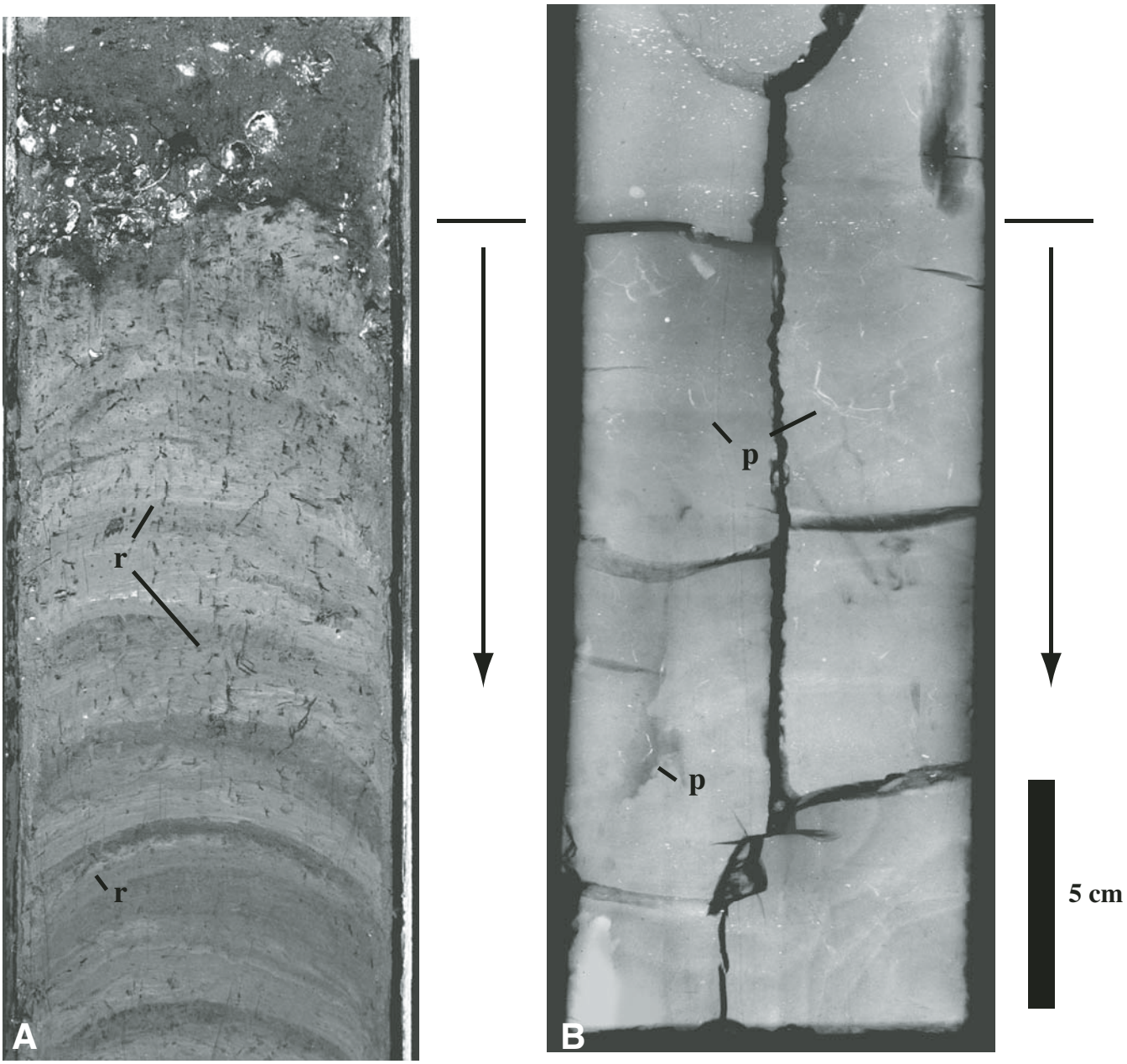

Figure 44. Core segments showing root structures. (A) Core BL2K-2 showing carbonaceous black roots (r) decreasing in abundance away from an overlying graded shell-gravel contact (arrow). The carbonaceous cylinders are coated with framboidal pyrite. Note how vertical features crosscut lamination. (B) X-radiograph of BL96-2 showing hollow cylinders of framboidal pyrite (p) decreasing in abundance away from a contact with calcitic siliciclastic mud with blebs (arrow). The cylinders are interpreted as former root casts similar to those in A.

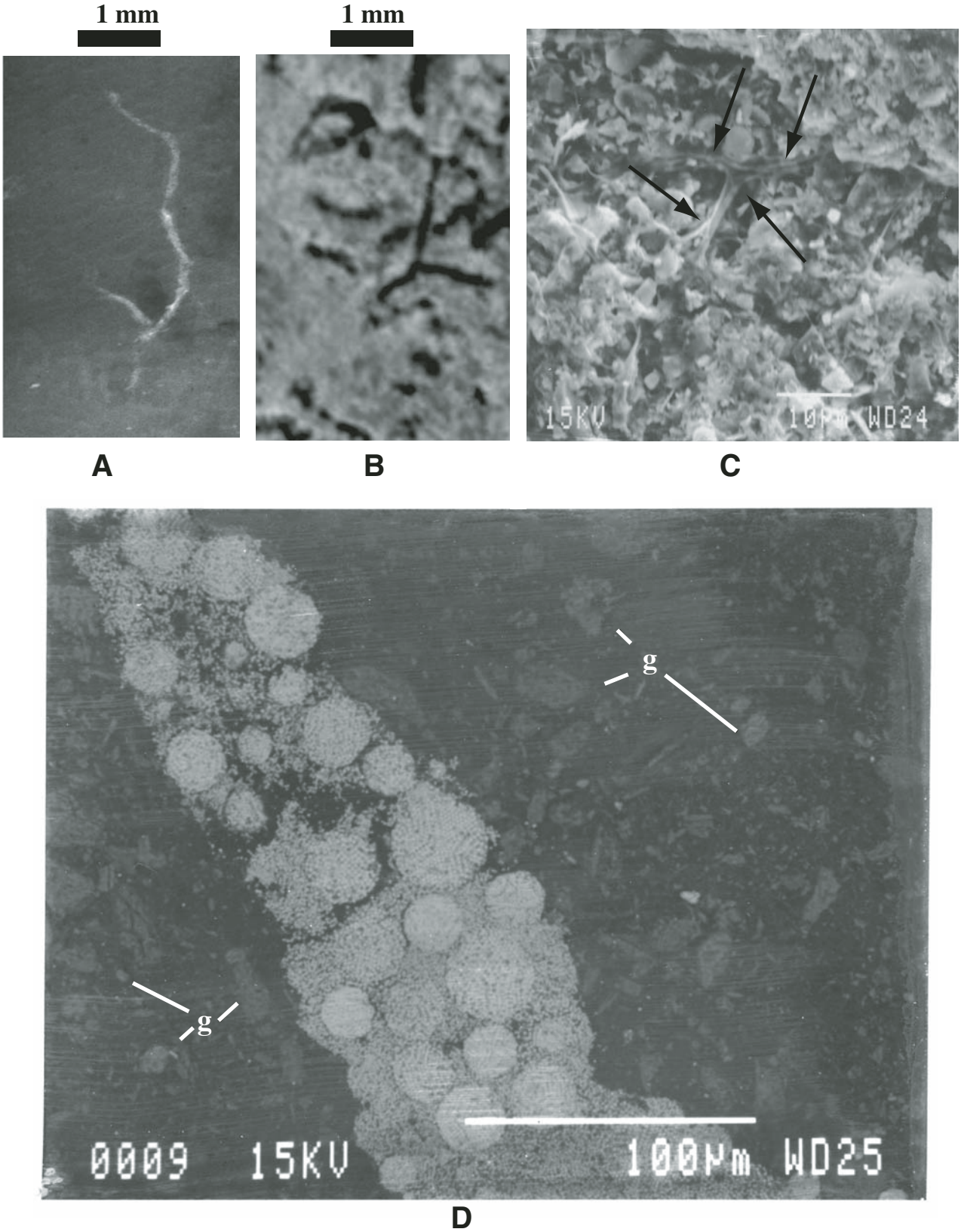

Figure 45. Details of root structures in cores. Comparison of X-radiograph of hollow pyrite tube from BL96-2 (A) and cut surface of carbonaceous tube from BL2K-2 (B), both showing characteristic branching. (C) SEM (Scanning Electron Microscope) image from BL96-2 showing a sheet of clay partially defining a branching set of tubes (arrows). The sheet of clay is interpreted as a cutan lining a root hair cast. (D) SEM backscatter image from BL96-2 showing framboidal pyrite coating a hollow cylinder. Surrounding matrix is full of euhedral gypsum crystals (g).

was probably spilling to the north and re-entering the Bear River (Reheis et al., this volume). Over most of this time span, laminated siliciclastic mud formed in the area adjacent to the northern margin of Bear Lake as distal equivalents to deltaic deposits of the Bear River (Fig. 51). To the south, the deposits were dominated by mud and silt over most of the basin floor. Fluctuations in the Bear River discharge and distributary channel avulsion caused shifts in the distance of silt sedimentation from the delta mouth. The lake margins probably had sandy shorelines with sandy mud and muddy sand in transition to the siliciclastic mud. At ca. 18 ka, the lake level dropped abruptly, leaving an exposed muddy bottom to at least 43 m below the modern highstand. Vegetation became established on the surface and gypsum-rich soils formed. At ca. 17 ka, the lake level rose to at least 33 m below the modern highstand, and then rapidly dropped to the former low, allowing a second vegetated surface with gypsum soils to form. The gypsum horizons suggest at least semiarid conditions during the lowstand intervals. The relatively rapid transition from spilling, glacier-fed lake to a nearly completely desiccated flat was probably caused by diversion of Bear River flow northward from the basin during an extended drought. The low-flow Bear River incised into delta deposits making avulsion away from the lake basin very possible. The minor transgression between the two gypsum-bearing soils may not have been caused by a return of Bear River water to the basin. Increased discharge of local drainages may have reworked the older subaerial deposits. When

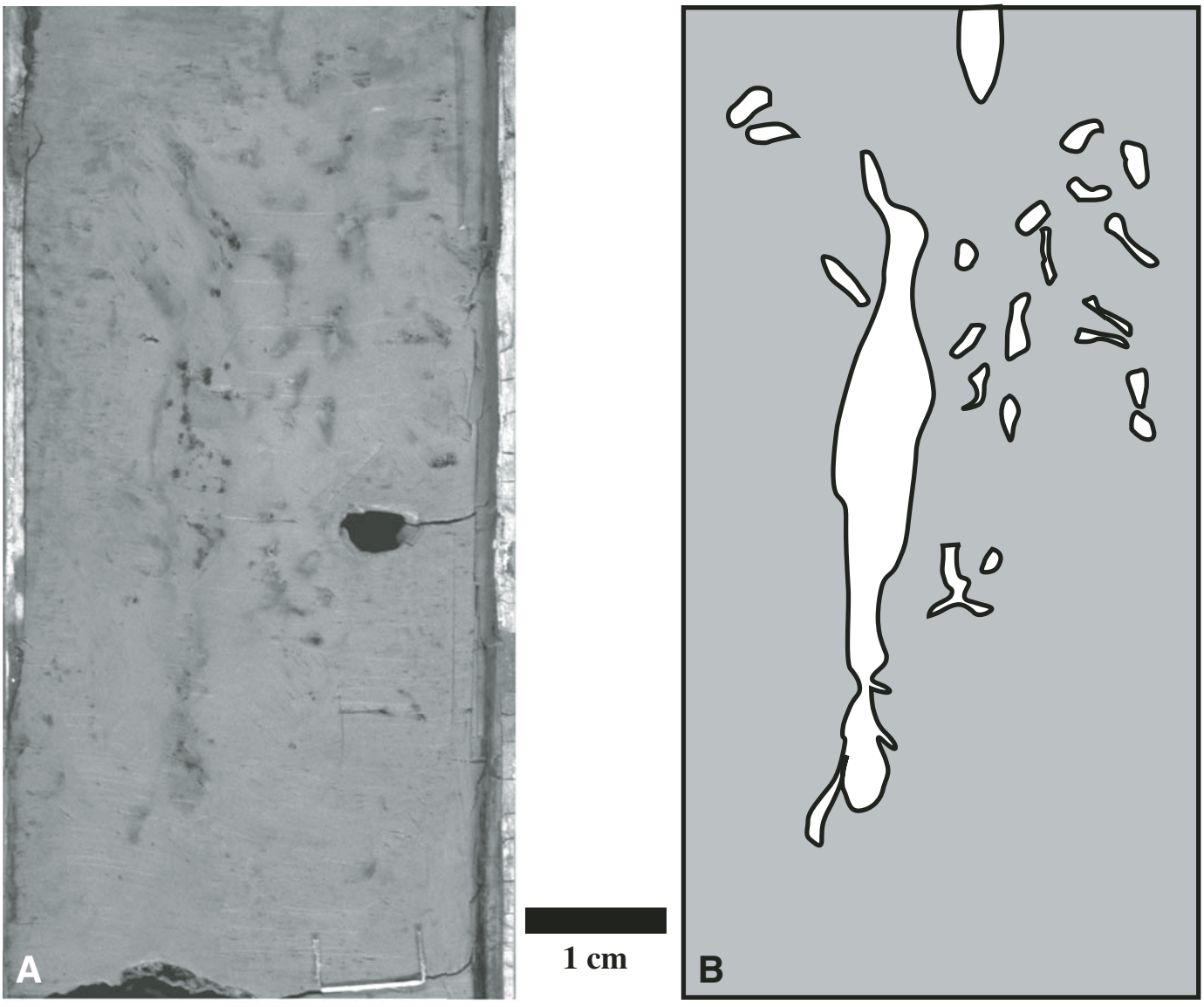

Figure 46. Cut surface (A) and schematic drawing (B) of sediment-filled root casts in BL96-3. Root outlines (darker gray in A and white in B) are defined by changes in grain texture and rims of iron oxide. Small blebs of pyrite (black) occur within the largest cast. Only largest root casts are shown in the schematic sketch.

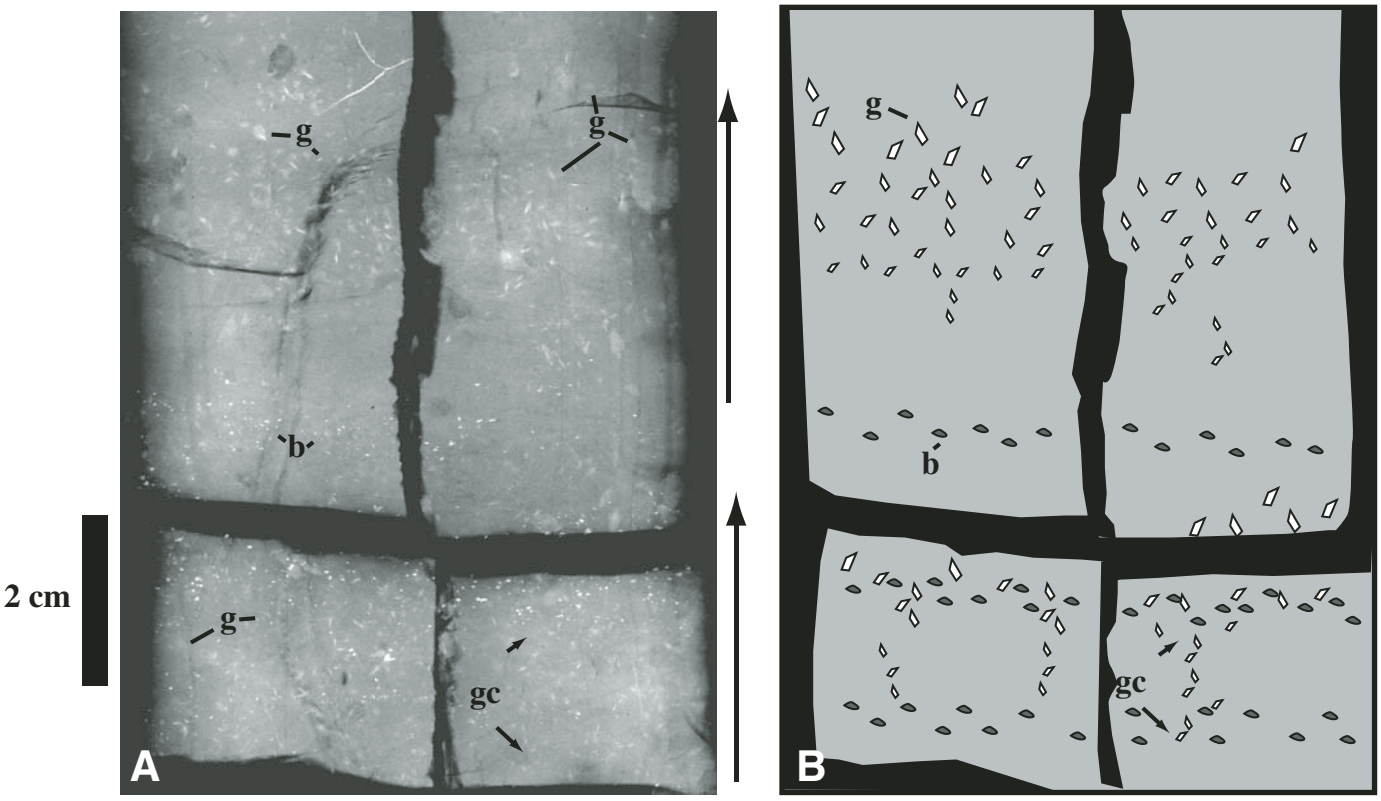

Figure 47. Gypsum crystals in core segment at BL96-2 in X-radiograph (A) and schematic sketch (B). Gypsum crystals (g) occur as two upward-coarsening sequences. Smaller crystals are arranged in vertical columns (gc) which probably follow roots or soil structures. Background sediment includes numerous pyrite-coated blebs (b), which are mostly *Daphnia* egg casings.

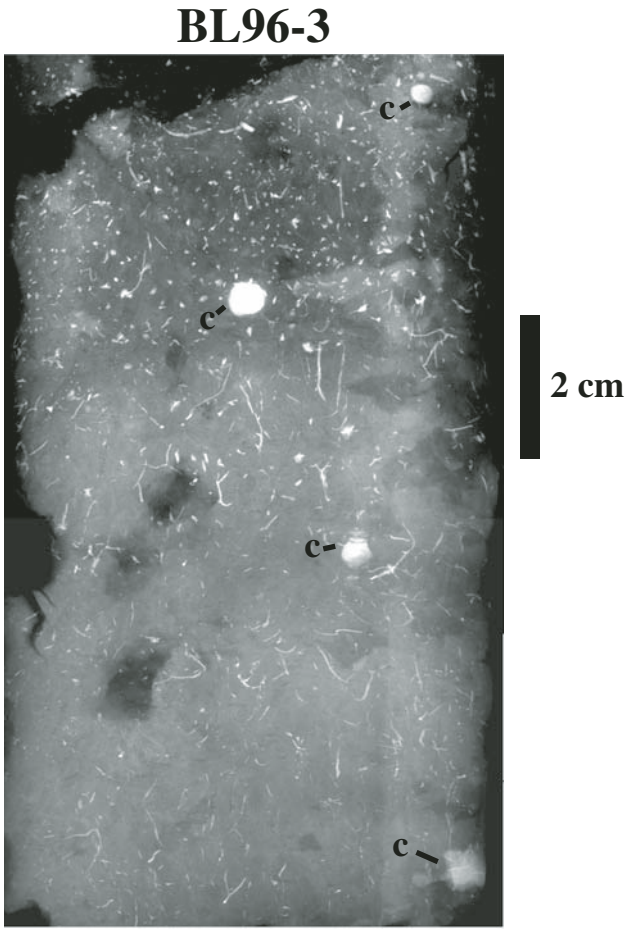

Figure 48. Carbonate concretions (c) associated with root structures (bright white stringers) in X-radiograph of BL96-3. Note how root structures decrease in size and abundance downward from top of segment.

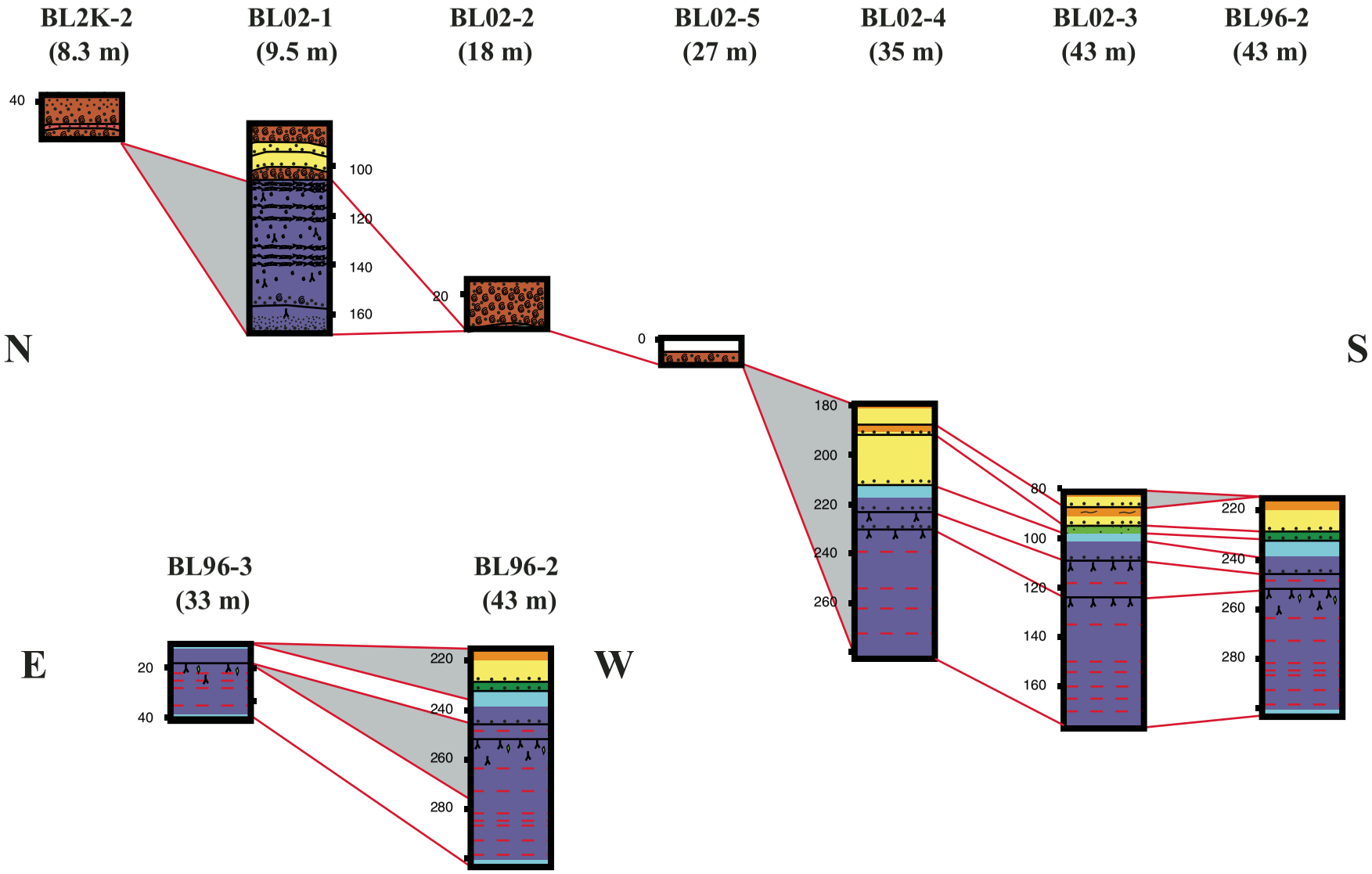

Figure 49. Correlation of core segments representing the time interval 15–10 ka along a north-south and an east-west transect. Formatting, scales, and data sources are the same as for Figure 31.

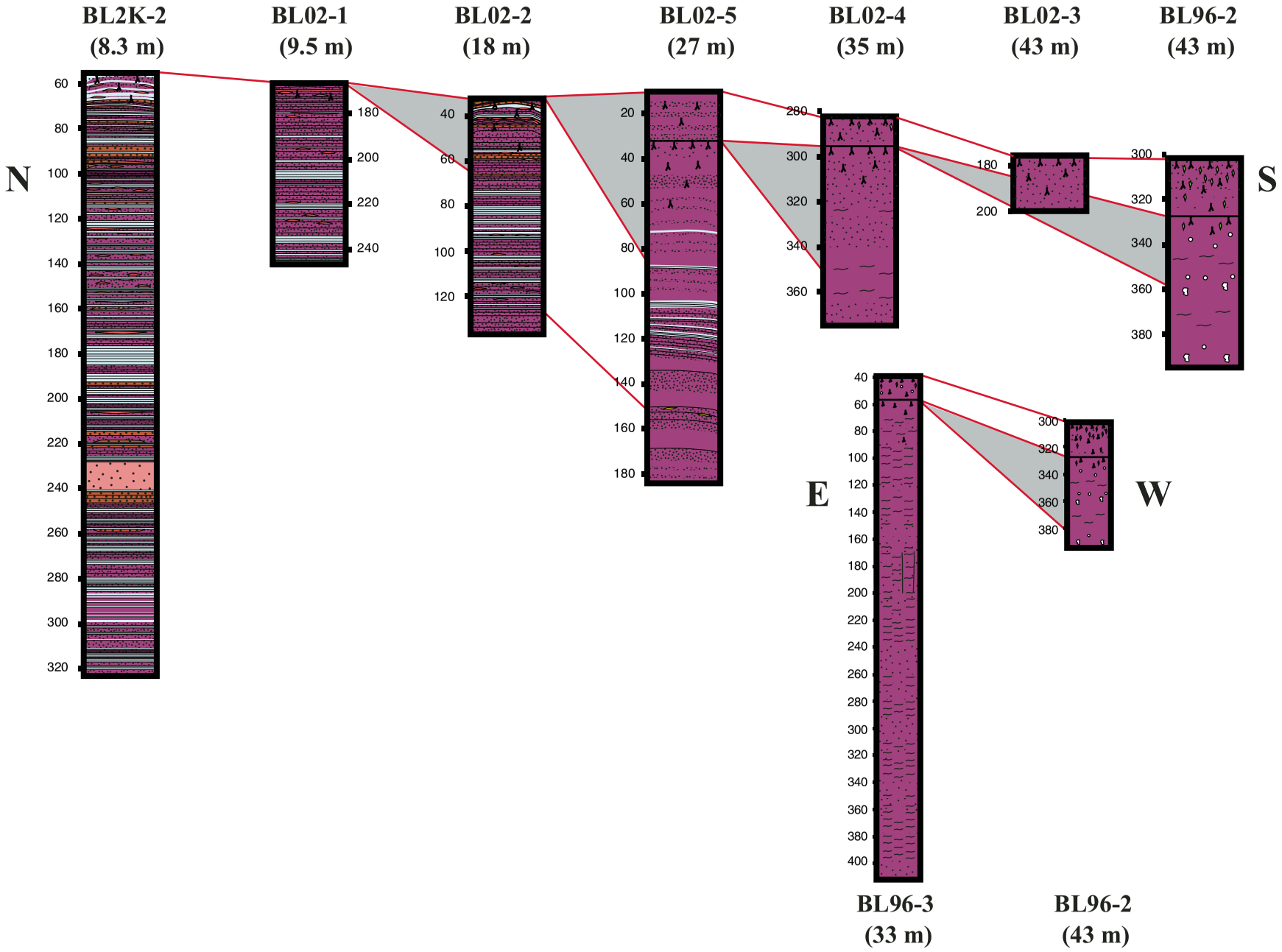

Figure 50. Correlation of core segments older than 15 ka along a north-south and an east-west transect. Formatting, scales, and data sources are the same as for Figure 31. Note the change of scale for the east-west correlation.

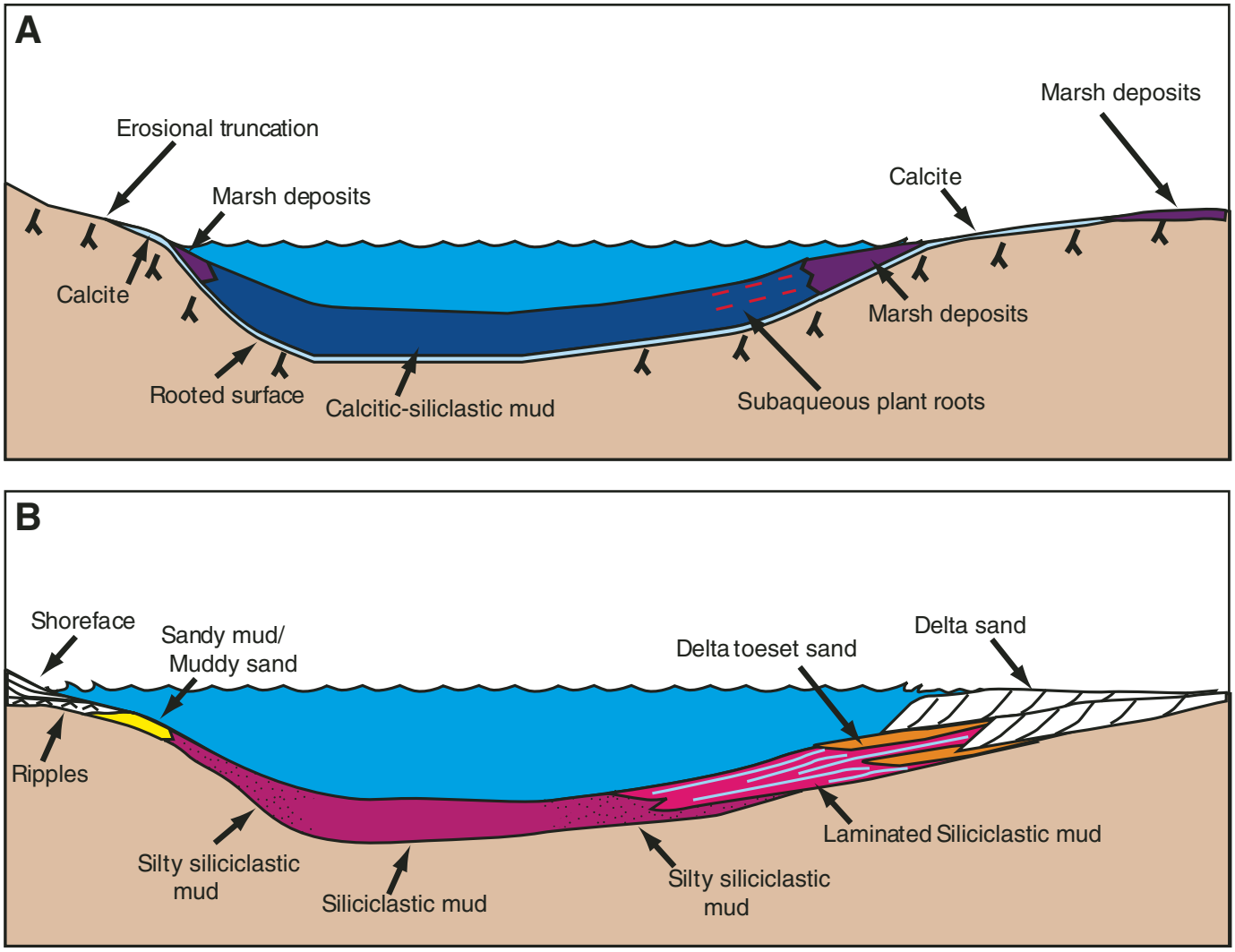

Figure 51. Schematic illustration of Pleistocene depositional facies in Bear Lake during calcitic-siliciclastic mud deposition (A) and siliciclastic mud deposition (B). The right side represents the northern margin of the basin. The left side is shown steeper to illustrate changes that also occur along the east-west transect. (A) The time of Bear Lake deposition following the highstand, which produced a widespread calcite layer overlying the lowstand rooted surface, itself superimposed on siliciclastic mud. Calcite and siliciclastic mud are eroded from the subaerial deposits and redeposited into the shallower lake. Subaqueous plants grow in the broad shallow areas to the north. (B) The time of siliciclastic deposition in Bear Lake before the first subaerial surface. Deltas fed by the Bear River form on the north margin of the lake in the area that is now Mud Lake. Siliciclastic mud becomes sandy near shorelines south of the delta area.

the lake level next rose ca. 15 ka, it signaled a return of Bear River inflow, but with virtually no siliciclastic sediment. This may indicate that only a minor distributary of the river entered the basin and that the lake-level rise was rapid enough to make sediment reworking unimportant.

DISCUSSION

Although the sedimentary record of Bear Lake records changes in climate over the past 26,000 years, the signals of change were modified by changes in the basin hydrology that were not directly linked to climate. Up to ca. 18 ka, the Bear River flowed into the basin, draining glaciers in the Uinta Mountains. Climate changes while the lake was spilling to the north were probably not well recorded in the sediment. The dry episode was probably an exaggerated representation of the actual climate change, because the loss of Bear River inflow contributed to the regression. In the 4000 years before the next major lake-level rise, the lack of Bear River inflow may have prevented the recording of wetter conditions in the drainage area. The return of Bear River water was probably related to a wetter climate, but the contrast with the exposed deposits was more a measure of having fluvial input into the basin. The transition to an aragonite precipitating lake was not exclusively due to a transition from spilling lake to

closed lake, because there is no record of aragonite precipitation associated with any of the rooted horizons. One possible explanation is that the root structures and gypsum-bearing soils are misinterpreted and that the lake did not experience the extreme desiccation (e.g., Dean et al., 2006). This is unlikely given the range of evidence for subaerial exposure, so the cause must be related to a change in the hydrology. It is possible that the groundwater systems that feed the modern lake were not established until the end of the Pleistocene. The well-documented active faulting around the lake margin could have provided the needed changes in groundwater flow paths.

Another important implication of this sedimentological study is that since ca. 18 ka, a large portion of the preserved sediment record in the basin is redeposited material, including both chemical precipitates and organisms. Furthermore, there are numerous gaps in the lacustrine record where the sediment was eroded and redeposited in the deeper parts of the basin. The fact that chemical and biological proxy measurements recognize variations in the lake level indicates that the actual lake changes are not completely masked by this mixing. Nonetheless, the sensitivity of these records has likely been reduced, because the chemical and biological proxy records presented in this volume show very little of the lake-level fluctuations inferred from the sedimentology.

SUMMARY

The sedimentary record of Bear Lake over the past 26,000 years can be divided into six episodes. The first episode is siliciclastic sedimentation as the Bear River deposited glacial flour derived from the Uinta Mountains. This episode ended ca. 18 ka, with a radical drop in lake depth probably due to a drought and diversion of the Bear River away from the basin. The second episode was a dry interval, with subaerial surfaces forming in areas now covered with over 40 m of water for most of the time between 18 and 15 ka. The third episode also included Bear River inflow, but clastic sediment was only a minor component. Calcite precipitation marked the initial transgression ca. 15 ka and the final transgression of this interval ca 11.5 ka. During the remainder of this time interval, the lake appeared to be shallow with intermittent periods of lowstands exposing the surfaces again to depths more than 40 m below the modern highstand. The fourth episode, ca 11.5–8 ka, is marked by aragonite precipitation from waters with no Bear River input. The lake was mostly shallower than the modern lake, with shorelines as much as 30 m below the modern highstand. The fifth episode marks a return of Bear River inflow and a major lake transgression ca. 8.5–8 ka. Once again, however, there was no siliciclastic input from the river and only calcite precipitation. Finally, the sixth episode is a shift to the modern Bear Lake hydrology, with no Bear River input and aragonite precipitation until the opening of the canal system in 1912. During this depositional episode lake level fluctuated between a few meters above the modern highstand to lowstands as much as 35 m below the modern highstand.

ACKNOWLEDGMENTS

All research for this paper was conducted with funding from the U.S. Geological Survey Western Lakes Catchment Project with Joe Rosenbaum as project chief. X-radiograph analysis of suspected gypsum samples was provided by Daniel Webster. Harvey Belkin provided access to an SEM and instructions for using it. Katrina Moser identified diatoms from photographs of smear slides, and Rick Forester identified the fragments of *Daphnia* and their egg casings. I thank Gail Ashley, Harland Goldstein, Tim Lowenstein, John Rayburn, and Joe Rosenbaum for their detailed reviews of this manuscript which greatly improved its clarity.

REFERENCES CITED

Bright, J., 2009, this volume, Ostracode endemism in Bear lake, Utah and Idaho, *in* Rosenbaum, J.G., and Kaufman, D.S., eds., Paleoenvironments of Bear Lake, Utah and Idaho, and its catchment: Geological Society of America Special Paper 450, doi: 10.1130/2009.2450(08).

Colman, S.M., 2005, Stratigraphy of lacustrine sediments cored in 1996, Bear Lake, Utah and Idaho, U.S. Geological Survey Open-File Report 2005-1288, 15 p.

Colman, S.M., 2006, Acoustic stratigraphy of Bear Lake, Utah-Idaho—Late Quaternary sedimentation patterns in a simple half-graben: Sedimentary Geology, v. 185, p. 113–125, doi: 10.1016/j.sedgeo.2005.11.022.

Colman, S.M., Rosenbaum, J.G., Kaufman, D.S., Dean, W.E., and McGeehin, J.P., 2009, this volume, Radiocarbon ages and age models for the past 30,000 years in Bear Lake, Utah and Idaho, *in* Rosenbaum, J.G., and Kaufman, D.S., eds., Paleoenvironments of Bear Lake, Utah and Idaho, and its catchment: Geological Society of America Special Paper 450, doi: 10.1130/2009.2450(05).

Dan, J., and Yaalon, D.H., 1982, Automorphic saline soils in Israel, *in* Yaalon, D.H., ed., Aridic soils and geomorphic processes: Catena Supplement, v. 1, p. 103–115.

Davis, M.B., and Ford, M.S., 1982, Sediment focusing in Mirror Lake, New Hampshire: Limnology and Oceanography, v. 27, p. 137–150.

Dean, W.E., 2009, this volume, Endogenic carbonate sedimentation in Bear Lake, Utah and Idaho, over the last two glacial-interglacial cycles, *in* Rosenbaum, J.G., and Kaufman, D.S., eds., Paleoenvironments of Bear Lake, Utah and Idaho, and its catchment: Geological Society of America Special Paper 450, doi: 10.1130/2009.2450(07).

Dean, W., Rosenbaum, J., Skipp, G., Colman, S., Forester, R., Liu, A., Simmons, K., and Bischoff, J., 2006, Unusual Holocene and late Pleistocene carbonate sedimentation in Bear Lake, Utah and Idaho, USA: Sedimentary Geology, v. 185, p. 93–112, doi: 10.1016/j.sedgeo.2005.11.016.

Drever, J.I., and Smith, C.L., 1978, Repeated wetting and drying of the soil zone as an influence on the chemistry of groundwater in arid terrains: American Journal of Science, v. 278, p. 1448–1454.

Harms, J.C., Southard, J.B., and Walker, R.G., 1982, Structures and sequences in clastic rocks: Tulsa, Oklahoma, SEPM Short Course no. 9, 249 p.

Hilton, J., 1985, A conceptual framework for predicting the occurrence of sediment focusing and sediment redistribution in small lakes: Limnology and Oceanography, v. 30, p. 1131–1143.

Hutchinson, G.E., 1975, Limnological botany, v. 3 of A treatise on limnology: New York, John Wiley and Sons, 660 p.

Kaufman, D.S., Bright, J., Dean, W.E., Rosenbaum, J.G., Moser, K., Anderson, R.S., Colman, S.M., Heil, C.W., Jr., Jiménez-Moreno, G., Reheis, M.C., and Simmons, K.R., 2009, this volume, A quarter-million years of paleoenvironmental change at Bear Lake, Utah and Idaho, *in* Rosenbaum, J.G., and Kaufman, D.S., eds., Paleoenvironments of Bear Lake, Utah and Idaho, and its catchment: Geological Society of America Special Paper 450, doi: 10.1130/2009.2450(14).

Kemp, A.S., Dean, J., Pearce, R.B., and Pike, J., 2001, Recognition and analysis of bedding and sediment fabric features, *in* Last, W.M., and Smol, J.P., eds., Physical and geochemical methods, v. 2 of Tracking environmental change using lake sediments: Dordrecht, Kluwer Academic Publishers, p. 7–22.

Kubiena, W.L., 1970, Micromorphological features of soil morphology: New Brunswick, New Jersey, Rutgers University Press, 254 p.

Laabs, B.J.C., and Kaufman, D.S., 2003, Quaternary highstands in Bear Lake Valley, Utah and Idaho: Geological Society of America Bulletin, v. 115, p. 463–478, doi: 10.1130/0016-7606(2003)115<0463:QHIBLV>2.0.CO;2.

Lamoureux, S.F., 1999, Spatial and interannual variations in sedimentation patterns recorded in nonglacial varved sediments from the Canadian High Arctic: Journal of Paleolimnology, v. 21, p. 73–84, doi: 10.1023/A:1008064315316.

Lamoureux, S.F., and Bradley, R.S., 1996, A late Holocene varved sediment record of environmental change from northern Ellesmere Island, Canada: Journal of Paleolimnology, v. 16, p. 239–255, doi: 10.1007/BF00176939.

McCalpin, J.P., 1993, Neotectonics of the northeastern Basin and Range margin, western U.S.A.: Zeitschrift für Geomorphologie N.F., Suppl. Bd., v. 94, p. 137–157.

Moser, K.A., and Kimball, J.P., 2009, this volume, A 19,000-year record of hydrologic and climatic change inferred from diatoms from Bear Lake, Utah and Idaho, *in* Rosenbaum, J.G., and Kaufman, D.S., eds., Paleoenvironments of Bear Lake, Utah and Idaho, and its catchment: Geological Society of America Special Paper 450, doi: 10.1130/2009.2450(10).

Reheis, M.C., Laabs, B.J.C., Forester, R.M., McGeehin, J.P., Kaufman, D.S., and Bright, J., 2005, Surficial deposits in the Bear Lake basin: U.S. Geological Survey Open-File Report 2005-1088, 30 p.

Reheis, M.C., Laabs, B.J.C., and Kaufman, D.S., 2009, this volume, Geology and geomorphology of Bear Lake Valley and upper Bear River, Utah and Idaho, *in* Rosenbaum, J.G., and Kaufman, D.S., eds., Paleoenvironments of Bear Lake, Utah and Idaho, and its catchment: Geological Society of America Special Paper 450, doi: 10.1130/2009.2450(02).

Retallack, G.J., 2001, Soils of the past: Oxford, Blackwell Science, 404 p.

Robertson, G.C., 1978, Surficial deposits and geologic history, northern Bear Lake Valley, Idaho [M.S. thesis]: Logan, Utah State University, 162 p.

Rosenbaum, J.G., and Heil, C.W., Jr., 2009, this volume, The glacial/deglacial history of sedimentation in Bear Lake, Utah and Idaho, *in* Rosenbaum, J.G., and Kaufman, D.S., eds., Paleoenvironments of Bear Lake, Utah and Idaho, and its catchment: Geological Society of America Special Paper 450, doi: 10.1130/2009.2450(11).

Rosenbaum, J.G., and Kaufman, D.S., 2009, this volume, Introduction to *Paleoenvironments of Bear Lake, Utah and Idaho, and its catchment*, *in* Rosenbaum, J.G., and Kaufman, D.S., eds., Paleoenvironments of Bear Lake, Utah and Idaho, and its catchment: Geological Society of America Special Paper 450, doi: 10.1130/2009.2450(00).

Rosenbaum, J.G., Dean, W.E., Reynolds, R.L., and Reheis, M.C., 2009, this volume, Allogenic sedimentary components of Bear Lake, Utah and Idaho, *in* Rosenbaum, J.G., and Kaufman, D.S., eds., Paleoenvironments of Bear Lake, Utah and Idaho, and its catchment: Geological Society of America Special Paper 450, doi: 10.1130/2009.2450(06).

Smith, N.D., and Ashley, G., 1985, Proglacial lacustrine environment, *in* Ashley, G., Shaw, J., and Smith, N.D., eds., Glacial sedimentary environments: Tulsa, Oklahoma, SEPM Short Course no. 16, p. 135–216.

Smoot, J.P., 2003, Impact of sedimentation styles on paleoclimate proxies in late Pleistocene through Holocene lakes in the western U.S.: Tucson, International Limnogeology Congress, 3rd, Abstracts, p. 273.

Smoot, J.P., and Benson, L.V., 1998, Sedimentary structures as indicators of paleoclimatic fluctuations: Pyramid Lake, Nevada, *in* Pitman, J.K., and Carroll, A.R., eds., Modern and ancient lake systems: Utah Geological Association, Guidebook 26, Salt Lake City, Utah, p. 131–161.

Smoot, J.P., and Benson, L.V., 2004, Mechanical mixing of climate proxies by sediment focusing in Pyramid Lake, Nevada: A cautionary tale: Geological Society of America Abstracts with Programs, v. 36, p. 473.

Smoot, J.P., and Lowenstein, T.K., 1997, Depositional environments of nonmarine evaporites, *in* Melvin, J.L., ed., Evaporites, petroleum and mineral resources: Amsterdam, Elsevier, Developments in Sedimentology, v. 50, p. 189–347.

Smoot, J.P., and Rosenbaum, J.G., 2009, this volume, Sedimentary constraints on late Quaternary lake-level fluctuations at Bear Lake, Utah and Idaho, *in* Rosenbaum, J.G., and Kaufman, D.S., eds., Paleoenvironments of Bear Lake, Utah and Idaho, and its catchment: Geological Society of America Special Paper 450, doi: 10.1130/2009.2450(12).

Sturm, M., 1979, Origin and composition of clastic varves, *in* Schluchter, C., ed., Moraines and varves: Rotterdam, A.A. Balkema, p. 281–285.

Terry, R.D., and Chilingar, G.V., 1955, Summary of "Concerning some additional aids in studying sedimentary formations," by M.S. Shvetsov: Journal of Sedimentary Petrology, v. 25, p. 229–234.

Manuscript Accepted by the Society 15 September 2008

Printed in the USA